STUDY OF BLAST-INDUCED MILD TRAUMATIC BRAIN INJURY:

LABORATORY SIMULATION OF BLAST SHOCK WAVES

STUDY OF BLAST-INDUCED MILD TRAUMATIC BRAIN INJURY:

LABORATORY SIMULATION OF BLAST SHOCK WAVES

By NEVEEN AWAD, M.B., B.Ch., M.A.Sc.

Thesis

Submitted to School of Graduate Studies in Partial Fulfilment of the Requirements for the Degree of Doctor of Philosophy

Doctor of Philosophy (2014) McMaster University

(School of Biomedical Engineering) Hamilton Ontario

TITLE: STUDY OF BLAST-INDUCED MILD TRAUMATIC BRAIN INJURY: LABORATORY SIMULATION OF BLAST SHOCK WAVES

AUTHOR: Neveen Awad

M.A.Sc. (McMaster University)

M.B., B.Ch. (Cairo University)

Supervisors: Dr. Wael W. El-Dakhakhni

Dr. Ammar Gilani

NUMBER of PAGES (i-xii, 1-173)

ABSTRACT

Blast-induced mild traumatic brain injury (BImTBI) is one of the most common causes of traumatic brain injuries. BImTBI mechanisms are not well identified, as most previous blast-related studies were focused on the visible and fatal injuries. BImTBI is a hidden lesion and long-term escalation of related complications is considered a serious health care challenging due to lack of accurate data required for early diagnosis and intervention.

The experimental studies presented in this thesis were performed to investigate aspects of blast shock wave mechanisms that might lead to mild traumatic brain injury. A compressed air-driven shock tube was designed and validated using finite element analysis (FEA) and experimental investigation. Two metal diaphragm types (steel and brass) with three thicknesses (0.127, 0.76, and 0.025mm) were utilized in the shock tube calibration experiment, as a new approach to generate shock wave. The consistency of generated shock waves was confirmed using a statistical assessment of the results by evaluating the shock waves parameters. The analysis results showed that the 0.127mm steel diaphragm induces a reliable shock waveform in the range of BImTB investigations.

Evaluation of the shock wave impacts on the brain was examined using two sets of experiments. The first set was conducted using a gel brain model while the second set was performed using a physical head occupied with a gel brain model and supported by a neck model. The gel brain model in both the experimental studies was generated using silicone gel (Sylgard-527). The effects of tested models locations and orientations with

respect to the shock tube exit were investigated by measuring the generated pressure wave within the brain model and acceleration. The results revealed that the pressure waveform and acceleration outcomes were greatly affected by the tested model orientations and locations in relation to the path of shock wave propagation.

Keywords: Blast-induced mild traumatic brain injury; Biomechanics; Blast shock wave; Finite element analysis; Gel brain model; Intracranial pressure; Physical head and neck model; Shock tube.

DEDICATION

I dedicate my dissertation to my family. A special feeling of gratitude goes to my loving parents-Nabil Awad and Nawal El-Waseef- whose words of encouragement and push for tenacity ring in my ears. Thanks to my sisters Nesrin, Nermin and Nedaa and their families for their never ending support. I also dedicate this dissertation to my husband Waleed who has supported me throughout the process. You have been and continue to be a blessing; an oasis in the desert. I will always appreciate you helping me to accomplish our family's dreams. I dedicate this work and give special thanks to my wonderful kids Maryem, Marwan, Salma and Ramez for being there for me throughout the entire doctorate program. All of you have been my best cheerleaders.

ACKNOWLEDGMENTS

I wish to thank my committee members who were more than generous with their expertise and precious time. A special thanks to Dr. Wael El-Dakhakhni and Dr. Ammar Gilani, my supervisors, for their countless hours of reflecting, reading, encouraging, and most of all patience throughout the entire research. Thank you Dr. Laurie Doering for agreeing to help on my committee, your excitement and willingness to provide feedback made the completion of this research an enjoyable experience. Special thanks go to the staffs at Applied Dynamic Lab, Kent Wheeler and Paul Heerema for their technical support during experiments. I could always count on you both for experimental assistance.

Hamilton, Ontario Neveen Awad
September 2014

DECLARATION OF ACADEMIC ACHIEVEMENT

This work has been organized according to the guidelines for the sandwich thesis preparation required by the Faculty of Graduate Studies at McMaster University. The authors' contributions in each paper are intended to be reported in the following statements:

Paper 1: Neveen Awad, Laurie Doering, "***Neurological manifestations related to blast injury***"**.** Accepted by European Neurological Journal in 2011.

Paper I was prepared for publication as a review paper. The paper was written by Neveen Awad. Dr. Doering reviewed and revised the journal paper.

Paper 2: Neveen Awad, Wael W. El-Dakhakhni, and Ammar.Gilani, "***Compressed Air-Driven Shock Tube System To Simulate Blast-Induced Mild Traumatic Injuries*** ". Submitted to Shock Waves Journal in July 2014

In this manuscript, the design of experimental study and analysis of the data were performed by Neveen Awad. The paper was written by Neveen Awad. Dr. El-Dakhakhni and Dr. Gilani supervised the research work; reviewed and revised the journal paper.

Paper 3: Neveen Awad, Ammar Gilani, Wael W. El-Dakhakhni."***Analysis of Blast Shock Wave Effects on Surrogate Brain Gel Model for Traumatic Brain Injury Assessment*** ". Submitted to Annals of Biomedical Engineering in August 2014

Design of research study and analysis of the experimental data were performed by Neveen Awad. Paper 3 was written by Neveen Awad. Dr. Gilani and Dr. El-Dakhakhni supervised the research work; reviewed and revised the journal paper.

Paper 4: Neveen Awad, Wael W. El-Dakhakhni, Ammar Gilani," ***A Physical Head and Neck Surrogate Model to Investigate Blast-Induced Mild Traumatic Brain Injury*** ". Submitted to the Arabian Journal for Science and Engineering in August 2014

In this manuscript, the design of experimental study and analysis of the data were performed by Neveen Awad Paper 4 was written by Neveen Awad. Dr. El-Dakhakhni and Dr. Gilani supervised the research work; reviewed and revised the journal paper.

Table of Contents

LIST OF ACRONYMS AND ABBREVIATIONS

ANOV	Analysis of Variance
ALE	Lagrangian Eulerian
ATP	Adenosine triphosphate
BBB	Blood Brain Barrier
b-TBI	Blast-induced Traumatic Brain Injury
BImTBI	Blast-induced mild Traumatic Brain Injury
BPT	Back Pressure Transducer
CFD	Computational Fluid Dynamics
CNS	Central Nervous System
CON WEP	Conventional Weapons Effect
CSF	Cerebrospinal Fluid
CT	Computed Tomography
CV	Coefficient of Variation
DAI	Diffuse Axonal Injury
DTI	Diffusion Tensor Imaging
EthD-1	Ethidium homodimer-1
EOS	Equation of State
FEA	Finite Element Analysis
FPT	Front Pressure Transducer
g	Gram (metric unit of mass)
GCS	Glasgow Coma Scale
GFAP	Glial Fibrillary Acidic Protein
GPa	Gigapascal
ICP	Intracranial Pressure
IED	Improvised Explosive Devices
Kg	Kilogram (One thousand grams)

kPa	Kilopascal
LDH	Lactate dehydrogenase
LMWAs	Low Molecular Weight Antioxidants
LOC	Loss of Consciousness
LPT	Left Pressure Transducer
µm	Micrometer
mm	Millimeter
MRI	Magnetic Resonance Imaging
ms	Millisecond
mTBI	Mild Traumatic Brain Injury
NMDAR	N methyl-D-aspartate receptors
NPD	Negative Phase Duration
NPP	Negative peak pressure
PET	Positron Emission Tomography
PHNM	Physical Head and Neck Model
PI	Positive Impulse
PPD	Positive Phase Duration
PPP	Positive Peak Pressure
PT	Pressure Transducer
PTA	Post-Traumatic Amnesia
PTM	Pressure Transducer Mount
PTSD	Posttraumatic Stress Disorder
ROS	Reactive Oxygen Species
SPSS	Statistical Package for the Social Sciences
TBI	Traumatic Brain Injury

Chapter 1: Introduction

1.1 Background

Traumatic brain injury (TBI) is a serious lesion that either induces severe mortalities or leads to morbidity. The most common reasons of TBI used to be related to sport or car accidents. Nowadays, the extensive use of explosives in military conflicts and terrorist attacks as well as frequent industrial or domestic accident increases the frequency of shock wave related TBI. The shock wave can induce primary blast brain injuries when it infiltrates directly through the brain parenchyma. Moreover, the blast shock wave can induce brain damage not only by direct effects but also through indirect mechanisms such as the injury of other organs that may lead to serious brain injuries.

The cerebral ischemia is one of the most serious complications that may result from both direct and indirect injuries and lead to chronic lesions depending on the affected area in the brain. Furthermore, the proliferation of shock wave through the brain tissue especially at the gray-white matter interface can generate shearing stresses that may lead to diffuse axonal injury (DAI). Studies of the mechanisms leading to blast-induced traumatic brain injury are crucial to improve the health care by early diagnosis and appropriate interactions.

Many blast related studies have utilized different types of shock tubes to generate simulated shock waves. In accordance with the subject type and size, wide ranges of shock tubes were developed for the purpose of TBI investigations. Explosive-driven and compressed gas- (e.g. air, Helium, Nitrogen) driven shock tubes are usually used with large laboratory animals or Physical head models. Furthermore, laser-induced stress

waves have been used recently in blast injury-related research to evaluate the blast wave impacts on small animals and cells. The shortcomings of using the high explosive to generate shock waves for blast injury studies purposes including not only safety and security concerns but also it can damage the test subjects so it is not suitable for mild traumatic brain injury (mTBI) studies. Therefore, it is important to develop a shock tube that able to generate shock waves and able to interact with wide range of tested subjects.

1.2 Motivation

Various theories have been suggested to address the explosion mechanisms that may lead to mTBI. Blast shock wave propagation through brain plays a crucial role in brain damage. The prediction of the brain response to blast wave proliferation in accordance with the subject's location and orientation in relation to the blast source has not been completely examined. Further, investigations of the blast wave behavior inside the brain as well as the brain response are a challenging study for two reasons. First, it is required to utilize a simulated blast load in the range that can induce mTBI. The second reason is the need to develop a surrogate brain model with similar elastic properties of the actual brain tissue. The experimental data obtained from the study of the interactions of simulated blast loads with a surrogate brain will promote proper information that may help the early assessment of potential brain injuries and timely intervention.

1.3 Research Objectives

The objectives of the current research are to design and validate a compressed air-driven shock tube that has the ability to generate a non-lethal blast shock wave. As a new approach, two types of metal diaphragms (steel and brass) will be used aiming to generate

a reliable and controlled simulated shock wave in the range that induces mTBI. Shock tube numerical model will be conducted to validate the design prior to actual manufacturing. In addition experimental investigations will be performed to validate the shock tube numerical model analysis. Furthermore, experimental investigations of the blast wave role in developing brain injury will be evaluated using surrogate brain model and a complete physical head and neck model (PHNM). The brain model will be developed by curing silicone gel in a plastic brain mold, thus, the irregular character of the brain outer surface will be captured. Testing the brain model with and without a surrogate skull, will facilitate its movement so that the brain acceleration can be monitored. Previous studies used spherical molds to simulate the skull which was filled with a surrogate brain material that cured *within* skull model thus forming an integrated structure, so a parameter such as the independent brain acceleration could not be evaluated. Further, the PHNM will be assembled with a neck model and simulated skin.

1.4 Organization of the Dissertation

This dissertation demonstrates both numerically and experimentally, the analysis, designed and construction of a compressed-air-driven shock tube. Two sets of experimental studies were performed to investigate the shock wave mechanisms in the traumatic brain injury using the calibrated shock tube as well as brain model and PHNM. This dissertation provides a wide range of information that can facilitate a better understanding of the shock wave/brain interactions. The contents of the dissertation are as follows:

- Chapter 1 provides description of the background information related to the different aspects of blast mechanisms that may have direct or indirect role in developing brain damage. In addition, research motivation and objectives are also presented in this chapter.
- Chapter 2 presents a literature review which comprised a review paper including characterizations of blast shock wave, the classifications of blast-induced traumatic brain injury, explanations of different blast mechanisms that may have role in developing TBI and brain pathophysiological responses as well as the clinical symptoms/signs
- Chapter 3 provides a combination of the numerical and experimental analysis of the designed and constructed compressed-air-driven shock tube for the purpose of studying the outcomes of blast/brain interactions.
- Chapter 4 displays experimental research of blast induced mild traumatic brain injury (BImTBI) utilizing the pre-calibrated shock tube and surrogate gel brain model. Analysis of the gel brain material properties and its comparison to that of actual brain is provided in this chapter. A set of experiments that examine the brain model responses to blast shock waves at different locations and orientation from shock tube exit are described in this section.
- Chapter 5 shows the methodology of preparing the PHNM parts especially the preparation and calibration of the neck model to simulate the actual neck stiffness. Further, group of experimental studies that examine the effect of the PHNM locations and orientations in relation to the shock wave propagation path on the brain model responses are also presented in this section.
- Chapter 6 focuses on the research summary as well as recommendations for future studies

Chapter2: Literature Review-Neurological Manifestations Related to Blast Injury

Neveen Awad and Laurie Doering

2.1 Abstract:

Blast-induced neurotrauma, a consequence of military conflict or domestic explosions, becomes a major focus of healthcare around the world. In general, the most important medical concern of neurotrauma is the potential long-term manifestations of mild traumatic brain injury. Blast overpressure can induce hidden-mild neurotrauma, which is considered to be a critical health and socioeconomic problem. Increased research efforts to understand the mechanisms of blast-induced neurotrauma and the subsequent neuropathophysiological responses are required to address these problems. The objectives of this review are to highlight a range of neurochemical and pathological reactions as well as the clinical manifestations of patients with blast-related neurotrauma.

Keywords: brain trauma, blast wave, blast injury mechanisms, neurochemical reactions, neuropathophysiological responses

2.2 Introduction:

Traumatic brain injury (TBI) is a worldwide critical health problem as it is considered the main reason of traumatic mortality and morbidity. The extensive use of explosives in military conflicts and terrorist attacks on civilians, enhances the incidence of TBI among other leading causes of brain injuries and diseases [1]. The current missions in Afghanistan and Iraq have involved military personnel in major combat operations since the Korean War (1950-1953). Recent reports reveal a progressive deterioration of the security situation due to a marked increase in roadside bombs, known

as improvised explosive devices (IEDs) [2]. The blast-induced TBI (b-TBI) and the consequences of physical and mental disabilities from IEDs are considered long-term critical socioeconomic health problems. The aim of this review is to provide insight into the blast-related injuries, in particular the brain injuries, focusing on experimental and case studies to address the blast injury mechanisms and the related physical and mental health problems.

2.3 The mechanisms of blast that induce neurotrauma

Blast-related neurological lesion research was launched in 1915 during World War I, when many soldiers were exposed to a detonation with no external head injury, but suffered from neurological disorders. These included headache, tinnitus, hypersensitivity to noise, dizziness, amnesia, tremors, and gait disabilities [3]. The forms of this trauma are often described as shell shock, battle fatigue, combat stress, or Post-Traumatic Stress Disorder (PTSD). The symptoms from these conditions vary in intensity in accordance with individual resilience and usually depend upon the degree of trauma experienced. The blast injuries can be classified into four main categories: primary, secondary, tertiary and quaternary according to the mechanism of the injury. The primary blast injury occurs via direct infiltration of the blast wave through the tissues [4]. The most common primary blast injuries include pulmonary barotraumas, tympanic membrane rupture, hemorrhage, organ perforation, and brain concussion [5]. Concerning the brain, this type of blast injury may directly impact the brain against the skull (coup) or indirectly on the opposite side of the impact (countre-coup). The coup/countre-coup injuries result commonly in contusion of the brain tissue with neurological symptoms depending on the site of impact.

Shearing and stretching of the brain tissue, the movement of the brain structures relative to the skull and to each other, are additional tissue responses to the blast wave that can provoke diffuse axonal injury. In addition, rupture of the intracranial blood vessels, especially the ones located between the brain and dura mater, induces subdural hematomas, leading to elevated intracranial pressure and brain edema [6].

The secondary blast injury mechanism results from objects that are accelerated by the energy of the explosion that strike the victim and cause either blunt or penetrating ballistic trauma. Tertiary injuries occur when the victim's body or head collide with surrounding objects or the ground and subsequently cause head injuries, skull fractures, and bone fractures. The blast injuries from exposure to heat, toxic gases, dust or the exacerbation of existing injuries are defined as the quaternary blast injury [7]. Furthermore, b-TBI can be classified according to the type of pathological change, namely focal injury, teras in contusion and localized hematoma, and/or diffuse injury, in particular diffuse axonal injury. Another blast injury classification relates to the injury biomechanics and are categorized as closed or penetrating injury [8] **(Table 1)**.

2.4 Blast wave and its effects on brain tissue

The blast wave has a significant role in primary TBI. The blast wave occurs from a rapid chemical conversion of an explosive material (solid or liquid) into highly pressurized gases that expand rapidly and compress the surrounding air. This generates a high-pressure region (the positive phase) and a blast wind that propagates in all directions in the form of a shock wave [9]. The blast wind lasts milliseconds and its strength varies with the strength of the detonated explosive device. As the gas propagates away from the

explosion, the initial high-pressure region starts to decompress. This creates a region of negative overpressure (the negative phase) that also propagates away from the explosion and finally returns to the ambient value [10] (Figure 2.1).

These extreme fluctuations in pressure lead to significant neurological injuries that cannot be avoided by a helmet or body armor protection [11]. The severity of injuries is directly proportional to the distance between the victim and the place of the explosion. Other factors that determine the degree of tissue damage include orientation of the victim to the blast, the body mass of the victim, environment of the blast (open space versus closed space, underwater, or urban); and existence of protective barriers [12]. In fact, the field of the explosion is an important factor that determines the blast-wave forms. The blast-wave forms may interact with the surroundings and then develop reflective waves that integrate with the primary blast wave leading to complex wave forms [13]. Patients with TBI are commonly identified according to the duration of the loss of consciousness, with post-traumatic amnesia (PTA) and the Glasgow Coma Scale (GCS) score into severe, moderate or mild (b-TBI) [14]. In mild TBI (m-TBI) victims may reveal alteration or loss of consciousness (LOC) not more than 30 minutes with duration of (PTA) less than 24 hours. Patients with moderate TBI demonstrate a period of (LOC) less than 6 hours and recover from (PTA) within 7 days. Furthermore, individuals with severe cases complain of a long period of LOC that may exceed 6 hours and with duration of (PTA) more than 7 days [15]. The m-TBI is a complex process and its diagnosis can be overlooked due to the subjective nature of complaints and the difficulty to evaluate in the battlefield where the medical attentions are mostly to severe injuries. Furthermore, the GCS may potentially

fail to detect TBI cases with mild or absent symptoms [16]. Therefore, blast-related m-TBI is considered a concealed critical problem that makes a clinical diagnosis challenging.

2.5 Responses of the human body to blast waves

The blast waves are believed to affect tissues and organs in a number of different ways. These include spalling, where the shock wave moves between tissues of different densities such as the organs containing air (i.e. lung, gastrointestinal tract, sinuses and ear chambers) that disrupt and destroy the affected tissues. The brain has regions of different densities at the junctions between the gray and white matter areas that are especially vulnerable to the blast overpressure [17]. In addition, tissues with variable densities respond to shock waves at different speeds in turn creating shearing injuries. Furthermore, a shock wave may create compression/expansion of the trapped gases in hollow organs that leads to rupture [18]. In general, the blast overpressure has direct effects in brain tissue and on other organs that can indirectly induce brain injury. For instance, cerebral ischemia, considered the most important secondary event after direct or indirect brain impact, has a crucial role in the consequences of TBI [19].

2.6 Remote blast trauma and its impact on the brain

Results from animal experiments and case studies indicate that remote blast trauma can induce brain injury [20]. For instance, a range of neurological manifestations can be demonstrated following peripheral blast injury. Brain damage in this case may occur as a consequence of the induced hyperexcitability and the ensuing increased synthesis and release of different neurotransmitters and autacoids [21-27]. The following sections

illustrate different ways of how the blast wave can reach the brain and induce injury from a remote injury site.

2.6.1 Propagation of the blast wave from injured extremities to the brain

In the middle of the 1940's, Livingston et al [28] proposed that a shock wave created by high-energy missiles, can propagate with a velocity similar to that of sound in water and produce damage to tissues that are offset from the path of the projectile. During the same period, Harvey et al (29) showed that the reflection and absorption features of the pressure waves that developed from the impact of the high-velocity missile were variable according to the tissue type that was affected [29]. Consequently, the tolerance and response of each tissue type to the pressure wave is different [30]. Suneson et al (30) demonstrated that the brain can be affected after the impact of a high-energy missile in the thigh of a pig [22, 23]. The gross examinations showed no abnormal changes, while the electron and light microscopic analyses revealed brain damage in different regions. These included myelin invaginations, axonal shrinkage, a decrease in the number of microtubules and glial edema [31].

2.6.2 Localized pulmonary blast injury provokes indirect brain injury

It has been reported that the primary effects of the blast to the lungs can result in air emboli. These obstruct the blood vessels and subsequently reduce the blood supply to different organs including the brain [32]. Furthermore, Cernak et al [33] showed that the localized pulmonary or whole body blast exposure can induce damage to cerebral tissue. The hippocampus, the area responsible for cognitive functions such as learning and memory was examined after whole body or focal pulmonary blast impacts [33]. The

histological studies showed morphological changes in hippocampol neurons. In addition, there was evidence of an increase in the lipid peroxidation levels – an important biomarker of different neurological disorders.

2.6.3 Rupture of the tympanic-membrane and Traumatic Brain Injury

The tympanic-membrane (TM) rupture is the most common form of primary blast impact, caused by low pressures between 5 and 15 pounds per square inch [34]. The other air-filled organs such as the lungs and gastrointestinal tract are damaged at pressures ranging between 40 and 75 psi [9, 35]. The sensitivity of the TM to dramatic changes of the ambient pressures near to an explosion and the ensuing TM failure, is considered a protective mechanism that prevents serious damage of the middle and inner ear structures [36]. Case studies reported that the incidence of TM rupture ranging between 9% and 47% in blast-injured patients at the war zone [37, 38]. In a case study by Xydakis et al, a significant association between TM rupture and concussive brain injury was reported [26].

2.7 Pathophysiology of blast-related neurotrauma

Even though the brain is encased different protective layers, it is vulnerable to mechanical trauma such as acceleration, pressure, shearing, and strain injuries. The b-TBI induces primary and secondary neurological impairment. Primary injury, provoked by blast overpressure, takes place at the time of the brain insult, causing various effects such as contusion, laceration, shearing, and axonal injury [39]. Contusion is known as a focal brain lesion that can be detected by neuro-imaging, including computed tomography (CT) or magnetic resonance imaging (MRI), as an extradural or intradural hemorrhage [40].

The axonal injury promotes a cascade of biochemical reactions leading to secondary injuries, where the damage moves from the affected neurons to the spared neurons. Therefore, the primary and secondary injuries both contribute in the diffuse axonal injury (DAI). Other diffuse brain injuries include cerebral edema and cerebral ischemia [11, 41]. The former, frequently occurs after TBI and can be classified into 1) vasogenic brain edema, where the endothelial cell layer of the brain vessels is broken down, and 2) cytotoxic brain edema. Brain edema is characterized by intracellular water accumulation as a consequence of increased cell membrane permeability for ions and cellular re-absorption of osmotically active solutes [42]. Edema produces increased intracranial pressure (ICP), in turn inducing secondary brain ischemia [43]. Furthermore, the cerebral ischemia is considered as the initiator of various biochemical perturbations including energy failure, excitotoxicity, oxidative injury and inflammatory tissue responses following the primary and secondary brain insults [44]. The inflammatory events characterized by the release of cellular mediators such as proinflammatory cytokines, prostaglandins and complement, in turn facilitate the immune cells, including microglia, neutophils and T-lymphocytes to infiltrate the damaged tissue. These pathophysiological procedures are pivotal in both secondary injury and the recovery mechanisms [45].

2.7.1 Neuronal and glial cells response following neurotrauma

In TBI, regardless of the cause of injury, the wound healing responses of brain tissue are governed by special cell types, which are unique to the Central Nervous System (CNS) [46]. The neurons, which consist of a cell body, dendrites and an axon, are the functional unit of brain tissue [47, 48]. In addition, more than half of the total CNS

volume is occupied by three types of glial cells: oligodendrocytes, astrocytes, and microglia. Each glial cell type performs functions that are integral to the health of neurons in the CNS [49]. For instants, astrocytes, the most abundant glial cell type, create a glial network that supports neurons both physically and biochemically. Important functions performed by astrocytes include the release and uptake of the neurotransmitter glutamate from the extracellular space via glutamate transporters that are expressed on the astrocyte cell membranes [50]. Glutamate uptake is vital to prevent influx of sodium (Na+) and calcium (Ca2+) ions into the neurons [51]. In brain injury or disease, the pathological accumulation of glutamate occurs as a consequence of astrocyte damage. In turn, the glutamate activates the N methyl-D-aspartate receptors (NMDAR) that open the ion channels to promote the influx of Na+ and Ca2+ to the intracellular space. This results in prolonged depolarization, excitotoxicity and ATP depletion [8]. Additionally, the increase in the glutamate/calcium induces programmed cell death, either by stimulating the transcription factors for pro-apoptotic genes or by down-regulating the transcription factors for anti-apoptotic genes [52]. Furthermore, the cell apoptosis event can be enhanced by the mitochondria of damaged cells, which in turn release cytochrome c that activates the caspases, a Cysteine protease family responsible for cell apoptosis [53]. Therefore, astrocytes have a direct and indirect crucial role in protecting neurons from excitotoxicity (Figure 2.2). The oligodendrocytes are abundantly distributed in both gray and white matter of the CNS and are responsible for myelin sheath formation as well as influencing important pathophysiological changes ensue after neurotrauma [54]. The third type of glial cell is the microglial cell and this cell function as the resident

macrophage of the brain and spinal cord. Microglia are critical to CNS protection and function as the brain's immune cells by responding to different stimulations such as ischemic, metabolic, or mechanical injuries.

The reactions of glial cells in response to various brain injuries, including b-TBI, have been addressed in different tissue culture and animal-related studies [55-61]. For instance, it is now clear that the process of astrocyte activation starts shortly after a brain insult. This is characterized by hypertrophy of the astrocyte nuclei, cell bodies and processes (astrogliosis). There is an increase in the expression of astrocyte markers, especially glial fibrillary acidic protein (GFAP) – a major protein of the intermediate filaments that is linked with the glial scar [56]. The glial scar is formed by a dense network of reactive astrocytes and other cells that produce specialized extracellular matrix-containing axon growth inhibitors that impair axon regeneration [62]. Conversely, these pathophysiological cell reactions not only lead to damaging consequences, but also support the healing process. The positive side of this reaction is to localize the tissue injury and restore cellular homeostasis [63]. Various studies illustrate the effects of reactive gliosis and the role of gliosis in the neuronal cell death following mechanical trauma [64]. Using an *in vitro* model, Mukhin et al examined the responses of neuronal and glial cells following exposure to mechanical injury [57]. This model used a special punch device that consisted of blades that made parallel cuts in each well of a 96-well microplate. Secondary cell injury was examined in mixed neuronal-glial and glial cell cultures with Ethidium homodimer-1 (EthD-1) and lactate dehydrogenase (LDH) assays. The results showed that by extending the incubation period after trauma, the cell injury

responses were different when comparing the cell culture systems. The neuronal-glial cell cultures reveled a spreading type of cell damage away from the initial site of the trauma, while, the cell injury in glial cell cultures remain localized to the cells adjacent to the site of trauma. This indicates that neuronal survival is dependent on the integrity of the glial cells, which protect the neurons from different biochemical reactions and the ensuing cell death [65]. The role of the NMDA receptor was also investigated in light of its function in synaptic plasticity and neuronal development [57]. The results showed a remarkable decrease in cell injury by adding the antisense oligodeoxynucleotide (MK-801), a non-competitive antagonist of NMDAR. This antagonist prevented calcium ion influx and the subsequent cell injury that occurred secondary to the intracellular accumulation of calcium ions. In addition, for the observation that a mechanical brain insult is usually accompanied by ischemic/metabolic injury [66]; Allen et al conducted both type of injuries in a cell culture study. The effects of inhibiting the action of NMDAR and caspase-3 were examined after inducing both mechanical and metabolic insults [67]. The mechanical trauma was performed using the same punch device used by Mukhins et al, while the metabolic impairment was conducted by inducing hypoglycemia. The combined inhibition of NMDAR and caspase-3 in cell cultures, exposed to both mechanical injury and metabolic impairment resulted in a significant reduction of the neuronal cell death. Another group, utilizing rodent fetal neurons, studied the effect of mechanical shear injury and/or hypoxic injury on neurons [68]. In this experiment, six-well plates with a flexible silastic membrane culture surface were used to apply a range of stretch injury using a Controller Cell Injury-II system. This system provides a variable

controlled pressure value for duration of 50 ms for each individual well in the culture dish. The pressure induces deformation of the silastic membrane and subsequently to the cell membrane interface with the substrate. The hypoxic injury was performed by replacing the growth medium with media that had been exposed to a gas mixture of 5% CO2 and 95% nitrogen for one hour. Following incubation in the previously mentioned free oxygen-gas mixture, the results demonstrated a significant increase in cell damage after exposure to both injuries compare to cells exposed for each injury alone. Therefore, the prognosis of neuronal cell damage depends on various factors, such as the type of injury and the integrity of the glial cells.

2.7.2 Diffuse axonal injury in brain trauma

DAI is the most serious type of diffuse brain injury, as the damage spreads to involve many brain regions resulting in a range of neurological manifestations. Other types of the diffuse brain injury include hypoxic brain damage and brain edema, which in turn promote DAI [69]. The DAI is a pathological sign that can be present with any degree of the TBI (mild, moderate or severe), resulting in acute and chronic neurological abnormalities [70, 71]. Therefore, TBI-related research focuses on understanding the mechanism as well as the pathophysiological changes that lead to DAI. The DAI represents damage to the white matter, more specifically to those structures that provide the connection within and across the cerebral hemispheres. This damage occurs as a result of mechanical trauma such as strain or the shearing forces generated by acceleration, deceleration or rotation of the brain [72]. In blast, this type of mechanical injury occurs as a consequence of the transmission of the blast wave crossing the

protective layers of the brain (bone, meninges, and cerebrospinal fluid (CSF)). The secondary injuries to the spared axons occur as a result of the biochemical reaction cascades that are induced by the non-neuronal components, such as astrocytes; as well as the injured axons. For example, an elevation in the levels of proinflammatory cytokines and chemokines as well as activation of brain inflammatory cells after a closed TBI has a critical role in axonal damage [45]. The activated parenchymal cells contribute to an increase in endogenous proinflammatory modulators that can promote cellular responses to trauma and contribute to neuronal death [73]. Furthermore, the mechanical injury may result in damaging of the Blood-Brain Barrier (BBB), which has a key role in CNS protection by selecting the molecules or cells that can reach the brain milieu from the blood circulation. This results in the infiltration of systemic inflammatory cells, such as macrophages as well as fibroblasts that promote scar tissue formation and subsequently interfere with axonal regeneration [74]. The histological changes of DAI are characterized by widespread axonal swelling, the formation of axonal bulbs known as retraction balls at the site of the trauma as well as the contralateral site of trauma [75]. As a result of the histological analyses, DAI was graded into three levels based on the distribution of axonal damage in different brain regions as well as the association of other abnormalities [76]. In grade-I DAI, the signs of axonal injury are determined in the corpus callosum, white matter of cerebral hemispheres, brain stem, and rarely in the cerebellum. The grade-II DAI is represented with a similar distribution as grade-I plus petechial hemorrhage in the corpus callosum. The features of grade-III DAI include the grade-I and II findings as well as petechial hemorrhage in the rostral brain stem [77].

Therefore, the severity of DAI is dependent on the distribution of injury in the white matter and can be correlated to the post-traumatic consciousness level [72]. In concussion syndromes, which are considered the least severe of white matter injury, patients usually complain of some neurological deficits with no loss of consciousness. The most severe DAI state presents with post-traumatic coma including signs of a developing vegetative state. This occurs when the cortex is severely damaged, the brain stem being spared and with the cardio-respiratory function preserved [69]. Clinical diagnosis of DAI is relatively difficult, as axonal damage may develop with no signs of external injuries or history of a loss of consciousness [78]. Brain imaging procedures especially CT and MRI are valuable investigation techniques when the detection of intra or extra cranial hematomas and concussion are the major apprehension [79, 80]. Some TBI studies have postulated that neurological damage with no hemorrhages at the microscopic level (such as DAI) is barely detected by CT or MRI. Furthermore, MRI is not ideal for routine emergency imaging of b-TBI patients due to the long processing times and availability [79]. In contrary, a recent clinical study revealed that by using an advanced technique of MRI, known as diffusion tensor imaging (DTI), traumatic axonal injury can be detected in veterans previously diagnosed with m-TBI [81]. Other techniques such as Positron Emission Tomography (PET) and Single Photon Emission Computed Tomography (SPECT) techniques can provide valuable data regarding the cognitive abnormalities that may be associated with DAI. In contrary, these techniques are very expensive and they require a long time to prepare patients [82]. For that reason, an investigative tool is required to scan cases with potential TBI.

2.7.3 The role of reactive free radicals and oxidative stress in TBI

Reactive oxygen species (ROS), such as the superoxide anion, hydrogen peroxide, and hydroxyl radical, are free radicals that can react readily with other biological molecules due to the presence of unpaired electrons in their outer orbits. ROS are a physiological byproduct of cellular respiration and normal metabolism. Under physiological conditions there is a balance between the free radical production and removal; therefore, the destructive effects of these molecules are prevented. In fact the high rate of oxygen demand and over production of free radicals by the brain make it the most vulnerable organ to oxidative stress [80]. The cells are able to inactivate these harmful hyperactive small molecules by efficient antioxidant compounds. These include antioxidant enzymes, such as superoxide dismutases, catalases, peroxidases, and low molecular weight antioxidants (LMWAs), including glutathione, ascorbic acid, carotenoids, and lipoic acid [83]. In certain pathological conditions such as TBI, there is an imbalance between the production of the free radicals and the body's ability to remove them. This leads to a phenomenon called oxidative stress, in which the elevation of free radical level promotes cellular destruction [84]. This occurs when the free radicals react with DNA, RNA, lipids, proteins, and thus interfere with the activation of certain enzymes within cells. Astrocytes play a pivotal role in eliminating ROS by releasing glutathione, the main antioxidant in the brain [44]. In traumatic brain injury, the production of ROS with depletion of antioxidant enzymes occurs leading to various pathological reactions such as elevation of the lipid peroxidation and mitochondrial dysfunction [85]. The perturbation of mitochondrial function as a consequence of

glutamate accumulation in the extracellular compartment stimulates the production of different enzymes that are responsible for creating more free radicals. Furthermore, the damaged mitochondria lead to leakage of the superoxide, the most common free radical in the body [86].

2.8 Clinical aspects of blast-induced traumatic brain injuries:

There is a wide spectrum of injuries induced by the detonations of explosive devices that can affect several organs through penetrating and/or non-penetrating trauma. Victims who are diagnosed with moderate or severe b-TBI usually suffer from a range of chronic symptoms and signs, including cognitive dysfunction, weakness or paralysis, cranial neuropathy, impaired speech and swallowing, lack of coordination, visual and hearing abnormalities [87]. While, patients with blast-related m-TBI may complain from the same symptoms as the moderate and severe cases, these patients may report other serious psychological symptoms including depression, anxiety, irritability, attention deficit and relationship difficulties [5]. In fact, case studies that involved veterans with a history of blast exposure showed that developing PTSD is more frequent with blast-related m-TBI than moderate or severe brain injuries [88]. The battlefield PTSD is a psychological outcome after exposure to traumatic events which threatened or caused great physical harm. Furthermore, many battlefield PTSD symptoms, such as depression, anxiety and memory deficit, overlap with symptoms of m-TBI. Hoge et al performed a case study on returning soldiers from the battlefield [89]. The study included a clinical examination as well as questionnaires for soldiers with a history of m-TBI and soldiers with other injuries. The results of this study indicated that victims with a history of blast-

related m-TBI are more susceptible to suffer from physical and mental health problems than others with different injuries. It showed that about 44% of soldiers with a history of loss of consciousness demonstrated signs of developing PTSD. Therefore, blast-related m-TBI is a critical risk factor for PTSD and other psychiatric disorders such as depression that requires early diagnosis and treatment to prevent disease deterioration and increasing health care and rehabilitation demands [90]. In order to address the socioeconomic problems as well as finding the proper health care for PTSD victims, a range of clinical studies by Richardson et al were performed to analyze veterans who have manifestations of battlefield PTSD [91]. One of these studies examined the health-related quality of life (HRQOL) in 125 Canadian veterans who were referred to Veterans Affairs Canada by their medical providers or pension officer [92]. The HRQOL analysis is frequently used to measure the effects of chronic disease and how this disease can interfere with the patient's day to day life. This study was performed using several scales including the Clinician-Administered PTSD Scale (CAPS), Hamilton Depression Scale (HDRS), Short-Form-36 Health Survey (FS-36), as well as an evaluation of the participants' socio-demographic characteristics. This study as well as another clinical study by Classen et al [93] demonstrated that veterans who had diagnoses of m-TBI and PTSD presented physical, cognitive, or personality changes that affect their work and daily life. The mechanisms under which the blast-related m-TBI and battlefield PTSD still remain unclear, however most studies suggest that blast wave plays a crucial role in developing such disorders [94].

2.9 Conclusions

The central nervous system is a vulnerable target for blast injury, triggering complex pathophysiological events that are responsible for both secondary brain damage and the ability to recover from damage. A range of fundamental information has been obtained through experimental and clinical studies of b-TBI. Nevertheless, there is a considerable lack of information regarding the early diagnosis of blast-induced m-TBI and the prediction of its biological consequences. It is important to establish additional experimental models that simulate blast overpressure- induced TBI in order to address the hallmarks of the early stages of brain injury after blast exposure. These models will be important to understand the cellular and molecular biology of the CNS milieu in response to blast overpressure to effectively improve the prognosis of blast-induced m-TBI.

2.10 References

1. Cassidy, J.D., et al., *Incidence, risk factors and prevention of mild traumatic brain injury: Results of the WHO Collaborating Centre Task Force on Mild Traumatic Brain Injury.* Journal of Rehabilitation Medicine, 2004. **36**: p. 28-60.
2. Champion, H.R., J.B. Holcomb, and L.A. Young, *Injuries From Explosions: Physics, Biophysics, Pathology, and Required Research Focus.* Journal of Trauma-Injury Infection and Critical Care, 2009. **66**(5): p. 1468-1477.
3. Salmon, T.W., *The care and treatment of mental diseases and war neuroses ("Shell Shock") in the British Army* Ment Hyg, 1917. **1**: p. 509-547.
4. Hill, J.F., *Blast Injury with Particular Reference to Recent Terrorist Bombing Incidents.* Annals of the Royal College of Surgeons of England, 1979. **61**(1): p. 4-11.
5. DePalma, R.G., et al., *Current concepts: Blast injuries.* New England Journal of Medicine, 2005. **352**(13): p. 1335-1342.
6. Cernak, I., *Animal Models of Head Trauma.* Neuro RX, 2005. **2**(3): p. 410-422.
7. David F. Moore, A.J., Michelle Nyein, Ludovic Noels, Michael S. Jaffe, Paul A. Radovitzky, *Computational biology-Modeling of primary blast effects on the central nervous system.* J NeuroImage, 2009.
8. *Gulf War and Health: Long-Term Consequences of Traumatic Brain Injury* 2008. **7**: p. 1-397.
9. Finkel, M.F., *The neurological consequences of explosives.* Journal of the Neurological Sciences, 2006. **249**(1): p. 63-67.
10. Mayorga, M.A., *The pathology of primary blast overpressure injury.* Toxicology, 1997. **121**(1): p. 17-28.

11. Okie, S., *Traumatic brain injury in the war zone.* New England Journal of Medicine, 2005. **352**(20): p. 2043-2047.

12. Crabtree, J., *Terrorist homicide bombings: A primer for preparation.* Journal of Burn Care & Research, 2006. **27**(5): p. 576-588.

13. Elsayed, N.M., *Toxicology of blast over-pressure.* Toxicology, 1997. **121**(1): p. 1-15.

14. Arciniegas, D.B. and T.W. McAllister, *Neurobehavioral Management of Traumatic Brain Injury in the Critical Care Setting.* Critical Care Clinics, 2008. **24**(4): p. 737-+.

15. Ruff, R.L., S.S. Ruff, and X.F. Wang, *Headaches among Operation Iraqi Freedom/Operation Enduring Freedom veterans with mild traumatic brain injury associated with exposures to explosions.* Journal of Rehabilitation Research and Development, 2008. **45**(7): p. 941-952.

16. Park, E., J.D. Bell, and A.J. Baker, *Traumatic brain injury: Can the consequences be stopped?* Canadian Medical Association Journal, 2008. **178**(9): p. 1163-1170.

17. Goh, S.H., *Bomb blast mass casualty incidents: initial triage and management of injuries.* Singapore Medical Journal, 2009. **50**(1): p. 101-106.

18. Horrocks C. , B.S., *Blast injury.* current Anethesia & critical care, 2000. **11**: p. 7.

19. DeWitt, D.S. and D.S. Prough, *Blast-Induced Brain Injury and Posttraumatic Hypotension and Hypoxemia.* Journal of Neurotrauma, 2009. **26**(6): p. 877-887.

20. Clemedson, C.-J., *Blast injury.* Physiol Rev, 1956. **36**: p. 336.

21. Suneson, A., H.A. Hansson, and T. Seeman, *Peripheral High-Energy Missile Hits Cause Pressure Changes and Damage to the Nervous-System - Experimental Studies on Pigs.* Journal of Trauma-Injury Infection and Critical Care, 1987. **27**(7): p. 782-789.

22. Suneson A, H.H., Seeman T, *Pressure wave injuries to the nervous system caused by high-energy missile extremity impact: Part II. Distant effects on the central nervous*

system--a light and electron microscopic study on pigs. J Trauma, 1990. **30**(3): p. 295-306.

23. Suneson A, H.H., Seeman T, *Pressure wave injuries to the nervous system caused by high-energy missile extremity impact: Part I. Local and distant effects on the peripheral nervous system--a light and electron microscopic study on pigs.* J Trauma, 1990. **30**(3): p. 281-294.
24. Cernak, I., et al., *Involvement of the central nervous system in the general response to pulmonary blast injury.* Journal of Trauma-Injury Infection and Critical Care, 1996. **40**(3): p. S100-S104.
25. Courtney, A.C. and M.W. Courtney, *A thoracic mechanism of mild traumatic brain injury due to blast pressure waves.* Medical Hypotheses, 2009. **72**(1): p. 76-83.
26. Xydakis, M.S., et al., *Tympanic-membrane perforation as a marker of concussive brain injury in Iraq.* New England Journal of Medicine, 2007. **357**(8): p. 830-831.
27. Bhattacharjee, Y., *Neuroscience - Shell shock revisited: Solving the puzzle of blast trauma.* Science, 2008. **319**(5862): p. 406-408.
28. Livingston, W., *"Delayed Recovery" in Peripheral Nerve Lesions Caused by High Velocity Projectile Wounding.* J Neurosurg, 1945. **2**: p. 170.
29. HARVEY, E.N., *An experimental study of shock waves resulting from the impact of high velocity missiles on animal tissues.* J. Exp. Med, 1946. **85**: p. 321.
30. Suneson, A., et al., *Physiological changes in pigs exposed to a blast wave from a detonating high-explosive charge.* Military Medicine, 2000. **165**(2): p. 119-126.
31. Ooigawa, H., et al., *The Fate of Nissl-Stained Dark Neurons Following Traumatic Brain Injury in Rats: Difference Between Neocortex and Hippocampus Regarding Survival Rate.* Acta Neuropathologica, 2006. **112**(4): p. 471-481.

32. Courtney, A. and M. Courtney, *Links between traumatic brain injury and ballistic pressure waves originating in the thoracic cavity and extremities.* Brain Injury, 2007. **21**(7): p. 657-662.

33. Cernak, I., et al., *Ultrastructural and functional characteristics of blast injury-induced neurotrauma.* Journal of Trauma-Injury Infection and Critical Care, 2001. **50**(4): p. 695-706.

34. Danielidis, V., et al., *Short-term pathophysiologic changes and histopathologic findings of the auditory pathway after closed head injury, using a rabbit model.* Audiology and Neuro-Otology, 2007. **12**(3): p. 145-154.

35. Wightman, J.M. and S.L. Gladish, *Explosions and blast injuries.* Annals of Emergency Medicine, 2001. **37**(6): p. 664-678.

36. Jensen, J.H. and P. Bonding, *Experimental Pressure-Induced Rupture of the Tympanic Membrane in Man.* Acta Oto-Laryngologica, 1993. **113**(1): p. 62-67.

37. Ritenour, A.E. and T.W. Baskin, *Primary blast injury: Update on diagnosis and treatment.* Critical Care Medicine, 2008. **36**(7): p. S311-S317.

38. Ritenour, A.E., et al., *Tympanic membrane perforation and hearing loss from blast overpressure in operation enduring freedom and operation Iraqi freedom wounded.* Journal of Trauma-Injury Infection and Critical Care, 2008. **64**(2): p. S174-S178.

39. Grujicic, M., et al., *Blast-Wave Impact-Mitigation Capability of Polyurea When Used as Helmet Suspension-Pad Material.* Materials & Design, 2010. **31**(9): p. 4050-4065.

40. Foley, K., R.E. Kast, and E.L. Altschulerc, *Ritonavir and disulfiram have potential to inhibit caspase-1 mediated inflammation and reduce neurological sequelae after minor blast exposure.* Medical Hypotheses, 2009. **72**(2): p. 150-152.

41. Unterberg, A.W., et al., *Edema and brain trauma.* Neuroscience, 2004. **129**(4): p. 1021-1029.

42. Tatsuro Kawamata, T.M., Shoshi Sato, Yoichi Katayama,, *Tissue hyperosmolality brain edema in cerebral contusion.* Neurosurgical Focus 2007. **22**(5): p. 1-7.

43. Werner, C. and K. Engelhard, *Pathophysiology of traumatic brain injury.* British Journal of Anaesthesia, 2007. **99**(1): p. 4-9.

44. Xu, L.J., R.M. Sapolsky, and R.G. Giffard, *Differential sensitivity of murine astrocytes and neurons from different brain regions to injury.* Experimental Neurology, 2001. **169**(2): p. 416-424.

45. Schmidt, O.I., et al., *Closed head injury - an inflammatory disease?* Brain Research Reviews, 2005. **48**(2): p. 388-399.

46. Lazarov-Spiegler, O., et al., *Restricted inflammatory reaction in the CNS: a key impediment to axonal regeneration?* Molecular Medicine Today, 1998. **4**(8): p. 337-342.

47. Rolls, A., R. Shechter, and M. Schwartz, *Neuron - Glia interactions- opinion the bright side of the glial scar in CNS repair.* Nature Reviews Neuroscience, 2009. **10**(3): p. 235-U91.

48. William D. Snider, F.-Q.Z., Jian Zhong, and Annette Markus, *Signaling the Pathway to Regeneration.* Neuron Glia Biology, 2002. **35**: p. 13-16.

49. Qian, X.M., et al., *Timing of CNS cell generation: A programmed sequence of neuron and glial cell production from isolated murine cortical stem cells.* Neuron, 2000. **28**(1): p. 69-80.

50. Yi, J.H. and A.S. Hazell, *Excitotoxic mechanisms and the role of astrocytic glutamate transporters in traumatic brain injury.* Neurochemistry International, 2006. **48**(5): p. 394-403.

51. Swanson, R.A., W. Ying, and T.M. Kauppinen, *Astrocyte influences on ischemic neuronal death.* Current Molecular Medicine, 2004. **4**(2): p. 193-205.

52. Smaili, S.S., et al., *Mitochondria, calcium and pro-apoptotic proteins as mediators in cell death signaling.* Brazilian Journal of Medical and Biological Research, 2003. **36**(2): p. 183-190.

53. Daniel J. Payette, J.X., Najeeb Shirwany and Qing Guo, *Exacerbation of Apoptosis of Cortical Neurons Following Traumatic Brain Injury in Par-4 Transgenic Mice.* Int J Clin Exp Pathol, 2008. **1**: p. 44-56.

54. Dewar, D., S.M. Underhill, and T.P. Goldberg, *Oligodendrocytes and ischemic brain injury.* Journal of Cerebral Blood Flow and Metabolism, 2003. **23**(3): p. 263-274.

55. Norton, W.T., et al., *Quantitative Aspects of Reactive Gliosis - a Review.* Neurochemical Research, 1992. **17**(9): p. 877-885.

56. McMillian, M.K., et al., *Brain Injury in a Dish - a Model for Reactive Gliosis.* Trends in Neurosciences, 1994. **17**(4): p. 138-142.

57. Mukhin, A.G., et al., *Mechanical injury to neuronal/glial cultures in microplates: Role of NMDA receptors and pH in secondary neuronal cell death.* Journal of Neuroscience Research, 1998. **51**(6): p. 748-758.

58. Raghupathi, R., *Cell death mechanisms following traumatic brain.* Brain Pathology, 2004. **14**(2): p. 215-222.

59. Cernak, I., et al., *Role of the cell cycle in the pathobiology of central nervous system trauma.* Cell Cycle, 2005. **4**(9): p. 1286-1293.

60. Mrak, R.E. and W.S.T. Griffin, *Glia and their cytokines in progression of neurodegeneration.* Neurobiology of Aging, 2005. **26**(3): p. 349-354.

61. Yiu, G. and Z.G. He, *Glial inhibition of CNS axon regeneration.* Nature Reviews Neuroscience, 2006. **7**(8): p. 617-627.

62. Sandvig, A., et al., *Myelin-, reactive glia-, and scar-derived CNS axon growth inhibitors: Expression, receptor signaling, and correlation with axon regeneration.* Glia, 2004. **46**(3): p. 225-251.

63. Hampton, D.W., et al., *The responses of oligodendrocyte precursor cells, astrocytes and microglia to a cortical stab injury, in the brain.* Neuroscience, 2004. **127**(4): p. 813-820.

64. Silver, J. and J.H. Miller, *Regeneration beyond the glial scar.* Nature Reviews Neuroscience, 2004. **5**(2): p. 146-156.

65. Zhao, X.R., et al., *Early loss of astrocytes after experimental traumatic brain injury.* Glia, 2003. **44**(2): p. 140-152.

66. Siegel, J.H., *The Effect of Associated Injuries, Blood Loss, and Oxygen Debletion on Death and Disability in Blunt Traumic Brain Injury- the Need for Early Physiological Predictors of Severity.* Journal of Neurotrauma, 1995. **12**(4): p. 579-590.

67. Allen, J.W., S.M. Knoblach, and A.I. Faden, *Combined mechanical trauma and metabolic impairment in vitro induces NMDA receptor-dependent neuronal cell death and caspase-3-dependent apoptosis.* Faseb Journal, 1999. **13**(13): p. 1875-1882.

68. Glass, T.F., B. Reeves, and F.R. Sharp, *Modeling both the mechanical and hypoxic features of traumatic brain injury in vitro in rats.* Neuroscience Letters, 2002. **328**(2): p. 133-136.

69. Graham, D.I., et al., *Recent advances in neurotrauma.* Journal of Neuropathology and Experimental Neurology, 2000. **59**(8): p. 641-651.

70. Taber, K.H., D.L. Warden, and R.A. Hurley, *Blast-related traumatic brain injury: What is known?* Journal of Neuropsychiatry and Clinical Neurosciences, 2006. **18**(2): p. 141-145.

71. Povlishock, J.T., D.E. Erb, and J. Astruc, *Axonal Response to Traumatic Brain Injury - Reactive Axonal Change, Deafferentation, and Neuroplasticity.* Journal of Neurotrauma, 1992. **9**: p. S189-S200.

72. Blumbergs, P.C., N.R. Jones, and J.B. North, *Diffuse Axonal Injury in Head Trauma.* Journal of Neurology Neurosurgery and Psychiatry, 1989. **52**(7): p. 838-841.

73. Fellin, T., *Communication between neurons and astrocytes: relevance to the modulation of synaptic and network activity.* Journal of Neurochemistry, 2009. **108**(3): p. 533-544.

74. Wanner, I.B., et al., *A New In Vitro Model of the Glial Scar Inhibits Axon Growth.* Glia, 2008. **56**(15): p. 1691-1709.

75. Adelson, P.D., et al., *Histopathologic response of the immature rat to diffuse traumatic brain injury.* Journal of Neurotrauma, 2001. **18**(10): p. 967-976.

76. Adams, J.H., et al., *Diffuse Axonal Injury in Head-Injury - Definition, Diagnosis and Grading.* Histopathology, 1989. **15**(1): p. 49-59.

77. Blumbergs, P.C., *Changing concepts of diffuse axonal injury.* Journal of Clinical Neuroscience, 1998. **5**(2): p. 123-124.

78. Niess, C., et al., *Incidence of axonal injury in human brain tissue.* Acta Neuropathologica, 2002. **104**(1): p. 79-84.

79. Shen, Y.M., et al., *In vivo measurement of tissue damage, oxygen saturation changes and blood flow changes after experimental traumatic brain injury in rats using susceptibility weighted imaging.* Magnetic Resonance Imaging, 2007. **25**(2): p. 219-227.

80. Ansari, M.A., K.N. Roberts, and S.W. Scheff, *Oxidative stress and modification of synaptic proteins in hippocampus after traumatic brain injury.* Free Radical Biology and Medicine, 2008. **45**(4): p. 443-452.

81. Mac Donald, C.L., et al., *Detection of blast-related traumatic brain injury in u.s. military personnel.* New England Journal of Medicine, 2011. **364**(22): p. 2091-2100.

82. Molteni, E., et al., *Combined behavioral and EEG power analysis in DAI improve accuracy in the assessment of sustained attention deficit.* Annals of Biomedical Engineering, 2008. **36**(7): p. 1216-1227.

83. Liu, R.L., et al., *Iron toxicity in organotypic cultures of hippocampal slices: role of reactive oxygen species.* Journal of Neurochemistry, 2003. **85**(2): p. 492-502.

84. Petronilho, F., et al., *Oxidative stress in brain according to traumatic brain injury intensity.* Journal of Surgical Research, 2010. **164**(2): p. 316-320.

85. Opii, W.O., et al., *Proteomic identification of oxidized mitochondrial proteins following experimental traumatic brain injury.* Journal of Neurotrauma, 2007. **24**(5): p. 772-789.

86. Robertson, C.L., et al., *Mitochondrial mechanisms of cell death and neuroprotection in pediatric ischemic and traumatic brain injury.* Experimental Neurology, 2009. **218**(2): p. 371-380.

87. Ling, G., et al., *Explosive Blast Neurotrauma.* Journal of Neurotrauma, 2009. **26**(6): p. 815-825.

88. Thompson, J.M., K.C. Scott, and L. Dubinsky, *Battlefield brain Unexplained symptoms and blast-related mild traumatic brain injury.* Canadian Family Physician, 2008. **54**(11): p. 1549-1551.

89. Hoge, E.A., et al., *Broad Spectrum of Cytokine Abnormalities in Panic Disorder and Posttraumatic Stress Disorder.* Depression and Anxiety, 2009. **26**(5): p. 447-455.

90. Peterson, A.L., M.T. Baker, and K.R. McCarthy, *Combat stress casualties in Iraq. Part 2: Psychiatric screening prior to aeromedical evacuation.* Perspectives in Psychiatric Care, 2008. **44**(3): p. 159-168.

91. Richardson, J.D., J. Pekevski, and J.D. Elhai, *Post-traumatic stress disorder and health problems among medically ill Canadian peacekeeping veterans.* Australian and New Zealand Journal of Psychiatry, 2009. **43**(4): p. 366-372.

92. Richardson, J.D., et al., *Posttraumatic stress disorder and health-related quality of life among a sample of treatment- and pension-seeking deployed Canadian Forces peacekeeping veterans.* Canadian Journal of Psychiatry-Revue Canadienne De Psychiatrie, 2008. **53**(9): p. 594-600.

93. Classen, S., et al., *Simulated driving performance of combat veterans with mild tramatic brain injury and posttraumatic stress disorder: A pilot study.* American Journal of Occupational Therapy, 2011. **65**(4): p. 419-427.

94. Chen, Y. and W. Huang, *Non-impact, blast-induced mild TBI and PTSD: Concepts and caveats.* Brain Injury, 2011. **25**(7-8): p. 641-650.

2.11 List of Table and Figures

Table 2.1: Different classifications of Blast-induced Traumatic Brain Injury

Mechanism of injury	**1) Primary blast injury** • Direct effects of the pressure wave on the body. **2) Secondary blast injury** • Results from objects (e.g. flying debris) that cause blunt or penetrating trauma. **3) Tertiary blast injury** • Consequences of the victim's body or head colliding with surrounding objects or the ground. **4) Quaternary blast injury** Occurs due to exposure to heat, toxic gases, or dust.
Pathological outcomes	**1) Focal** • Hematomas • Contusions **2) Diffuse** • Diffuse axonal injury • Hypoxic-ischemic brain damage •
Biomechanics of injury	**1) Closed** • Static • Dynamic **2) Penetrating or perforating injury** • Flying debris generated by the explosion (the injury depends on shape and mass)

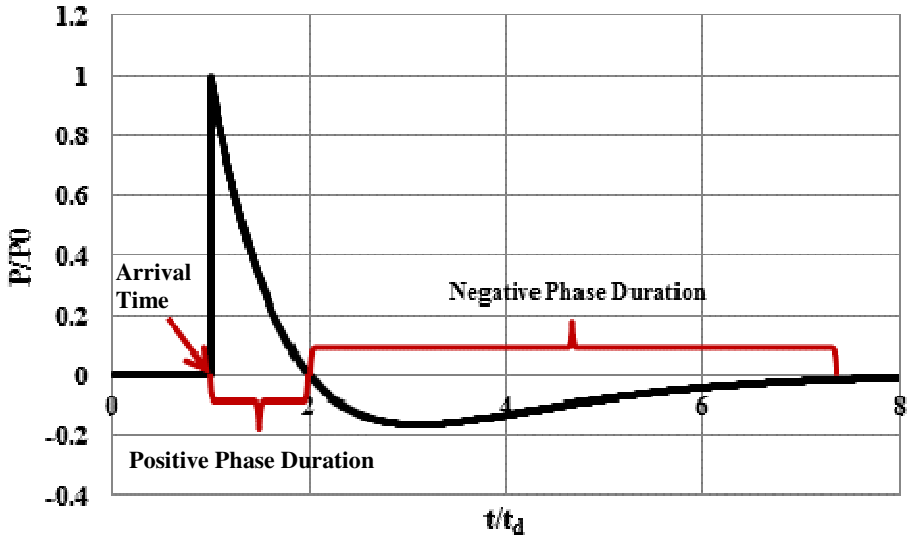

Figure 2.1: The blast wave components in an open-air field

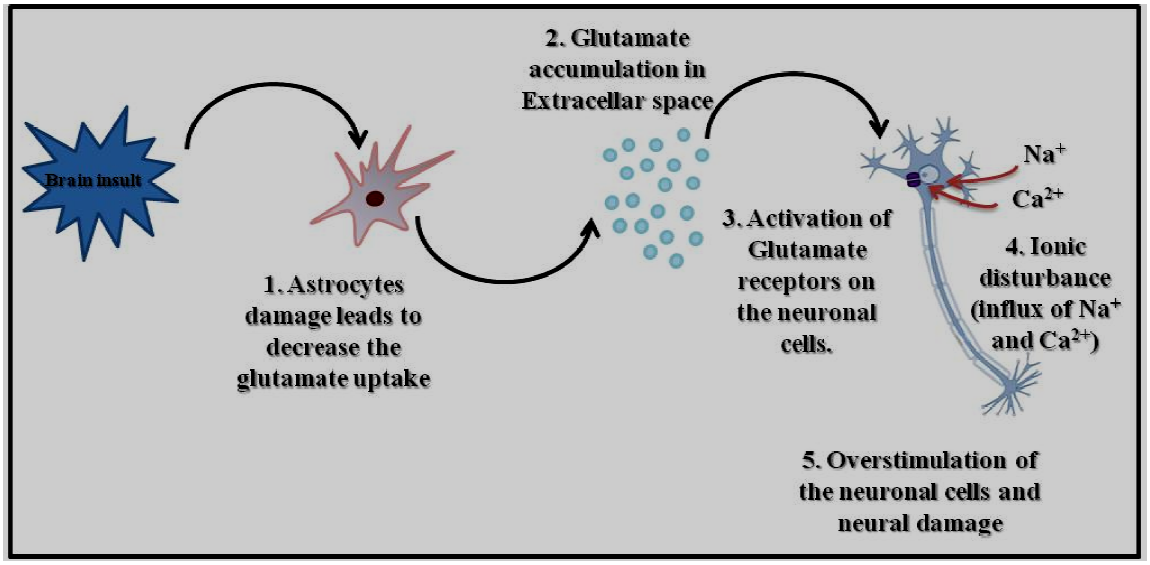

Figure 2.2: Schematic diagram demonstrates the role of astrocytes in neuronal damage

Chapter 3: Compressed Air-Driven Shock Tube System to Simulate Blast-induced Mild Traumatic Injuries

Neveen Awad, Wael W. El-Dakhakhni and Ammar.Gilani

3.1 Abstract

The use of Improvised Explosive Devices (IED) in conflict areas worldwide has created a research need to develop reliable and reproducible blast wave generators to study blast induced injuries. With the mechanisms by which Blast-induced mild Traumatic Brain Injury (BImTBI) develops not being fully understood, there is a need to design reduced-scale (bench-top size) shock tube with characteristics aiming at simulating shock waves parameters consistent with those observed to cause BImTBI.

In the current study, a unique air-driven shock tube capable of producing blast wave profiles simulating those induced by IED producing BImTBI was designed. The finite element model (FE) of the shock tube design was verified experimentally. The experimental study addressed the effects of different parameters on the blast wave development and characterized the shock wave features to be used subsequently in BImTBI research. The blast overpressure and positive phase duration (and thus the blast impulse) are the two characteristics of shock waves that govern BImTBI. Two types of metallic diaphragm (steel and brass) with three different thicknesses were used to perform the blast tests. The steel and brass diaphragms rupture occurred at 204 kPa and 279 kPa, respectively. Monitoring the free field blast and shock pressure wave profiles showed that the amplitude values of the positive overpressure and positive impulse were

found to be significantly affected by the shock tube diaphragm thickness and material type. The results demonstrated that the designed shock tube can generate a wide range of controllable shock wave profiles that can be utilized in various blast-related injury researches.

Keywords: Compressed air-driven shock tube, FEA, Shock wave, Friedlander wave, Mild traumatic brain injury.

3.2 Introduction

Shock tubes have been widely used in various blast-related research studies to simulate explosion shock waves. Laboratory animal tests and physical models have been used in conjunction with shock tubes to identify injury mechanisms and detect injury thresholds [1-3]. A shock wave can be generated by several means including detonating high explosive charges, or using explosive-driven and compressed gas- (e.g. air, Helium, Nitrogen) driven shock tubes [4-6]. More recently, laser-induced stress waves have been used recently in blast injury-related research to address the blast wave effects on small animals [7]. Although utilizing high explosive in blast wave-related studies facilitates attaining higher overpressures, there are many disadvantages associated with this approach related to logistical and safety and security concerns, making them limited to a small number of published studies [8], whereas large-scale compressed air-driven shock tubes are extensively used in blast investigations due to its ability to generate controllable and repeatable shock wave profiles [9, 10], making them ideal for research applications. In this respect, the design parameters of air-driven shock tubes are key to generating the

desired shock wave profiles [11]. A typical free-field blast wave profile takes the form of a Friedlander waveform at a certain distance from the explosion source location [12]. The main characteristics of the blast pressure waveform are the positive-pressure phase decaying to ambient pressure, followed by a negative pressure phase, arrival time, and rise time as shown in Figure (3.1). The arrival time is defined as the time elapsed by a shock wave where pressure experiences an abrupt change from its initial/ambient value to peak value. In addition, the rise time is defined as the time period starting from the shockwave front arrival time and ending when the overpressure reaching its maximum value. From the mechanics point of view, one of the key aspects to study BImTBI, is the development of shock waves that accurately simulate field conditions created by IED [13, 14]. In addition, from the biomedical response aspects, it is widely accepted that the two most critical components of shock wave signatures are the positive peak pressure (PPP) and the positive phase duration (PPD) that are usually related to various hidden brain tissue damage [3, 15], whereas the magnitude of the peak overpressure and positive phase duration (and thus the positive impulse) control the severity of injuries [3, 16-19].

Blast induced injuries can be caused by four different mechanisms including primary, secondary, tertiary, and quaternary injuries [20]. In the case of traumatic brain injury, primary blast injury corresponds to the shock wave pressure loading, while secondary injury corresponds to ballistic/shrapnel penetration. The tertiary injury on the other hand corresponds to accelerations caused by blunt impact, and quaternary injury relates to all other injuries that follow such as chemical or burn injuries [16]. Although these three blast injury mechanisms usually lead to serious injuries and oftentimes to

fatalities, primary blast injuries are thought to cause hidden trauma that can chronically affect the human body [18, 21]. In this regard, a recent study has been completed with a focus of designing a shock tube that have capabilities to generate a reliable shock wave for different blast related research purposes [22].

The aim of the current study is to design and calibrate a laboratory-size shock tube that can generate a shock wave simulating the primary blast loading effects of an IED. Furthermore, the generated waveform should possess characteristics (PPP, PPD and PI) similar to that causing mTBI, which rather than being lethal, can induce instead chronic neurological deficits as reported in previous studies [23-25]. The design parameters of the shock tube were first optimized using Finite Element Analysis (FEA) prior to the experimental validation. The objective of the FEA simulations herein is to pre-evaluate the shock tube design that is capable of generating Friedlander-similar pressure-time profiles within the waveform parameter range that would cause BImTBI. Arbitrary Lagrangian Eulerian (ALE) formulation using multi material approach was used to model the compressed air-driven shock tube wave propagation inside and outside the shock tube. In this regard, the LSDYNA ALE solver has been used extensively on modeling fluid and gas dynamics [26] especially within extreme dynamic loading and shock wave problems[27, 28].

3.3 Design, Modeling and Experimental Validation

3.3.1 Shock Tube Design

The shock tube was designed as two compartments with one compartment being the compression chamber (250 mm in length) that is separated from the other component, the expansion chamber (2,000 mm in length) by a metallic rupture diaphragm with different materials and variable thicknesses. Utilizing an air compressor, the compression chamber is pressurized with air causing the diaphragms to rupture at a pressure level that is dependent on the thickness and the material of the diaphragm separating the two chambers. As specifying the diaphragm characteristics provided an easy tool to control the blast wave characteristics, selecting a diaphragm with specific (calibrated) rupture pressure threshold, was the first objective of the current study.

The layout of the shock tube is shown in Figure 3.2. The horizontally mounted hollow cylinder comprises the compression and expansion chambers with constant cross sections. The first chamber contains compressed air while the second volume is open to the atmosphere (expansion). The chambers are 250 mm and 2,000 mm long respectively, while their outer diameter is 200 mm. The two chambers are typically separated by a metallic diaphragm and are connected using sixteen 19 mm steel bolts. When the diaphragm ruptures suddenly (as plastic deformations exceed its material ultimate limits) the pressurized air is abruptly exposed to the zone of low (atmospheric) pressure in the expansion chamber. This creates a shock wave that propagates into the low-pressure chamber and then into the surrounding atmosphere and a rarefaction, or expansion, wave

that propagates into the high-pressure zone or the compression chamber. Depending on the travel length of the wave in both compression and expansion chambers of the shock tube, the initial pressure in the compression chamber and the volume of both chambers, a specific pressure-time profile (signature) is created. The type and temperature of the pressurized gas can also be altered depending on the desired shock flow properties, but were not evaluated in this study.

3.3.2 Finite Element Simulation

Finite Element Analysis (FEA) was conducted using LS-DYNA [29] to optimize the shock tube design and predict the experimental results by simulating the flow inside and outside of the shock tube. The initial conditions inside the compression and expansion chambers of the shock tube were used to simulate the shock wave in 2-D. The displacements degrees of freedom perpendicular to the shock tube wall elements were kept equal to zero to avoid air leakage through or expansion in the direction of the shock tube wall. This approach would maintain a planar shock front to develop and travel in the longitudinal direction without lateral flow. Using this approach did not only simplify the analyses and significantly reduced the computational time, but also was justifiable as the resulting membrane strains within the shock tube walls would only result in negligible elastic deformation in the hoop direction due to the moving shock wave front based on the pressure values within the focus of the current study. Under such boundary conditions, the shock tube walls can be assumed rigid and the focus of the analysis can

only be on the fluid component, thus accelerating the solution of this computational fluid dynamics (CFD) problem.

In order to be able to study the shock wave characteristics upon exiting the shock tube, a sufficient portion of the air zone surrounding the shock tube had to be modelled with the displacement degrees of freedom also kept equal to zero along the boundary of the air zone to simplify the analysis and minimize the computational time. This approach was favoured over using non-reflecting boundary conditions even though the propagation of the wave beyond the modelled portion of the air would cause the generation of a reflected wave along these boundaries. This is attributed to the fact that using non-reflecting boundary conditions is known to amplify the pressure and impulse if the boundary is close to the wave source [28]. However, the pressure-time profiles will only be studied up to the time at which reflected wave starts to impinge the shock wave and alter its characteristics.

The mesh generated to represent the air was conducted using solid elements with 5 mm in size. The Air was modeled as MAT_NULL with a linear-polynomial equation of state (EOS). The Mach number of the shock front is expected to be slightly above 1.0. Hence, the ideal gas assumption in the EOS was acceptable, as the ratio of specific heats do not change drastically at this Mach number level. The linear-polynomial EOS is of the internal energy yields a pressure value that is given by:

$$P = C_0 + C_1\mu + C_2\mu^2 + C_3\mu^3 + (C_4 + C_5\mu + C_6\mu^2)E \quad (1)$$

In the above equation, the parameters $C_2\mu^2$ and $C_6\mu^2$ are set to zero if$\mu < 0$, where ;

$$\mu = \frac{\rho}{\rho_0} - 1 \quad (2)$$

and $\frac{\rho}{\rho_0}$ is the ratio of the current density to the reference density. The air density was taken as 1.225 kg/m^3 at 15°C for the current study.

For the current analysis, the value of C_0, C_1, C_2, C_3 and C_6 were set to zero and C_4 and C_5 to γ-1, where,

$$\gamma = \frac{C_p}{C_v} = 1.4 \quad (3)$$

3.4 Experimental and Design Validation

3.4.1 Shock Tube Pressure-Time Signature Evaluation

Four Pressure Transducer (PT) transducers (Model type-2115B, Kistler Instrument Corp., Armherst NY 14228) were inserted inside the shock tube. The first pressure transducer was mounted in the compression chamber while the remaining three pressure transducers were mounted at the beginning, middle and end of the expansion chamber. Therefore, the pressure required for rupturing the diaphragms within the compression chamber and the generated wave inside the expansion chamber can be monitored. The four pressure transducers inside the shock tube were installed flush with the inner walls of both the compression and expansion chambers. An air foil board was used as a blast Pressure Transducer Mount (PTM) to hold four PTs (Model type-2115B, Kistler Instrument Corp., Armherst NY 14228) at four different locations (50, 100, 150 and 450 mm) outside the shock tube to measure the resultant free-field peak pressure at the exit of

the expansion chamber. Two identical 500 MHz high-speed data acquisition systems (Tektronix TDS744A) with four channels each were linked and used to record the pressure wave profile. To ensure signal capturing during the shock wave development, one of the linked data acquisition systems was set to act as the main trigger and the other as the auxiliary trigger. Therefore, capturing pressure transducers signals using data acquisition system would provide an effective mean to track the pressure wave inside and outside the shock tube. For safety, the shock tube was controlled using a wireless control panel, which is connected to the shock tube as well as four air solenoid control cables (fill, dump, diaphragm rupture control, and common valves).

3.4.2 Diaphragms Preparation

In the current study, two different types of diaphragms (Branded® Shim, Downers Grove, IL, 60515 USA) were used to study their effect on the wave pressure profiles. Three different steel and brass diaphragm thicknesses (0.127, 0.076, and 0.025 mm) were used in order to obtain a wide range of blast wave profiles. The tensile strength of the steel diaphragms is 552 MPa and 393 MPa for brass diaphragms. Each diaphragm used in the shock tube test was prepared by perforating a total of sixteen holes that corresponding to the blots' location between the compression and expansion chambers using punch set (SP-9 Fractional, Trinity Brand Industries, INC, USA) with a 19 mm size. The high pressure that is required to rupture the diaphragm was generated using an electrical motor-driven compressor that pumps the compressed air into the compression chamber. Depending on the diaphragm thickness and material type, a controlled and repeatable

pressure wave signature can be created. As shown in Figure 3.3, the shock tube is also provided with a mechanically-operated sharp metal striker that can puncture the diaphragm when the air inside the compression chamber reaches the target level.

3.4.3 Statistical Analysis

All experiments were carried out at least in triplicate for each rupture diaphragm type and thickness, so the reliability of the developed shock wave can be evaluated. Furthermore, the experimental results were correlated with the shock tube FEA model. Comparative analyses were performed with SPSS for Windows (version 13.0; SPSS Inc, Chicago, IL, USA) using One-Way ANOVA test to evaluate the variance of positive pressure values among shock tube tests. On the other hand, Independent-Samples-*T* test was used to compare between the experimental and model results. Statistical significance was set at a probability (*P*)-value less than 0.05 [30].

3.5 Results and Discussion

3.5.1 FEA Model of the Shock Tube

The FEA numerical model was developed to simulate the performance of the physical shock tube model, in which pressurizing air into the compression chamber would increase the membrane stresses, and subsequently the strains, in the metallic diaphragm, leading to the diaphragm rupture. Such behaviour was numerically simulated by instantaneously exposing the compressed air to the expansion chamber pressure at time *t=0* ms (Figure 3.4a). At this instant of time, the expansion of the high pressure air causes the formation

of a shock wave that travels towards the low pressure side of the shock tube (the expansion chamber) and a rarefaction wave that propagates back toward the pressure chamber (Figure 3.4b). As the length of the compression chamber is much less than that of the expansion part of the shock tube, the rarefaction wave reaches the other end of the compression chamber and reflects back (Figure 3.4c). Following this, the reflected rarefaction wave travels behind the shock wave front inside the expansion chamber (Figure 3.4d). Once they both reach the exit of the expansion chamber (Figure 3.4e) the shock wave front expands into the open air (under atmospheric pressure) at the shock tube exit (Figure 3.4f).

3.5.2 Experimental Validation of the Shock Tube Performance

Figures (3.5a) and (3.5b) show the pressure waves generated using the steel and brass diaphragms, respectively. The pressure rises inside the compression chamber with increased compressed air flow until the membrane stresses reaches the diaphragm rupture threshold due to significant plastic deformations develop. The pressure inside the compression chamber increases until it reaches its maximum value resulting in creating the first peak in the pressure-time profile. Following this, the pressure in the compression chamber starts to decay to the value of the ambient (atmospheric) pressure level. All three thicknesses of both diaphragm types show secondary peaks of lesser values just before decaying to the ambient pressure. This secondary peak corresponds to the rarefaction wave propagating towards the high-pressure chamber of the shock tube. The average values of the pressure ± standard deviation and the (CV value) at the onset of the steel

diaphragm rupture increase with diaphragm thickness and were 204 ± 5 kPa (CV = 0.02), 110 ± 12 kPa (CV = 0.11), and 30 ± 5 kPa (CV = 0.16) for the thicknesses of 0.127 mm, 0.076 mm and 0.025 mm, respectively. With brass diaphragm of similar thicknesses (Figure 3.5b), diaphragm rupture occurred at higher-pressure values (300 ± 7 kPa with CV = 0.02, 120 ± 20 kPa with CV = 0.2, and 110 ± 20 kPa with CV = 0.18) comparing to the steel ones. On the other hand, the mean blast overpressures measured by PTs on the board (± standard deviation) from the generated shock waves range from 92.4 ± 2 kPa to 5 ± 2 kPa, while, the Coefficient of Variation (CV) values are 0.02 and 0.4, respectively, at 50 mm distance from the shock tube exit using steel diaphragm with three different thicknesses. At the same location, the brass diaphragms with same thicknesses generated blast overpressures that range from 110 ± 2 kPa to 53 ± 9 kPa with a CV equal to 0.02 and 0.17, respectively. These positive peak pressures of the generated shock waves are in the range that was shown to induce BImTBI [13, 31, 32].

In addition, as expected, the resultant wave profiles of each diaphragm type and thickness demonstrated that the values of the maximum peak pressure of the tested diaphragms are directly proportional to the diaphragm thicknesses and inversely proportional to the distance from the shock tube opening.

Figures (3.6a) and (3.6b) are examples of the waveform of steel and brass at 50 mm from the shock tube exit. The plots are good agreement with the generated positive pulse shape of free-field blast wave demonstrating a rapid rise in pressure followed by an almost exponential decay. Table 1 demonstrates a comparison between the parameters of the incident shock wave pressure and free field pressure at 50 mm from shock tube exit

using the 0.127mm steel and brass diaphragms. Depending on the diaphragm type the PPP in the free field is always higher than the incident pressure. On the other hand, because the incident pressures of both materials have a longer PPD, therefore, their resultant PI values are higher than the free field results. Previous studies related to blast injuries tested the effects of peak overpressures on brain damage utilizing a wide range of PPP values that varied from 20 kPa to 10,000 kPa [33, 34]. Moreover, the range of PPD of the incident shock wave varied from 0.3 to 53 ms in blast related studies [35, 36]. Therefore, the current shock tube, by using the 0.127 mm steel or brass, is considered to produce a shock pressure wave that able to induce mTBI, as the previous studies showed that animal models survived, but suffered from neurological manifestations, after exposing to a similar blast overpressure value [37].

Arrival time for the wave front shows a significant dependence on diaphragm thicknesses where the time for the wave front to reach a certain location decreases with the increase in diaphragm thickness. These values ± standard deviation (and CV value) for steel 0.127 mm, 0.076 mm, and 0.025 mm were 5.0 ± 0.15 ms (CV = 0.03), 5.3 ± 0.08 ms (CV = 0.02), and 5.53 ± 0.22 ms (CV = 0.04), respectively. While the arrival time values for the brass with the same thickness were 4.3 ± 0.04 ms (CV = 0.03), 4.6 ± 0.16 ms (CV = 0.03), and 4.59 ± 0.09 ms (CV = 0.02). In addition, the 0.076 mm and 0.025 mm thicknesses brass diaphragms behave similarly with minimal difference in terms of their maximum peak pressure waveform and arrival time values. On the other hand, by comparing waveforms from both diaphragm types it is clear that the wave characteristics are completely dependent on the diaphragm type (Figure 3.6c). As brass is more ductile

than steel [38], brass diaphragm will allow higher air pressure in the compression chamber, as it will plastically deform before rupturing. However, steel diaphragms prematurely fail, which allow relatively less air pressure in the compression chamber. Therefore, the brass diaphragms produced waveforms with higher maximum overpressure comparing to the steel diaphragms, which was observed in all shock tube tests. In addition, as the brass diaphragm requires higher pressure to rupture than the steel therefore, it has a faster wave front compared to that of steel diaphragm (Figure 3.6c).

In addition, pressure Rise Rate (PRR), another important factor that influences the blast wave damage level, was calculated [39]. The PRR values for each pressure wave of steel and brass diaphragms increase with the diaphragm thickness and the brass diaphragm are generally higher than that for the steel. Figures (3.7a) and (3.7b) are examples of the (PRR) for steel and brass, respectively, at 50 mm from the shock tube opening for the three thicknesses. The values of (PRR) of the steel diaphragms are 1.50E+03 (kPa/ms), 1.25E+03 (kPa/ms), and 3.40E+01 (kPa/ms), while for the brass the values are 1.59E+03 (kPa/ms), 9.03E+02 (kPa/ms), and 8.07E+02 (kPa/ms), respectively. This is also attributed to the pressure in the compression chamber before the rupture of diaphragms. As a result, the air pressure in the compression chamber is directly proportional to the maximum positive pressure, the wave arrival time and the pressure rise time.

As explained earlier, the two most critical components of the shock waveform, that are thought to induce a wide range of BImTBI, are the maximum overpressure and the positive phase duration [1, 13, 40]. Subsequently, one of the main goals of the current study was to evaluate the variation of the Positive Peak Pressure (PPP) as well as the

Positive Phase Duration (PPD) and the Positive Impulse (PI) values, for both diaphragm types, inside and outside the shock tube. Figures (3.8a) and (3.8b) show the maximum pressure of 0.127 mm steel and brass diaphragms at four different locations from the shock tube opening, which indicates decay in both positive and negative peak pressures. In addition, Figure (3.9a) displays the average PPP of both diaphragm types at different locations inside and outside the shock tube. The PPP diminishes as the wave moves away from the shock tube exit. Moreover, by evaluating the values of PPD of steel and brass (Figure 9b); it is clear that they generally increase by moving away from the shock tube exit. On the other hand, the PI values of steel and brass (Figure 3.9c) decrease as the shock wave propagates away from the shock tube opening. The PPD and PI values for both steel and brass resultant shock waves are summarized in Tables (3.2) and (3.3) for the four locations outside the shock tube exit. By comparing these parameters produced by 0.127 mm steel and brass diaphragms, it appears that the PPD of the former is relatively longer than the latter. In contrary, the brass diaphragm induces higher positive impulse in comparing with the steel type. Table (3.4) shows the statistical analyses using One-Way ANOVA test for the positive pressure wave profile. The results demonstrate that there are no evidence to reject the null hypothesis for the 0.127 mm steel diaphragm at the four locations (50 mm, 100 mm, 150 mm, and 450 mm) from the shock tube exit (P value $>$ 0.05) (Table-3.4). Comparing the positive waveforms of the other steel diaphragm thicknesses (0.076 mm and 0.025 mm) at the four points from the shock tube opening reveal that there are significant variances among the sample means (P value $<$ 0.05). On the other hand, the One-Way ANOVA test for the brass diaphragm

demonstrates that there is no evidence to reject the null hypothesis for the 0.127 mm brass diaphragm at locations 50 mm and 100 mm from the shock tube opening. On the contrary, statistical analysis results for the brass 0.076 mm and 0.025 mm revealed that there are significant variances for both thicknesses at the four distances outside the shock tube exit. This suggests that utilizing these thicknesses results in generating unpredictable shock wave signature.

Based on the above, the current study shows that the designed bench-top shock tube can provide reliable results of blast waves, which have pressure-time profiles similar to that from actual blast tests. This pressure wave profiles can be correlated to that of the Friedlander waveform of free-field blast [41, 42]. This is confirmed by the statistical analysis of shock tube tests using three thicknesses of steel and brass diaphragms, where it is found that the 0.127 mm steel produce the most reliable waveform (Table 3.4). Moreover, the designed shock tube is capable of generating non-lethal pressure levels in the effective range of producing BImTBI [23].

3.5.3 Correlation between Shock Tube FEA model and Experimental Results

The 0.127 mm steel diaphragm results of the three shock tube tests show that there are no significant variances between the values, therefore, the FEA model has been correlated to the experimental study using 0.127 mm steel diaphragm. The initial pressure that have been used in the FE model was alike to the average pressure induced the 0.127 mm steel diaphragm rupturing in the three typical shock tube tests (Figure 3.10). The average values ± standard deviation (and CV value) of the pressure at the onset of the

steel diaphragm rupture is 204 ± 5 kPa (CV = 0.02) and the three tests show very similar results. In addition, the correlation between the shock tube experiments and the FEA model shows that there is no significant difference between the PPP values at the four locations outside the shock tube exit (Table 3.5).

Figures (3.11a, b, c & d) show the pressure wave profiles of both shock tube experiments and FEA model at 50 mm, 100 mm, 150 mm and 450 mm from the shock tube exit. The figures clearly show the close agreement between of the results from physical shock tube tests and the FEA numerical model. In addition, Table (3.6) summaries the 0.127 mm steel diaphragm experimental and model results showing the correlation between the shock tube test parameters and the corresponding ones obtained from the FEA model. This demonstrates the ability of the shock tube design to generate predictable waveforms that can be used in BImTBI researches.

3.6 Conclusions

This paper presents a unique design for compressed air-driven shock tube that can produce reliable pressure wave profiles, which typically represent the Friedlander waveform of free-field blast waves. The validation of the shock tube FE model analysis has been confirmed using experimental study of the subsequently constructed shock tube. The effects of two different factors on the generated shock waves were examined. These factors include: i) diaphragm thickness that separates the compression and expansion chambers; ii) diaphragm material types (steel and brass) that can influence the shock

wave profiles. At least three tests for each diaphragm type and thickness (0.127, 0.076 and 0.025 mm) were conducted in free-field to minimize the reflection effects.

The two diaphragm types with three different thicknesses that have been used with the current compressed air driven shock tube played a crucial role in controlling the wave pressure profile. This is observed as the brass diaphragm is more ductile than the steel diaphragm; therefore, brass requires higher plastic deformations to rupture than the steel. Therefore, each membrane can be utilized in various studies depending on the desired pressure range. This results in producing different waveforms depending on the diaphragm type. Additionally, from the statistical analysis it is found that the steel (0.127mm) diaphragm showed no significant difference (P value > 0.05) in the maximum overpressure and the positive phase duration, the two most critical components of shock wave. Moreover, the brass (0.127 mm) diaphragm provides data with no significant difference at two locations (5 cm and 10 cm) from the shock tube exit., The steel and brass diaphragm with 0.076 mm and 0.025 mm thicknesses showed significant difference among the shock tube test results (P value < 0.05) This variation of the steel and brass diaphragms with small thicknesses may be attributed to the manufacturing process or stress concentration. This verifies that by increasing the diaphragm thicknesses, one may produce a higher reproducible positive peak pressure. Future studies can be performed using thicker steel and brass diaphragms and utilizing the mechanically-operated sharp tipped metal striker provided in the compression chamber of the shock tube. This can puncture the diaphragm when the air inside the compression chamber reaches the

required target level; therefore, a higher maximum peak pressure can be obtained for a wide range of blast-related studies.

The statistical analysis and correlation of pressure wave profiles in both shock tube FE model and experimental study confirmed their agreement. The shock tube design presented in this study is capable of generating reliable non-lethal pressure levels by utilizing the 0.127 mm steel diaphragm that can be used in BImTBI researches. Therefore, the presented validation of shock tube design provides valuable knowledge and a promising research tool, which is essential in a wide range of blast related applications utilizing shock tubes.

3.7 Acknowledgments

The authors gratefully acknowledge Kent Wheeler and Paul Heerema at the Applied Dynamics Lab for their help and useful discussions

3.8 References

1. Yang, Z.H., et al., *Biological effects of weak blast waves and safety limits for internal organ injury in the human body.* Journal of Trauma-Injury Infection and Critical Care, 1996. **40**(3): p. S81-S84.
2. Irwin, R.J., et al., *Shock after blast wave injury is caused by a vagally mediated reflex.* Journal of Trauma-Injury Infection and Critical Care, 1999. **47**(1): p. 105-110.
3. Bauman, R.A., et al., *An Introductory Characterization of a Combat-Casualty-Care Relevant Swine Model of Closed Head Injury Resulting from Exposure to Explosive Blast.* Journal of Neurotrauma, 2009. **26**(6): p. 841-860.
4. Courtney, M.W. and A.C. Courtney, *Note: A table-top blast driven shock tube.* Review of Scientific Instruments, 2010. **81**(12).
5. Hjördis Celander, C.-J.C., Ulf A. Ericsson, Holter Ison Hultman, *The Use of a Compressed Air Operated Shock Tube for Physiological Blast Research.* Acta Physiologica Scandinavica, 1955. **33**(1): p. 6-13.
6. Reneer, D.V., et al., *A multi-mode shock tube for investigation of blast-induced traumatic brain injury.* Journal of Neurotrauma, 2011. **28**(1): p. 95-104.
7. Satoh, Y., et al., *Pulmonary blast injury in mice: A novel model for studying blast injury in the laboratory using laser-induced stress waves.* Lasers in Surgery and Medicine, 2010. **42**(4): p. 313-318.
8. Courtney, A.C., L.P. Andrusiv, and M.W. Courtney, *Oxy-acetylene driven laboratory scale shock tubes for studying blast wave effects.* Review of Scientific Instruments, 2012. **83**(4).
9. Arun, P., et al., *Studies on blast traumatic brain injury using in-vitro model with shock tube.* Neuroreport, 2011. **22**(8): p. 379-384.

10. Hjordis Celander, C.C., Ulf A. Ericsson Aud Holter Ison Hultman, *The Use of a Compressed Air Operated Shock Tube for Physiological Blast Research.* From the Research Institute of National Defense, Physical Department, Stockholm, Sweden, and Medical Department, Sundbyberg, Sweden., 1954.

11. Yu, Q. and H. Gronig, *Shock waves from an open-ended shock tube with different shapes.* Shock Waves, 1996. **6**(5): p. 249-258.

12. Nakagawa, A., et al., *Mechanisms of Primary Blast-Induced Traumatic Brain Injury: Insights from Shock-Wave Research.* Journal of Neurotrauma, 2011. **28**(6): p. 1101-1119.

13. Ling, G., et al., *Explosive Blast Neurotrauma.* Journal of Neurotrauma, 2009. **26**(6): p. 815-825.

14. Zou, X.T., et al., *Rapid miniature fiber optic pressure sensors for blast wave measurements.* Optics and Lasers in Engineering, 2013. **51**(2): p. 134-139.

15. Leonardi, A.D., et al., *Intracranial pressure increases during exposure to a shock wave.* Journal of Neurotrauma, 2011. **28**(1): p. 85-94.

16. Chafi, M.S., G. Karami, and M. Ziejewski, *Biomechanical assessment of brain dynamic responses due to blast pressure waves.* Annals of Biomedical Engineering, 2010. **38**(2): p. 490-504.

17. Scherer, M.R. and M.C. Schubert, *Traumatic Brain Injury and Vestibular Pathology as a Comorbidity After Blast Exposure.* Physical Therapy, 2009. **89**(9): p. 980-992.

18. Cernak, I.N.-H., L. J., *Traumatic brain injury: an overview of pathobiology with emphasis on military populations.* Journal of Cerebral Blood Flow and Metabolism, 2010. **30**(2): p. 255-266.

19. Rosenfeld, J.V. and N.L. Ford, *Bomb blast, mild traumatic brain injury and psychiatric morbidity: A review.* Injury-International Journal of the Care of the Injured, 2010. **41**(5): p. 437-443.

20. Wightman, J.M. and S.L. Gladish, *Explosions and blast injuries.* Annals of Emergency Medicine, 2001. **37**(6): p. 664-678.

21. Hicks, R.R., et al., *Neurological effects of blast injury.* Journal of Trauma-Injury Infection and Critical Care, 2010. **68**(5): p. 1257-1263.

22. Sundaramurthy, A., et al., *Blast-induced biomechanical loading of the rat: an experimental and anatomically accurate computational blast injury model.* Journal of Neurotrauma, 2012. **29**(13): p. 2352-+.

23. Saljo, A., et al., *Mechanisms and pathophysiology of the low-level blast brain injury in animal models.* Neuroimage, 2011. **54**: p. S83-S88.

24. Burgess, P., et al., *Managing traumatic brain injury secondary to explosions.* Journal of emergencies, trauma, and shock, 2010. **3**(2): p. 164-72.

25. Skotak, M., et al., *Rat injury model under controlled field-relevant primary blast conditions: acute response to a wide range of peak overpressures.* Journal of Neurotrauma, 2013. **30**(13): p. 1147-1160.

26. Zhu, F., et al., *Numerical simulation of a shock tube for bio-dynamics study.* International Journal of Nonlinear Sciences and Numerical Simulation, 2012. **13**(1): p. 25-29.

27. Almagableh, A. and P.R. Mantena, *Experimental and finite element modeling of vinyl ester nanocomposites under blast and quasi-static flexural loading.* Journal of Applied Polymer Science, 2012. **126**(6): p. 1895-1905.

28. Tan, P., B. Lee, and C. Tsangalis, *Finite element analysis of sandwich panels subjected to shock tube blast loadings.* Journal of Sandwich Structures & Materials, 2011. **13**(3): p. 263-278.

29. *LS-DYNA. Keyword user's manual*, 2007. Version 971, Livermore, California CA, USA: Livermore Software Technology Cooperation (LSTC).

30. SPSS, *SPSS for Windows*, 2004. Version 13.0, Chicago, SPSS Inc.

31. Sogbesan, E., *Design and analysis of blast induced traumatic brain injury mechanism using a surrogate headform: instrumentation and outcomes*, in *Mechanical & Materials Engineering*2011, University of Nebraska-Lincoln.

32. Courtney, M.W. and A.C. Courtney, *Working toward exposure thresholds for blast-induced traumatic brain injury: Thoracic and acceleration mechanisms.* Neuroimage, 2011. **54**: p. S55-S61.

33. Moochhala, S.M., et al., *Neuroprotective role of aminoguanidine in behavioral changes after blast injury.* Journal of Trauma-Injury Infection and Critical Care, 2004. **56**(2): p. 393-403.

34. Kato, K., et al., *Pressure-dependent effect of shock waves on rat brain: induction of neuronal apoptosis mediated by a caspase-dependent pathway.* Journal of Neurosurgery, 2007. **106**(4): p. 667-676.

35. Cernak, I., et al., *Cognitive deficits following blast injury-induced neurotrauma: possible involvement of nitric oxide.* Brain Injury, 2001. **15**(7): p. 593-612.

36. Cheng, J., et al., *Development of a rat model for studying blast-induced traumatic brain injury.* Journal of the Neurological Sciences, 2010. **294**(1-2): p. 23-28.

37. Wang, Y., et al., *Tightly Coupled Repetitive Blast-Induced Traumatic Brain Injury: Development and Characterization in Mice.* Journal of Neurotrauma, 2011. **28**(10): p. 2171-2183.

38. Ravichandran, K.S., S.S. Sahay, and J.G. Byrne, *Strength and ductility of microscale brass-steel multilayer composites.* Scripta Materialia, 1996. **35**(10): p. 1135-1140.

39. F.I. Khan, S.A.A., *Risk assessment in chemical process industries*. 1998: Discovery publishing house.

40. Chavko, M., et al., *Measurement of blast wave by a miniature fiber optic pressure transducer in the rat brain.* Journal of Neuroscience Methods, 2007. **159**(2): p. 277-281.

41. Chandra, N., et al., *Evolution of blast wave profiles in simulated air blasts: experiment and computational modeling.* Shock Waves, 2012. **22**(5): p. 403-415.

42. Goel, M.D., et al., *An abridged review of blast wave parameters.* Defence Science Journal, 2012. **62**(5): p. 300-306.

3.9 List of Tables

3.10 List of Figures

Figure 3.11: Correlation between Pressure wave of 0.127 mm Steel diaphragm and model at four different locations from shock tube opening (a) 50 mm. (b) 100 mm. (c) 150 mm (d) 450 mm

Table 3.1: Demonstrates a comparison between the parameters of both incident shock wave pressure and free-field pressure at 50 mm using steel and brass 0.127 mm diaphragms: The parameters are the average values of Positive Peak Pressure (PPP), Positive Phase Duration (PPD), and Positive Impulse (PI) (± Standard deviation).

Parameters	**Incident Pressure**		**Free-Field Pressure**	
	Steel(0.127mm)	**Brass(0.127mm)**	**Steel(0.127mm)**	**Brass(0.127mm)**
PPP(kPa)	82.35±3.5	93.8±6.0	92±0.27	107.9±1.8
PPD(ms)	1.24±0.2	1.6±0.1	0.66±0.06	0.53±0.007
PI(kPa.ms)	50±8.9	69.0±2.8	20±0.6	29.80±0.63

Table 3.2: Positive Phase Duration (PPD) values (± Standard deviation) of the resultant positive pressure waves of steel and brass (0.127mm, 0.076 mm, 0.025 mm) diaphragms at four locations from the shock tube opening.

PTs-Board	Steel						Brass					
(PPD) (ms)	0.127 mm	CV	0.076 mm	CV	0.025 mm	CV	0.127 mm	CV	0.076 mm	CV	0.025 mm	CV
PT-50mm	0.66± 0.06	0.1	0.80± 0.15	0.2	1.08± 0.17	0.12	0.53± 0.01	0.02	0.64± 0.02	0.03	0.65± 0.04	0.06
PT-100mm	0.73± 0.01	0.01	0.65± 0.06	0.1	1.21± 0.21	0.2	0.67± 0.01	0.01	0.83± 0.09	0.11	0.72± 0.04	0.06
PT-150mm	1.10± 0.01	0.01	0.68± 0.02	0.03	1.29± 0.23	0.2	0.91± 0.13	0.14	0.78± 0.12	0.2	0.85± 0.15	0.2
PT-450mm	1.08± 0.12	0.1	0.52± 0.06	0.12	1.31± 0.03	0.02	1.14± 0.05	0.04	0.71± 0.16	0.2	0.40± 0.01	0.03

Table 3.3: Illustrates the Positive Impulse (PI) values (± standard deviation) of the resultant free field positive pressure waves of steel and brass (0.127mm, 0.076 mm, 0.025 mm) diaphragms at four locations from the shock tube opening.

PTs-Board	**Steel**						**Brass**					
PI-kPa.ms	**0.127 mm**	**CV**	**0.076 mm**	**CV**	**0.025 mm**	**CV**	**0.127 mm**	**CV**	**0.076 mm**	**CV**	**0.025 mm**	**CV**
PT-50 mm	20± 0.6	0.03	15± 3.9	0.3	2.9± 0.5	0.17	20± 0.63	0.03	11± 1.4	0.1	11± 1.9	0.17
PT-100 mm	14± 0.13	0.01	8.3± 0.83	0.1	2.3± 0.35	0.2	16± 0.06	0.004	9.0± 1.2	0.1	8.1± 2.1	0.3
PT-150 mm	13± 0.27	0.02	6.0± 0.69	0.1	1.6± 0.22	0.1	14± 0.18	0.01	6.6± 0.97	0.1	6.4± 2.0	0.3
PT-450 mm	5.7± 1.1	0.2	2.0± 0.16	0.1	0.67± 0.07	0.1	7.6± 0.4	0.05	1.7± 0.36	0.2	2.2± 0.47	0.2

Table 3.4: *P* value of the resultant positive pressure waves of steel and brass (0.127mm, 0.076 mm, 0.025 mm) diaphragms at four locations from the shock tube opening. P value > 0.05 means that there are no differences among the samples means.

PTs on the Board	**Steel thickness (mm)**			**Brass thickness (mm)**		
(*P* Value)	**0.127**	**0.076**	**0.025**	**0.127**	**0.076**	**0.025**
PT-50 mm	**0.113**	7.04E-04	~0	**0.41**	0.001	8.14E-09
PT-100 mm	**0.761**	2.15E-05	~0	**0.77**	1.53E-08	5.8E-09
PT-150 mm	**0.612**	0.012	~0	1.09E-07	0	1.95E-07
PT-450 mm	**0.07**	**0.073**	0	0.006	0.013	9.58E-11

Table 3.5: Demonstrates the pressure wave parameters of three shock tube experiments using 0.127 mm steel diaphragm and model results at four tested locations from shock tube exit.

Readings at distances in mm		Model	Experiment			Three Tests Average	CV
			Test-1	Test-2	Test-3		
PPP (kPa)	**50**	70	92	90	94	92±0.27	0.002
	100	66	60	80	83	75±9	0.12
	150	60	59	59	57	58±1.4	0.02
	450	37	22	20	20	29±1	0.03
PPD (ms)	**50**	0.97	0.73	0.57	0.68	0.66±0.06	0.09
	100	1.06	0.71	0.75	0.74	0.73±0.01	0.01
	150	1.17	1.08	1.11	1.12	1.10±0.016	0.01
	450	1.33	1.23	1.07	0.93	1.01±0.12	0.12
PI (kPa.ms)	**50**	28	21	19	2	20±0.61	0.03
	100	22	14	14	14	14±0.13	0.01
	150	2	14	13	12	13±0.27	0.02
	450	1.3	7.2	5	4.8	5.7±1.1	0.20

Table 3.6: Statistical analysis correlating the model results to experimental average positive peak pressure values. *P* values indicate that there are no significant differences between the model analysis and the experimental results at the examined locations in the free field.

PT	Locations from Shock Tube Opening (mm)	Experimental/Model (*P* Value)
PT1	50	0.60
PT2	100	0.30
PT3	150	0.52
PT4	450	0.20

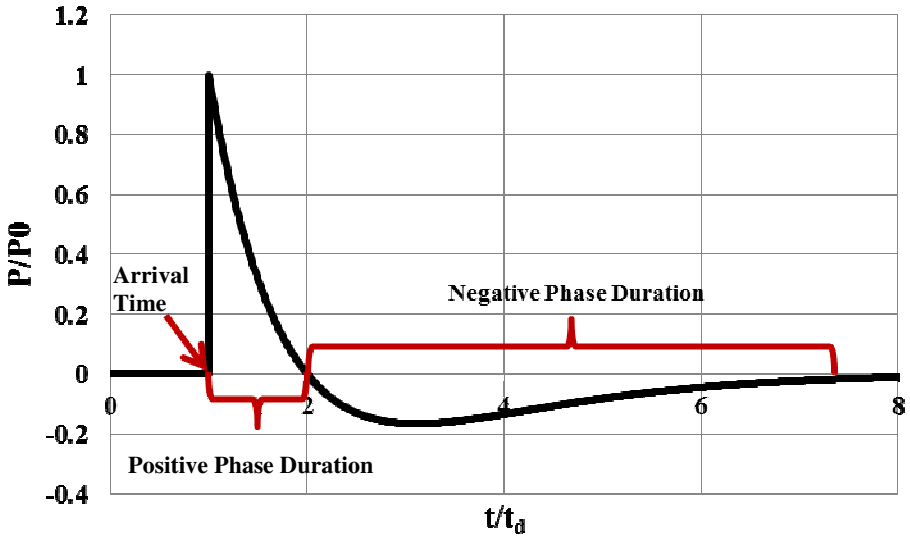

Figure 3.1: A typical pressure-time curve for a free air blast wave

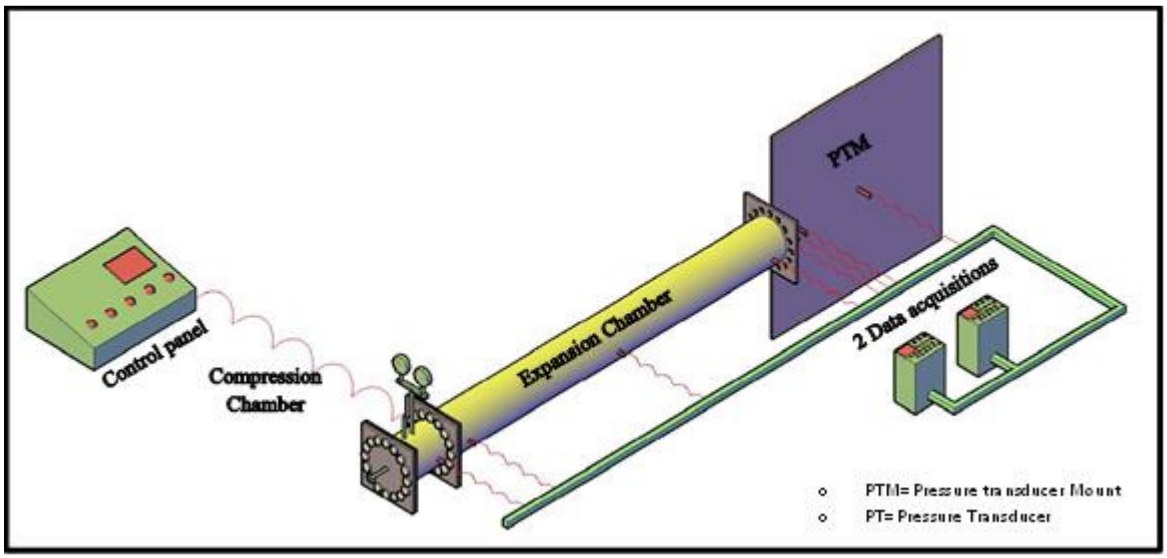

Figure 3.2: Schematic Diagram Showing Compressed air Shock Tube: 1 PT within the compression chamber, 3 PTs within the expansion chamber and 4 PTs are mounted on a board (PTM).

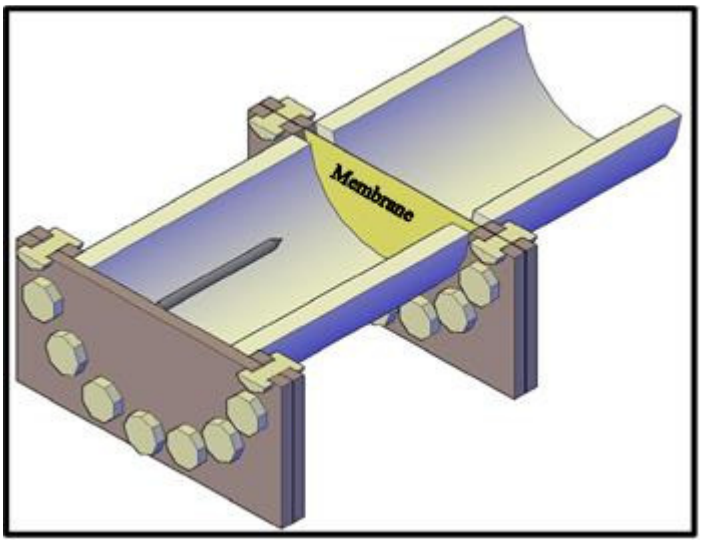

Figure 3.3: Schematic diagram showing a cross-section for a diaphragm between the compression and expansion chambers with the metal striker.

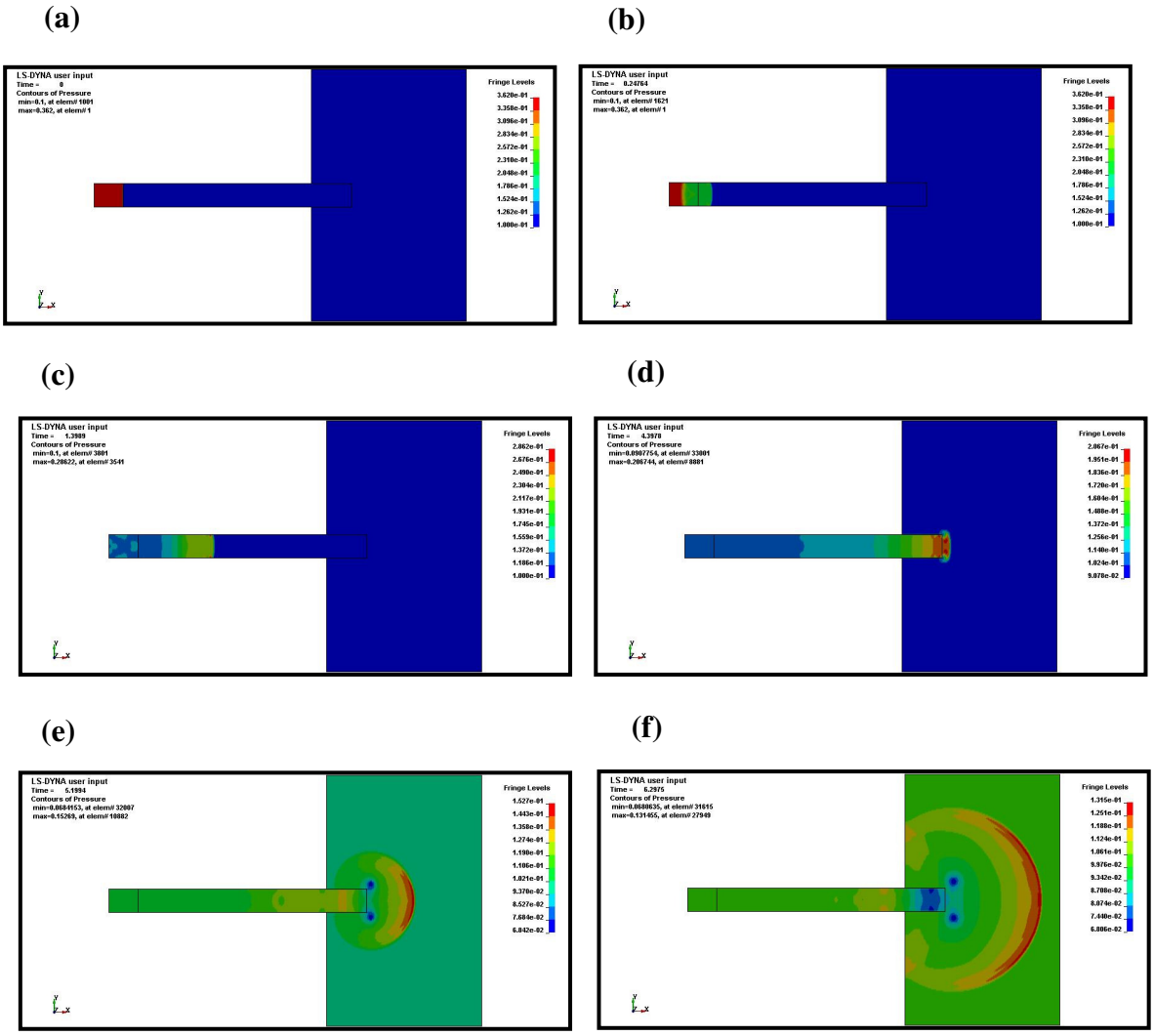

Figure 3.4: Finite Element Model for pressure contours at (a) t = 0 ms, (b) t = 0.25 ms, (c) t = 1.40 ms, (d) t = 4.40 ms, (e) t = 5.20 ms, and (f) t = 6.3 ms

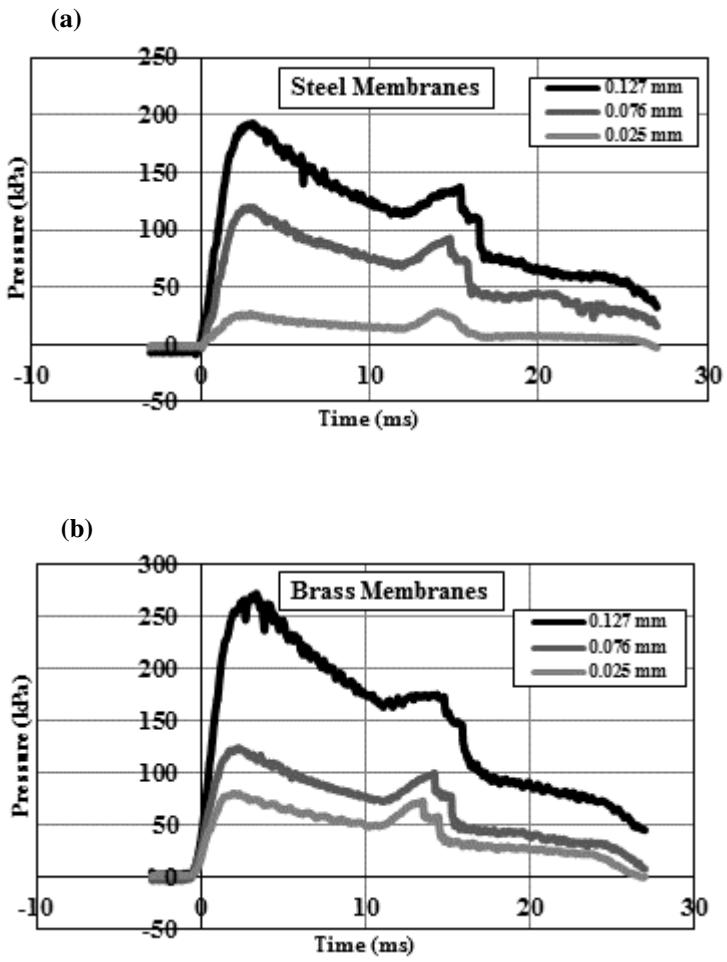

Figure 3.5: Pressure values in the compression chamber at which the diaphragms with 0.127 mm, 0.076 mm, and 0.025 mm thicknesses were ruptured. (a) Steel diaphragm (b) Brass diaphragm

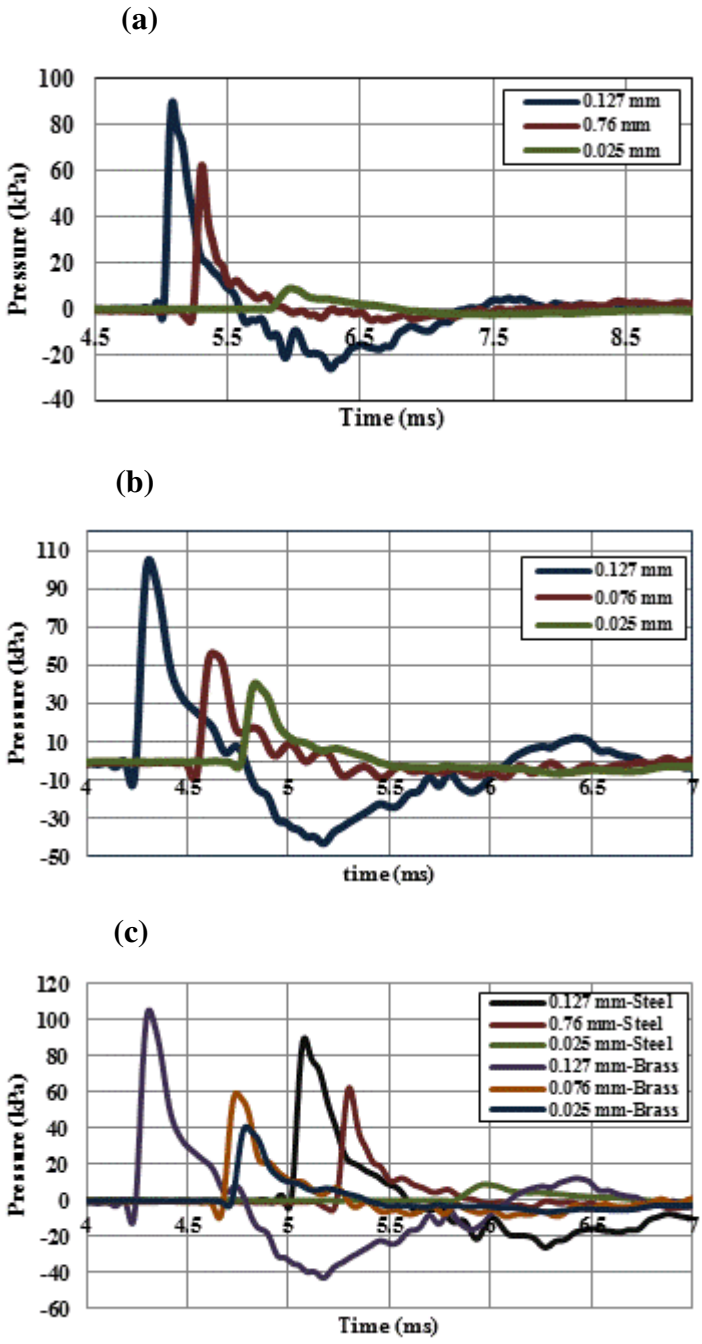

Figure 3.6: Pressure waves at 50 mm from the shock tube opening: (a). Three Steel diaphragm thicknesses (b). Three Brass thicknesses (c). Steel and brass diaphragm

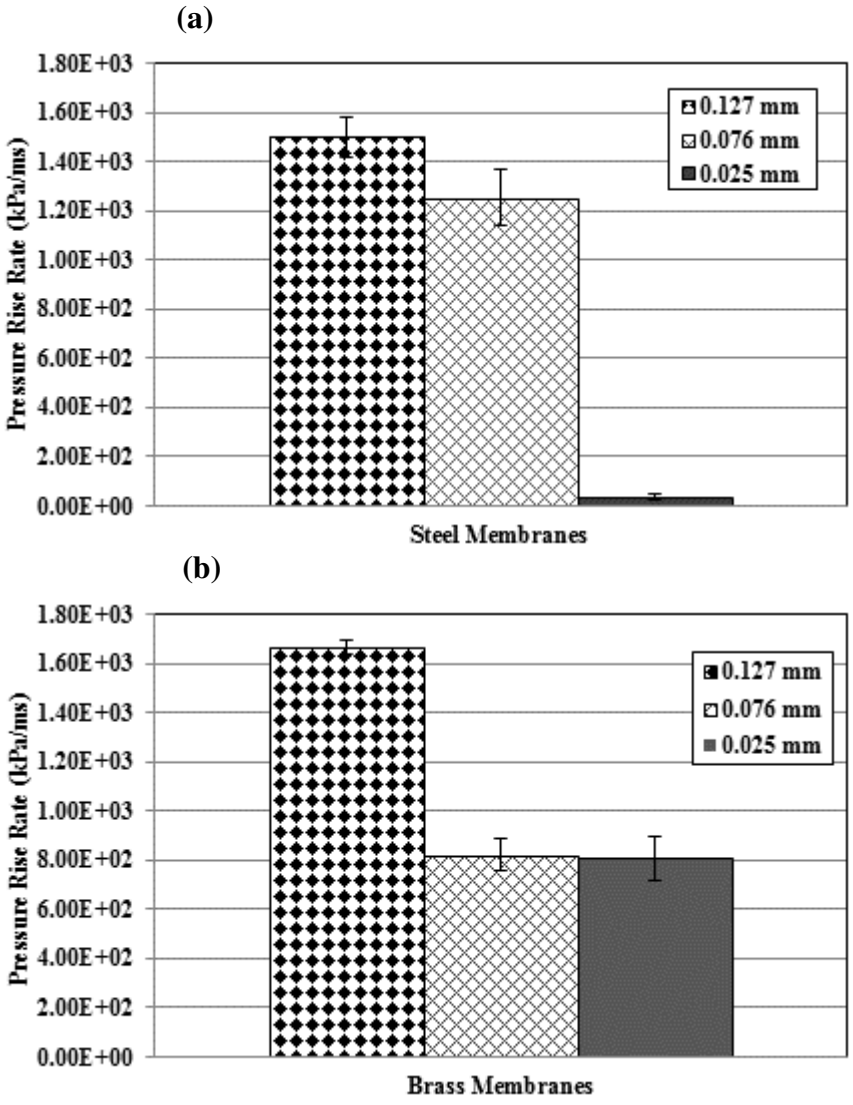

Figure 3.7: Pressure Rise Rate values at 50 mm from shock tube opening of (a). Steel diaphragms and (b). Three Brass diaphragms

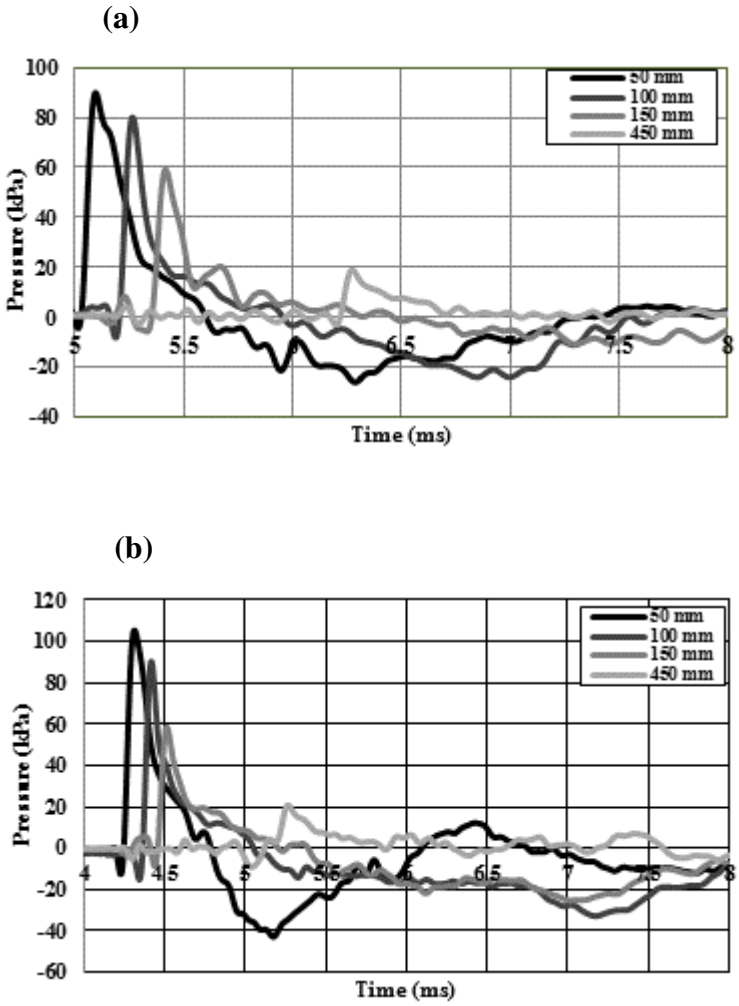

Figure 3.8: Pressure wave at four different locations from shock tube opening (a). Steel 0.127 mm (b). Brass 0.127 mm

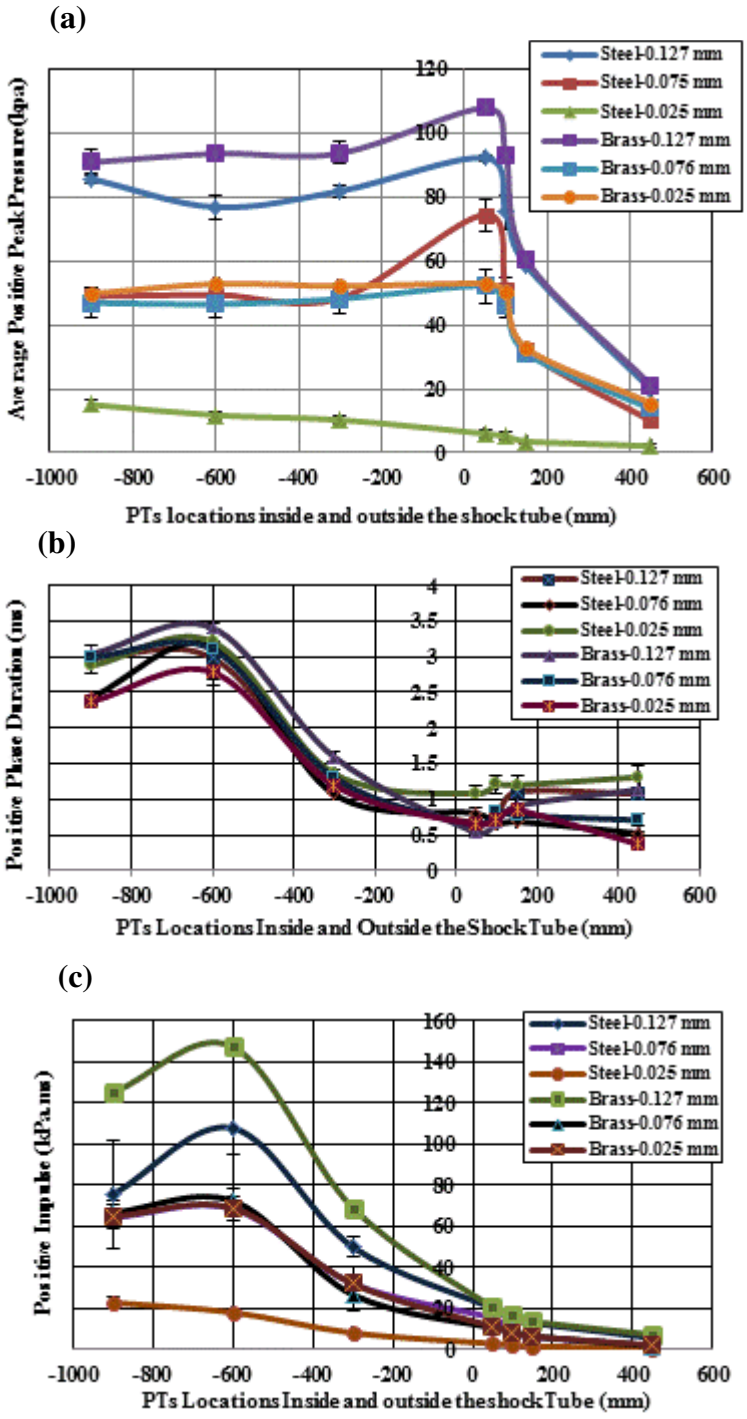

Figure 3.9: Steel and Brass diaphragms with 0.127 mm, 0.076 mm, and 0.025 mm thicknesses. Pressure Transducers (PTs) located at different locations inside and outside the shock tube. (a). Maximum Peak Pressure (kPa) (b). Positive Phase Duration (ms). (c). Shock wave Positive Impulse (kPa.ms)

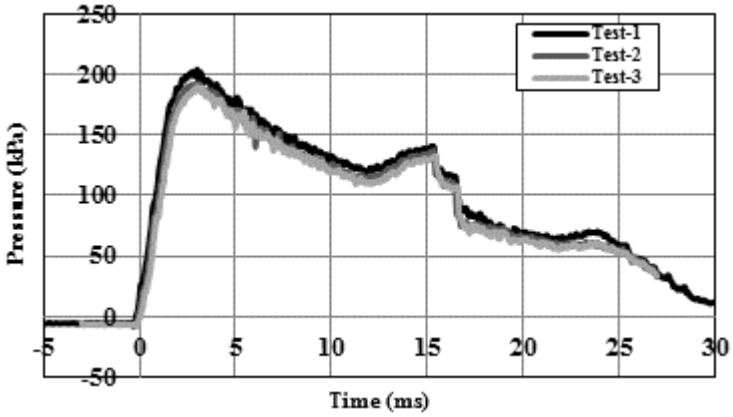

Figure 3.10: Initial pressure in the compression chamber at which the 0.127 mm steel diaphragm was ruptured in three identical shock tube tests.

(a)

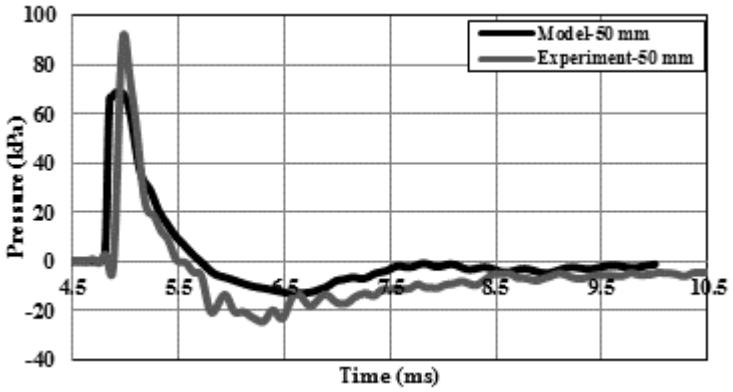
Model-50 mm
Experiment-50 mm
Pressure (kPa)
Time (ms)
100
80
60
40
20
0
-20
-40
4.5
5.5
6.5
7.5
8.5
9.5
10.5

(b)

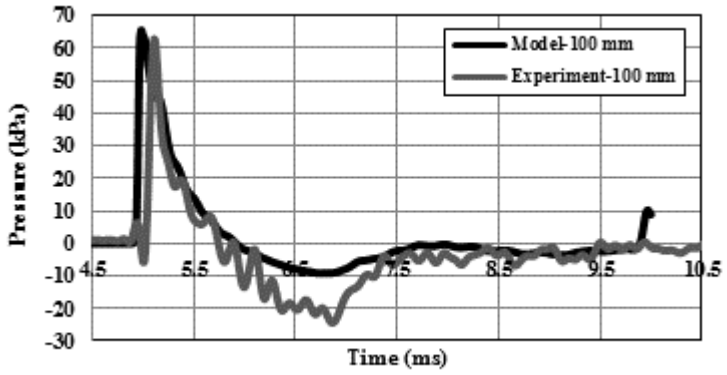
Model-100 mm
Experiment-100 mm
Pressure (kPa)
Time (ms)
70
60
50
40
30
20
10
0
-10
-20
-30
4.5
5.5
6.5
7.5
8.5
9.5
10.5

(c)

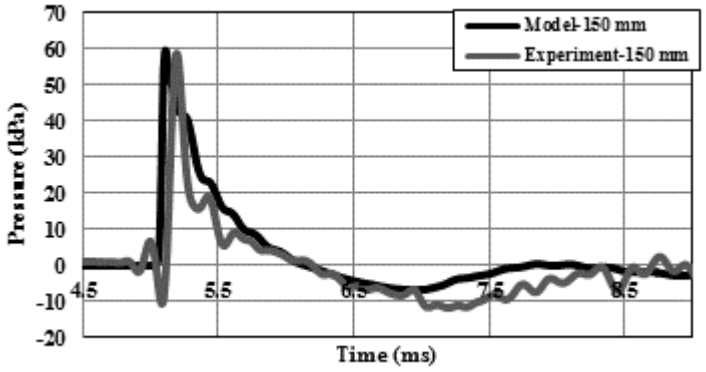

(d)

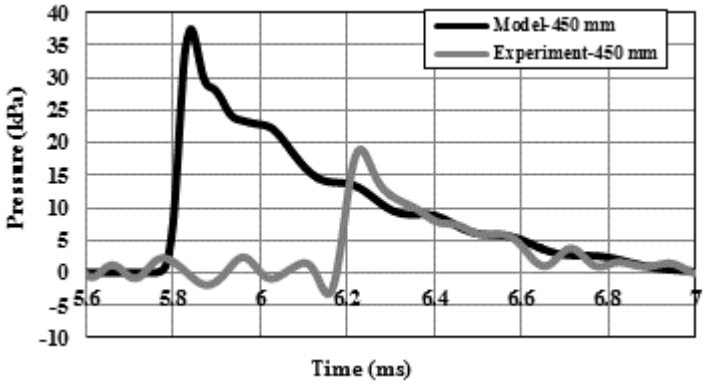

Figure 3.11: Correlation between Pressure wave of 0.127 mm Steel diaphragm and model at four different locations from shock tube opening (a). 50 mm. (b). 100 mm. (c). 150 mm (d). 450 mm

Chapter 4: Analysis of Blast Shock Wave Effects on Surrogate Brain Gel Model for Traumatic Brain Injury Assessment

Neveen Awad, Ammar Gilani, Wael W. El-DaKhakhni

4.1 Abstract

Introduction: The body exposure to Blast wave is the main cause of primary blast injury of different organs. The brain is one of the most vulnerable organs for the direct and indirect effects of shock waves. Due to improvements in the design of helmets and body armor, individuals who are exposed to Improvised Explosive Devices (IEDs) are often protected from the shrapnel, bullets and fragments that may cause the secondary blast injuries. However, blast/pressure waves can propagate through the protective equipment causing serious damage to different vital organs. Despite extensive research characterizing the brain injury produced by blast, the mechanism of blast induced mild traumatic brain injury (BImTBI) remains unclear. A thorough understanding of the contribution of each component of the shockwave to the mechanism of injury is essential. In order to understand the biomechanics of BImTBI, the current study investigated the blast wave-brain interactions after exposing a surrogate brain model to blast pressure wave.

Materials and Methods: The experimental study was conducted using a pre-designed compressed air-driven shock tube and a brain model created from Sylgard 527 silicone gel. The shock tube is capable of producing reliable blast wave forms simulating those induced by improvised explosive device (IED). The changes of shock wave behaviours

inside the brain model in relation to the distance from shock tube exit or the brain orientation were monitored using pressure transducers. The brain acceleration for tested locations and orientations with respect to the shock tube opening were also measured using an accelerometer.

Results and Discussion: The results from the current study demonstrated that positive peak pressure (PPP) and positive impulse (PI) values, which are considered the most vital parameters on mild traumatic brain injury (mTBI), were affected according to the changes of the brain locations/orientations from the shock tube exit., The pressure wave forms inside the brain model showed significant increases of negative pressure peak (NPP) values. The generation of negative pressure within the brain can results in development of cavitation, which is a potential mechanism of the brain tissue damage.

Keywords:

Blast-induced mild Traumatic Brain Injury, biomechanics, Explosions, Shock tube, Shock wave, surrogate brain.

4.2 Introduction

Recent war conflicts and increases in the prevalence of industrial and domestic/terrorist accidents have led to a dramatic increase in the number of explosive-related events [1]. This augments the frequency of primary Blast-Induced mild Traumatic Brain Injury (BImTBI) when victims are exposed to nonlethal levels of explosion [2]. Due to the devastating consequences of BImTBI, an understanding of the shock wave effects on the brain biomechanics is crucial in traumatic brain injury (TBI) related research in order to improve early diagnosis and management. A classical free-field blast

wave at a fixed location can be modeled by the Friedlander waveform, which is characterized by an instantaneous rise in pressure immediately followed by a decay curve [3]. Therefore, a detonation of any powerful explosive generates sudden and extreme differences in pressures known as blast shock wave. The blast wave is formed of positive pressure components followed by temporary negative components that may lead to significant injuries of different organs particularly at air-fluid interfaces [4]. Additionally, winds may propel fragments and people, causing penetrating or blunt injuries. The shock wave travelling outwards from the source is reflected when it meets with objects with higher density than atmospheric pressure (e.g. ground) and then travels back to the origin. The overpressure of the reflected wave exceeds the overpressure of the incident wave, and due to its higher velocity, it will eventually catch up with the incident wave [5, 6].

The mechanism of BImTBI has been controversial for a long time [7]. Direct head exposure to explosions is considered by most investigators as one of the mechanical mechanisms by which the blast wave causes mild traumatic brain injury (mTBI) [8]. Different theories have been proposed for BImTBI mechanisms [9]. One of these theories suggested that exposure of the body or local chest to blast overpressure may result in brain injuries [10, 11]. This is may be correlated to the difference in pressure between the ventral body cavity (high pressure) and cranial cavity (low pressure), which can induce mTBI by the sudden increase of cerebral perfusion pressure [12]. Therefore, the blood acts as a transmission medium, which propagates a pressure wave to the brain and subsequently enhances the damage of small cerebral blood vessels and the Blood-Brain Barrier (BBB) as a result of the sudden cerebral perfusion pressure fluctuation. [13-16].

The second theory suggests that transitional and rotational acceleration play a serious role in primary brain injury which, without a direct impact, may lead to brain lesions such as cerebral contusion, tears in arteries and veins, and tears of axons in brain white matter [17, 18]. In some cases of mTBI, brain function impairments such as attention, emotional, and memory problems may exist without any visible brain lesions [19, 20]. Further, the direct propagation of the blast waves through brain tissues, with different properties as white matter and gray matter, can induce severe damage through spalling and implosion mechanisms [21].

Animal and clinical studies have presented some of the critical pathophysiological findings in the acute stage of BImTBI [22-24]. These include rapid and marked diffuse brain tissue edema, intracranial hemorrhage within the white matter, and vasospasm. Additionally, survivors after explosions have a greater chance of suffering pseudoaneurysms, especially in association with vasospasm leading to cerebral hypotension and hypoxia [25, 26]. Other serious pathological changes include diffuse axonal injury (DAI) and subdural hemorrhage that play crucial role in the TBI chronic stage. As most of the BImTBI patients suffer from cognitive dysfunction and post-traumatic stress disorder (PTSD) [27, 28]. Further, the cumulative effects of multiple exposures are believed to lead to serious short-term and long-term health impairments [29]. As a result of limited available data about free-field blast pressure wave and associated BImTBI, the brain reactions under different pressure impact conditions require more investigation [30].

From the human injury point of view, the most important part of the wave energy is the one that is transmitted into the body in the form of both positive (compression) and negative (tension) stress waves. Additionally, the shear stress waves, where the compression by the stress wave portion is followed by a tensile wave portion, can promote mTBI [7]. Therefore, the positive/negative peak pressure, the rise time, and the impulse of the shock wave are vital parameters that can be measured to understand the brain tissue damage mechanisms [23].

The extensive investigations for the complex wave propagation and its role in mTBI is highly proposed. The hypotheses of the current study are: (1) The orientation of the brain in relation to the blast wave pathway would significantly influence the severity of the blast direct impact on the brain, and (2) Distance from the explosion would also alter the behaviour of the stress wave propagation into the brain. In the current study, a brain model was created from silicone gel Sylgard 527 after determining that this material has viscoelastic properties similar to those of actual human brain tissue [31, 32]. The brain model was exposed to the blast wave at three different orientations representing the brain anatomy-based region of interest to be analyzed. These include the back (occipital lobe), the right side (temporal lobe) and oblique 45^{o} positions (for the occipital lobe). Additionally, each orientation was examined at four distances from the shock tube opening (150, 500, 1000, and 1500 mm). In each test, the pressure waves were recorded using four pressure transducers (PT). PTs were imbedded intraparenchymally within the brain model at four different locations corresponding to frontal lobe (front), occipital lobe (back), temporal lobe (left side), and medially between two hemispheres at the anatomical

location of corpus callosum toward the right side. Additionally, the acceleration was recorded using one accelerometer that was always facing the shock tube opening at any brain model orientation. The brain model was exposed to at least three typical free-field blast tests with controlled consistent Positive Peak Pressure (PPP). This was controlled by using pre-calibrated steel diaphragm with thickness of 0.127mm that requires compressed air pressure around 204 kPa to rupture. The Conventional Weapons Effect (CONWEP) computer code (Hyde, 1992) was used to calculate the TNT equivalent of the simulate shock wave with peak pressure in the range that was used in experimental study [33].

4.3 Materials and Methods

4.3.1 Silicone Gel Preparation for Compression Test

The compression test samples were prepared from silicone gel, Sylgard 527 part A and B (Dow Corning Corporation, USA). The two parts of the silicone gel were added at 1:1 ratio of part A and B then mixed thoroughly together and poured inside pre-made silicone rubber mold (McMaster-Carr, USA) to cure at room temperature. In order to mitigate the substantial difficulties of preparing the silicone gel samples using different mold types, a silicone rubber sheet was used to generate special molds. The molds were prepared by dividing the silicone rubber sheet (6.35 mm thick) into 28 pieces that had the same dimensions as a glass slide (80 mm x 25 mm). In order to obtain perfect circles in the silicone rubber sheet, a hollow puncher with a diameter of 19 mm was used. Furthermore, two of the silicone rubber pieces were mounted together on top of a glass slide in order to obtain silicone gel samples with a thickness of 12.7 mm.

4.3.2 Compression Test

Instron® SFL-3366 (MMRI, McMaster University) equipped with a 50 N load cell was utilized to examine the mechanical properties of the silicone gel and to compare it with the human brain tissue. Uniaxial compression tests were performed using five crosshead speeds (10, 20, 50, 100, 150 mm/min)

4.3.3 Brain Gel Model Preparation

A plastic brain mold (SKS Sibley CO., El-Segundo, CA) (190 x 160 x 100 mm) was used to create a surrogate brain that had the characteristic appearance of the outer surface of the human brain. The brain mold was filled with Sylgard 527 A&B silicone gel. The two components of the gel were mixed in a one-to-one mass ratio and cured in the plastic mold, for at least one week at room temperature before experiments commenced.

4.3.4 Pressure-Time Profile and Acceleration Measurements of The Brain Model

Four pressure transducers (PTs) (Model type-2115B, Kistler Instrument Corp., Armherst NY 14228), were imbedded inside the brain model at four locations (front, back, inner surface of the right hemispheres, and left side). Thereby, the diaphragm parts were embedded internally and the connector parts were projected externally to be connected to the data acquisition systems. These PTs have the ability to measure transient/repetitive dynamic events as well as incorporate acceleration-compensation. Additionally, the accelerometer (Kistler Instrument Corp., Armherst NY 14228) was connected to the data acquisition system and was facing the shock tube opening at all orientations.

4.3.5 Recording Pressure/Acceleration Waveforms

Two identical 500 MHz high-speed data acquisition systems (Tektronix TDS744A) with four channels each were linked and used to record the pressure/acceleration waveforms. To ensure signal capturing during the shock wave development, one of the linked data acquisition systems was set to act as the main trigger and the other as the auxiliary trigger.

4.3.6 Shock Tube

The horizontally mounted steel shock tube consists of compression and expansion chambers of equal and constant cross section but with different lengths. The first chamber (shorter) contains compressed air while the second volume (longer) is open to the atmosphere (expansion). The chambers are 250 mm and 2000 mm long, respectively, while their inner diameter is 200 mm. The two chambers are separated by a metallic diaphragm and are tightly joined together using 16 of 19 mm steel bolts. When the diaphragm is suddenly removed (plastic deformation leading to rupture) the pressurized air is abruptly exposed to the area of low pressure. This creates a shock wave that propagates into the low pressure area and then into the surrounding atmosphere and a rarefaction or expansion wave that propagates into the high pressure area.

4.3.7 Diaphragm Preparation

Steel diaphragms with thicknesses of 0.127mm (Branded® Shim, Downers Grove, IL60515 USA) were used with the previously designed compressed air shock tube to create a simulated shock wave. The steel diaphragms were prepared by performing 16 holes using punch set (SP-9 fractional, Trinity Brand Industries, INC, USA) with a size of

19 mm. Each performed hole was corresponding to the bolts' location at the compression and expansion chambers of the shock tube.

4.3.8 Statistical Analysis

All experiments were carried out at least in triplicate for each brain orientation and distance from the shock tube opening, so the reliability of the effects of shock wave on the brain model can be verified. Comparative analyses were performed using The Statistical Package for Social Sciences (SPSS), Version 13.0. One-Way ANOVA tests were performed in order to evaluate the variance of positive pressure values among the experiments.

4.4 Results and Discussion

BImTBI mechanisms are difficult to study experimentally due to many important ethical issues involving the use of human cadavers and animals. Therefore many physical head and/or brain models have been developed and tested. The aim of the current study is to evaluate the effects of blast wave propagation, particularly those typical of IEDs, in the brain and its crucial role on potential causes of BImTBI. In this work, a set of experiments were performed to study the shock wave-brain model interactions as the blast wave transverse the brain.

4.4.1 Simulated Brain Model

In order to investigate the propagation of pressure/blast wave and its role in the brain, a simulated brain was developed (Figure 4.1). Silicone dielectric gel, Sylgard 527 A&B, has been demonstrated to have viscoelastic properties approaching those of actual brain tissue and has gained widespread acceptance as a physical substitute for human

brain tissue [34, 35]. In this light, the brain model was prepared utilizing the silicone gel (Sylgard 527) and its mechanical properties were tested using the Instron to compare it with the brain tissue mechanical properties. Figure 4.2 (a and b) shows stress-strain curves (Figure 4.2a) and Young's modulus of silicone gel under uniaxial compression test using five crosshead speeds. The Young's modulus was determined by the slope of the resultant curves (Figure. 4.2b). The Young's modulus values of the Sylgard 527 ranged between 3.6 ± 0.3 kPa to 5.6 ± 1.8 kPa depending on the cross section speed, while the corresponding coefficient of variation values (CV) were 0.09 and 0.23, respectively. These values are consistent with the reported Young's modulus value of human brain tissue in different studies [35-37]. Consequently, the prepared brain model was used in a series of experimental studies to investigate the mechanisms of wave propagation according to the brain orientation and location from the shock tube opening. The pressure wave inside the brain model was recorded using four pressure transducers that were imbedded at different locations. These PTs consist of two ends, a diaphragm at one side (sensor part) and a connector from the other side, therefore, its orientation inside the brain model affects the resultant waves. The diaphragm side of PTs at front, back and left side were embedded internally; while the PT diaphragm of right side was embedded to face outward. Interpretation of the pressure waves recorded inside the brain model is dependent on the PTs' orientations inside the brain model (Front, Back, Left side and Right side) (Figure 4.3).

4.4.2 Characterization of Shock Waves

The main goal of this work is to investigate the responses of simulated brain model to reliable shock waves in the range capable of inducing mTBI. According to a previous study of the compressed air-driven shock tube calibration conducted at Applied Dynamic Lab [38], the amount of compressed air was controlled by using pre-tested steel diaphragm with a thickness of 0.127 mm. Therefore, the peak overpressure, which is required for the steel diaphragm to rupture in each blast, was controlled and approximately equal to 204 kPa. The average of resultant free-field peak pressure values at 50, 100, 150 and 450 mm from the shock tube exit were 92, 75, 58 and 29 kPa, respectively [38]. These results from the previous study are important to correlate the reflected pressure wave recorded by four PTs mounted on the air-foil board with the brain model pressure wave at four locations from shock tube opening (150, 500, 1000 and 1500 mm). The common reference location, at 150 mm, is used to extrapolate the results and estimate the pressure wave characteristics at the other brain model locations using ConWep (Protection Engineering Consultants, 2010). Using free filed measured wave profile at 150 mm, it was found to be equivalent to 68 g of TNT at 2745 mm. Table (4.1) shows the blast wave parameters at 150 mm from shock tube calibration tests and its ConWep equivalent. Table 4.2 demonstrates the pressure wave parameters at the four tested locations from shock tube exit using ConWep.

The incident pressure profile at the shock tube exit follow the Friedlander waveform fairly well (Figure 4.4) and its average PPP value in all blast test were equal to 82.35 kPa and the PPD was 1.24 ms. The incident shock wave results are in line with the results of

previous studies and demonstrate that there is no evidence to reject the null hypothesis of the incident pressure waves (P value > 0.05).

4.4.3 Pressure Wave Profiles within the Brain Model at Various Orientations

Each test of the brain model was examined with three brain orientations (right, back and oblique). Figure (4.5a) shows four pressure waves inside the brain model with right side orientation at 150 mm from shock tube. The right pressure transducer (RPT) was embedded medially from the inner surface of the right hemisphere at the anatomical site of corpus callosum. Therefore, the diaphragm part of The RPT was facing the travelling pressure wave inside the brain model. As a result the recorded wave at RPT for the right side orientation test showed a significant higher value (104 kPa) of the positive peak pressure compared to the other recoded waves at the rest PTs inside the brain. The average positive peak pressure values of recorded waves at the left side PT (LPT), Front PT (FPT) and Back PT (BPT) were 21, 41, and 20 kPa respectively. In addition, the recorded right side pressure waveform for right orientation showed different characteristics from the other recorded pressure waveforms within the brain model (LPT, FPT, and BPT). The latter waveforms showed similar profiles (the shape was almost identical) to that of the incident pressure profile where the positive peak pressure decayed rapidly and was then followed by a negative peak pressure. Due to the setting orientation of RPT, the waveform showed no negative pressure as the sensor part, inside the brain model, was directly facing the travelling shock wave. By comparing the resultant waveforms of the back and oblique 45^{o} orientations with the right side orientation at 150 mm, it showed that all pressure waveforms have positive and negative peak pressure at all

PTs locations inside the brain including RPT (Figure 4.5b and c). Similarly, at the other three distances (500, 1000, and 1500 mm) the pressure waveform at RPT for right side orientation, also showed no negative pressure. Furthermore, the pressure waves' analyses inside the brain model revealed that at each distance (500, 1000, and 1500 mm) the PPP experiences a rapid pressure drop followed by a long duration before the NPP starts. This duration along with the NPP values increase by moving away from shock tube exit (Figures 4.6, 4.7 &4.8). Possible explanation of increase NPP is the overlapping of both incident negative phase with the negative phase of internally reflected pressure wave, which leads to the magnification effect. Additionally, the rapid pressure drop within the brain model is induced by the rapid gas expansion in the three dimensions within the blast free field tests. Table 4.3 summarises the PPP and NPP values for all PTs within the brain model with three tested orientations at four locations from shock tube exit. Thus, from the pressure wave analysis, it is found that the brain was exposed to two different types of strains, compressive and tensile. As the shock wave travels toward the brain model two interaction phenomena occur. One is the positive pressure phase that results from a compression loading on the area facing shock wave, while the other side is under tensile loading that leads to negative pressure or rarefaction wave [39]. Compressive phenomena most often cause injury at the point of impact (coup injury), whereas rarefaction phenomena often cause serious damage at sites distant from the site of impact (countercoup injury). Moreover, a rarefaction wave may cause much brain injuries than the incident shock wave due to its cavitation effects [40].

4.4.4 Positive Peak Pressure and Positive Impulse Comparison

Calculating the PI is an important method of examining the energy delivered. Figure 4.9 (a and b) displays comparisons between the average PPP values and the corresponding positive impulse at 150mm for all orientations, respectively. It reveals that even though the RPT has the highest average PPP value for the right orientation, it also has a lower PI average compared to the LPT and FPT for the back and oblique orientations. This is due to the shorter PPD of the RPT waveform (0.38 ms) compared to the PPD values of LPT and FPT (1.41 ms and 1.01 ms, respectively) for the back and oblique orientations. Moreover, at 500 mm the PI at the LPT has higher values for the right and back orientations, while the FPT only has higher PI values at the right orientation compared to the other PTs locations and the brain model orientations (Figure 4.10). Figures 4.11 and 4.12 reveal the PPP and PI at 1000 mm and 1500 mm have no significant differences between average values. Figure 4.13 demonstrates the pressure waveforms at three different locations: 1) shock tube exit, 2) PT mounted on air-foil board at 150 mm and 3) RPT inside the brain model at 150 mm. Not only are the magnitudes of PPPs different among the three waveforms, but also the duration of PPD, thus the impulses, which are the integration of a pressure history, are significantly different. Even though the pressure waveform inside the brain has a significantly higher average PPP value than shock tube and board waveforms, its impulse is significantly less than shock tube waveform impulse and close to the average value of board wave PI. This is due to the long PPD of incident shock wave and short PPD of waveform inside the brain. Table 4.4 shows a comparison between PPP, PPD, and PI at the three formerly

mentioned locations (shock tube end, PT mounted on air-foil board at 150 mm and RPT inside the brain model at 150 mm).

4.4.5 Brain Model Acceleration Analysis

Acceleration/deceleration is the key mechanism of the brain damage that results in diffuse axonal injury (DAI), contusion, and acute subdural hematoma. The brain injury occurs if local strains and strain rates exceed a critical threshold that leads to axonal damage [15]. Strain rate was hypothesized to be a key biomechanical parameter to explain the cause of brain injury. It was claimed that the tethering of the brain at the sellar and suprasellar region has crucial role in the mechanical brain response during linear acceleration [41]. As the brain exhibits asymmetry, both linear and angular displacement of the brain can occur. Since there is no direct way to verify acceleration mechanisms on a living human brain, these studies are typically performed on laboratory animals, cadavers, physical models, and/or through the use of computer models. In the current experimental study, only the linear accelerations were evaluated. The accelerations for three brain model orientations were assessed using an accelerometer, which was set in the direction of the traveling shock wave. Figure 4.14 (a and b) shows the resultant acceleration pulses for the right side, back and oblique orientations at 1500 mm, and the average positive and negative acceleration values for all orientations at the four tested locations. The right side orientation showed higher peak acceleration values at all distances than back and oblique orientations (Table 4.5). This may be due to the fact that the brain surface area exposed to the shock wave is larger on the right side orientation

than on the back and oblique orientations. Additionally, the maximum peak acceleration was reached by the brain gel model before the end of the positive phase duration.

4.5 Conclusions

TBI, especially mTBI, is a common consequence of modern warfare. Given the frequency at which mTBIs occur in modern warfare, a clear understanding of the explosive blast injury mechanisms is required. Current research regarding the effects of primary blast waves upon the central nervous system is limited and areas of active investigation are required to improve early diagnosis and management. The mimic critical features of blast injury sustained in combat or terrorist explosions are of particular importance for an in-depth and comprehensive study of the biomechanisms, the pathophysiology, and long-term neurological consequences of blast-induced TBI. The current experimental study provides a satisfactory design and implementation that can control key parameters (PPP, PPD, and PI) of the blast shock waves and examine their interactions with the physical brain model. In this work, the brain model was exposed to a reliable shock wave in the range that can induce mTBI and three orientations were examined at four distances. The characteristics of the blast wave used in this study are representative of ideal free-field blast. The resultant pressure wave profiles inside the brain model showed significant differences depending on the brain orientation and location from the shock tube exit. At the right orientation, irrespective of distance, the RPT pressure wave did not show negative phase, where, the positive pressure decayed and remained at the ambient pressure. Other PTs pressure wave profiles for all

orientations and locations showed positive and negative phases. At the 150 mm distance from shock tube exit the pressure waves showed positive and negative peak pressures that are similar to the incident shock wave profile. As the decay of the positive peak pressure is followed by a drop in the pressure and then return to ambient pressure. In contrast, by moving away from the shock tube exit, the duration between positive and negative phase is significantly increased and the PPP reduced while the NPP increased. As a result, the risk of cavitation as a possible brain injury mechanism needs to be evaluated. Based on the measured pressure waves, the PI values for the three orientations showed that they are close at the far distances. This indicates that the orientation effects on the brain injury are minimized by moving away from the explosion site.

4.6 Acknowledgments

The authors gratefully acknowledge Kent Wheeler and Paul Heerema at Applied Dynamic Lab for their help and useful discussions.

4.7 References

1. Cernak, I.N.-H., L. J., *Traumatic brain injury: an overview of pathobiology with emphasis on military populations.* Journal of Cerebral Blood Flow and Metabolism, 2010. **30**(2): p. 255-266.
2. Leonardi, A.D., et al., *Intracranial pressure increases during exposure to a shock wave.* Journal of Neurotrauma, 2011. **28**(1): p. 85-94.
3. James H. Stuhmiller, Y.Y.P., And Donald R. Richmond, , *The Physics And Mechanisms of Primary Blast Injury* 1991, Office of the Surgeon General. p. 241-270.
4. Ohnishi, M., et al., *Reflex nature of the cardiorespiratory response to primary thoracic blast injury in the anaesthetised rat.* Experimental Physiology, 2001. **86**(3): p. 357-364.
5. Sundaramurthy, A., et al., *Blast-induced biomechanical loading of the rat: an experimental and anatomically accurate computational blast injury model.* Journal of Neurotrauma, 2012. **29**(13): p. 2352-+.
6. Kakogiannis, D., et al., *Assessment of pressure waves generated by explosive loading.* Cmes-Computer Modeling in Engineering & Sciences, 2010. **65**(1): p. 75-93.
7. Leonardi, A.D., et al., *Methodology and evaluation of intracranial pressure response in rats exposed to complex shock waves.* Annals of Biomedical Engineering, 2013. **41**(12): p. 2488-2500.
8. Moore, D.F. and M.S. Jaffee, *Military traumatic brain injury and blast.* Neurorehabilitation, 2010. **26**(3): p. 179-181.
9. Neveen Awad, L.C.D., *Neurological manifestations related to blast injury.* European Neurological Journal 2011: p. 8.

10. Cernak, I., et al., *Ultrastructural and functional characteristics of blast injury-induced neurotrauma.* Journal of Trauma-Injury Infection and Critical Care, 2001. **50**(4): p. 695-706.

11. Courtney, A.C. and M.W. Courtney, *A thoracic mechanism of mild traumatic brain injury due to blast pressure waves.* Medical Hypotheses, 2009. **72**(1): p. 76-83.

12. Chen, Y., W. Huang, and S. Constantini, *The Differences between Blast-Induced and Sports-Related Brain Injuries.* Frontiers in neurology, 2013. **4**: p. 119-119.

13. Chen, Y. and W. Huang, *Non-impact, blast-induced mild TBI and PTSD: Concepts and caveats.* Brain Injury, 2011. **25**(7-8): p. 641-650.

14. Abdul-Muneer, P.M., et al., *Induction of oxidative and nitrosative damage leads to cerebrovascular inflammation in an animal model of mild traumatic brain injury induced by primary blast.* Free Radical Biology and Medicine, 2013. **60**: p. 282-291.

15. Yeoh, S., E.D. Bell, and K.L. Monson, *Distribution of blood-brain barrier disruption in primary blast injury.* Annals of Biomedical Engineering, 2013. **41**(10): p. 2206-2214.

16. Yamakami, I. and T.K. McIntosh, *Effects of Traumatic Brain Injury on Regional Cerebral Blood-Flow in Rats as Measured with Radiolabeled Microspheres.* Journal of Cerebral Blood Flow and Metabolism, 1989. **9**(1): p. 117-124.

17. Li, X.Y., et al., *Diffuse axonal injury induced by simultanous moderate linear and angular head accelerations in rats.* Neuroscience, 2010. **169**(1): p. 357-369.

18. Zhang, L.Y., K.H. Yang, and A.I. King, *A proposed injury threshold for introduction mild traumatic brain injury.* Journal of Biomechanical Engineering-Transactions of the Asme, 2004. **126**(2): p. 226-236.

19. Gupta RK, P.A., *Mathematical models of blast-induced TBI: current status, challenges, and prospects.* Frontiers in Neurology., 2013. **4**(59).

20. Moss, W.C., M.J. King, and E.G. Blackman, *Skull Flexure from Blast Waves: A Mechanism for Brain Injury with Implications for Helmet Design.* Physical Review Letters, 2009. **103**(10).

21. Wightman, J.M. and S.L. Gladish, *Explosions and blast injuries.* Annals of Emergency Medicine, 2001. **37**(6): p. 664-678.

22. Cernak, I., et al., *The pathobiology of moderate diffuse traumatic brain injury as identified using a new experimental model of injury in rats.* Neurobiology of Disease, 2004. **17**(1): p. 29-43.

23. Skotak, M., et al., *Rat injury model under controlled field-relevant primary blast conditions: acute response to a wide range of peak overpressures.* Journal of Neurotrauma, 2013. **30**(13): p. 1147-1160.

24. Armonda, R.A., et al., *Wartime traumatic cerebral vasospasm: Recent review of combat casualties.* Neurosurgery, 2006. **59**(6): p. 1215-1225.

25. Rosenfeld, J.V. and N.L. Ford, *Bomb blast, mild traumatic brain injury and psychiatric morbidity: A review.* Injury-International Journal of the Care of the Injured, 2010. **41**(5): p. 437-443.

26. Bass, C.R., et al., *Brain injuries from blast.* Annals of Biomedical Engineering, 2012. **40**(1): p. 185-202.

27. Richardson, J.D., J.A. Naifeh, and J.D. Elhai, *Posttraumatic stress disorder and associated risk factors in Canadian peacekeeping veterans with health-related disabilities.* Canadian Journal of Psychiatry-Revue Canadienne De Psychiatrie, 2007. **52**(8): p. 510-518.

28. Ling, G., et al., *Explosive Blast Neurotrauma.* Journal of Neurotrauma, 2009. **26**(6): p. 815-825.

29. Ahlers, S.T., et al., *Assessment of the effects of acute and repeated exposure to blast overpressure in rodents: toward a greater understanding of blast and the potential ramifications for injury in humans exposed to blast.* Frontiers in neurology, 2012. **3**: p. 32-32.

30. Nakagawa, A., et al., *Mechanisms of primary blast-induced traumatic brain injury: insights from shock-wave research.* Journal of Neurotrauma, 2011. **28**(6): p. 1101-1119.

31. Hossain, S.G.M., *Material modeling and analysis for the development of a realistic blast headform* in *Mechanical Engineering* 2010, University of Nebraska

32. Zhang, J., et al., *Experimental Study of Blast-Induced Traumatic Brain Injury Using a Physical Head Model*, in *Stapp Car Crash Journal, Vol 53*, A.I. King, J.W. Melvin, and L.W. Schneider, Editors. 2009. p. 215-227.

33. Hyde, D., *ConWep " Conventional weapons effects program"*, 1992, ERDC Vicksburg MS.

34. Palchesko, R.N., et al., *Development of polydimethylsiloxane substrates with tunable elastic modulus to study cell mechanobiology in muscle and nerve.* Plos One, 2012. **7**(12).

35. Sogbesan, E., *Design and analysis of blast induced traumatic brain injury mechanism using a surrogate headform: instrumentation and outcomes*, in *Mechanical & Materials Engineering*2011, University of Nebraska-Lincoln.

36. Ruan, J.S., T. Khalil, and A.I. King, *Human head dynamic-response to side impact by finite-element modeling.* Journal of Biomechanical Engineering-Transactions of the Asme, 1991. **113**(3): p. 276-283.

37. Pettikiriarachchi, J.T.S., et al., *Biomaterials for brain tissue engineering.* Australian Journal of Chemistry, 2010. **63**(8): p. 1143-1154.

38. Neveen Awad, W.W.E.-D., and Ammar Gilani, *Compressed air-driven shock tube system to simulate blast-induced mild traumatic injuries*: Submitted July 2014 to Shock Waves Journal

39. Chandra, N., et al., *Evolution of blast wave profiles in simulated air blasts: experiment and computational modeling.* Shock Waves, 2012. **22**(5): p. 403-415.

40. Engelhard, C.W.a.K., *Pathophysiology of traumatic brain injury.* British Journal of Anaesthesia 2007. **99**(1): p. 4–9

41. Sabet, A.A., et al., *Deformation of the human brain induced by mild angular head acceleration.* Journal of Biomechanics, 2008. **41**(2): p. 307-315.

3.8 List of Tables

3.9 List of Figures

Figure 4.10: (a) Average Positive Peak Pressure (kPa). (b) Average Positive Impulse (kPa.ms) of three Brain Model orientations (Right side, Back, and Oblique 45^{o}) at 500 mm.

Figure 4.11: (a) Average Positive Peak Pressure (kPa). (b) Average Positive Impulse (kPa.ms) of three Brain Model orientations (Right side, Back and Oblique 45^{o}) at 1000 mm.

Figure 4.12: (a) Average Positive Peak Pressure (kPa). (b) Average Positive Impulse (kPa.ms) of three Brain Model orientations (Right side, Back, and Oblique 45^{o}) at 1500 mm.

Figure 4.13: Pressure waveform at three different locations: Shock tube exit, PT mounted on air-foil board and RPT inside the brain model.

Figure 4.14: (a) Acceleration profiles for the three Brain Model orientations. The accelerometer was facing the shock tube opening at 1500 mm. (b) Average of the acceleration positive and negative values for three brain model orientations at four distances from shock tube exit.

Table 4.1: Demonstrates a comparison between experimental shock wave characteristics at 150 mm and its Con Wep equivalents.

	Pressure wave-(Shock Tube) at 150 mm	**Con Wep (68 g of TNT at 2745 mm)**
PPP (kPa)	58	59
PPD (ms)	1.1	1.26

Table 4.2: Con Wep equivalents to shock tube pressure at four distances

Con Wep	PPP (kPa)	PPD (ms)
150 mm	59	1.26
500 mm	50	1.34
1000 mm	37	1.46
1500 mm	31	1.53

Table 4.3: Positive and negative peak pressure peak recorded at four locations inside the brain model with three different orientations at four distance points from shock tube exit.

Orientation	**Right**								**Back**								**Oblique 45^o**							
Pressure (kPa)	**Right**		**Left**		**Back**		**Front**		**Right**		**Left**		**Back**		**Front**		**Right**		**Left**		**Back**		**Front**	
Distance (mm)	+ve	-ve	+ve	-ve	+ve	-ve	+ve	-ve	+ve	-ve	+ve	-ve	+ve	-ve	+ve	-ve	+ve	-ve	+ve	-ve	+ve	-ve	+ve	-ve
150	104	-	21	-13	20	-11	41	-14	23	-11	19	-13	21	-8	28	-11	26	-7	21	-10	21	-11	36	-11
500	17	-	12	-12	17	-13	18	-16	12	-7	11	-9	10	-5	10	-6	14	-3	10	-7	11	-12	15	-8
1000	8	-	5	-9	8	-12	8	-14	4	-6	4	-6	4	-3	5	-5	5	-4	5	-6	5	-12	6	-4
1500	6	-	3	-9	4	-9	5	-8	3	-8	3	-8	3	-2	4	-5	2	-4	2	-3	3	-6	2	-3

Table 4.4: Comparison between Positive Peak Pressure (PPP), Positive Phase Duration and Positive Impulse (PI) values (± stander deviation and Coefficient of Variation (CV)) at three locations (exit of shock tube, PT mounted on air-foil board and the brain model RPT).

Location of PTs	Shock tube-End	CV	PT-Board at 150mm	CV	RPT-Brain model at 150mm	CV
PPP (kPa)	82.35±3.5	0.04	58 ± 1.4	0.02	104 ± 7.5	0.07
PPD (ms)	1.24±0.2	0.16	1.10 ± 0.01	0.009	0.38 ± 0.004	0.01
PI (kPa.ms)	49 ± 0.25	0.005	13 ± 0.27	0.02	14.6 ± 0.11	0.008

Table 4.5: Comparison between acceleration average values (± stander deviation and Coefficient of Variation (CV)) for three orientations at four distances from shock tube exit.

Acceleration (g)	**Right**				**Back**				**Oblique 45^{o}**			
Distance (mm)	**+ve**	**CV**	**-ve**	**CV**	**+ve**	**CV**	**-ve**	**CV**	**+ve**	**CV**	**-ve**	**CV**
150	311±4.45	0.01	-332±23.8	0.07	225±88	0.4	-148±70	0.4	173±6.8	0.04	-125±44	0.3
500	113±4.2	0.04	-145±2.8	0.02	11±4.3	0.3	-19±8.5	0.2	7.4±0.2	0.02	-5.7±0.5	0.08
1000	17±2	0.12	-27±3	0.1	4.8±0.08	0.01	-1.9±0.1	0.05	8.7±1.3	0.15	-4.6±0.9	0.2
1500	7.1±0.09	0.01	-2.8±0.37	0.1	3.9±0.2	0.06	-9.7±0.47	0.05	7±1.8	0.25	-8.9±2.6	0.3

Figure 4.1: Silicone gel brain model after curing in a plastic brain mold

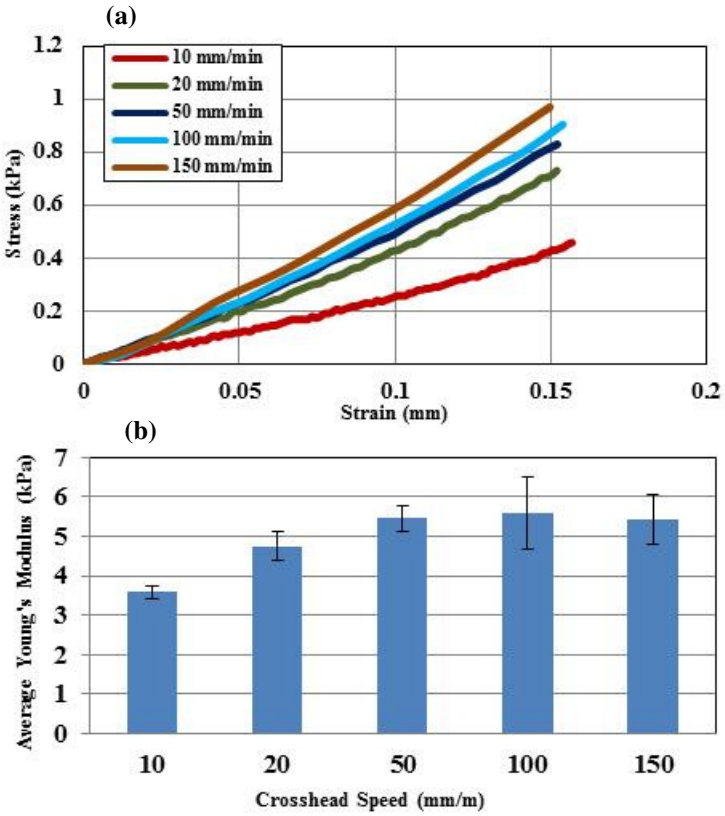

Figure 4.2: The results of Silicone gel compression test: (a) stress-strain curve and (b) average of young's Modulus (kPa)

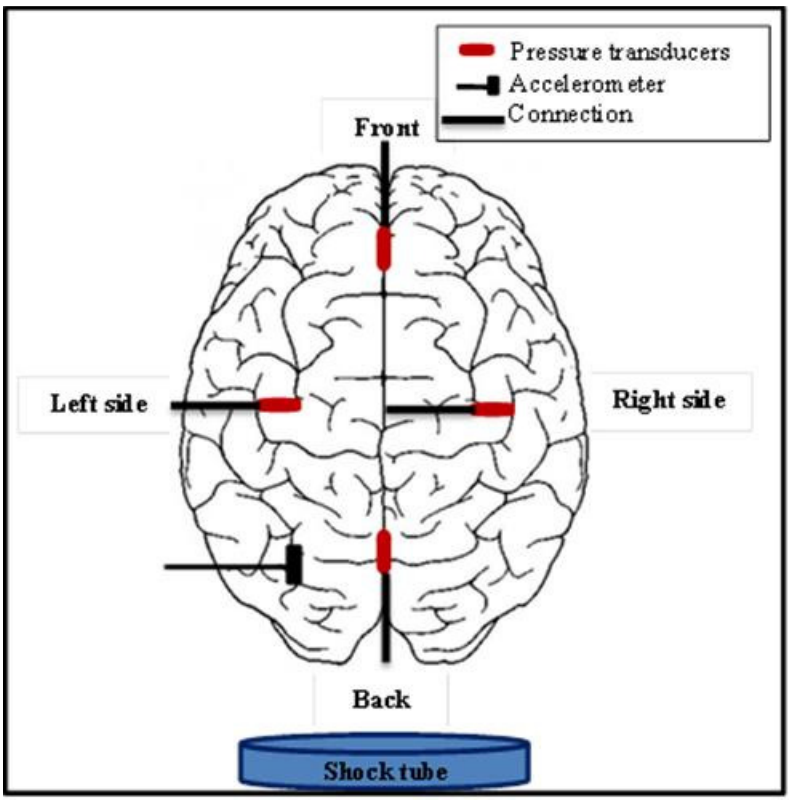

Figure 4.3: Schematic diagram shows the pressure transducers and the accelerometer locations in relation to the shock tube opening. It also demonstrates the back orientation of the brain model as an example

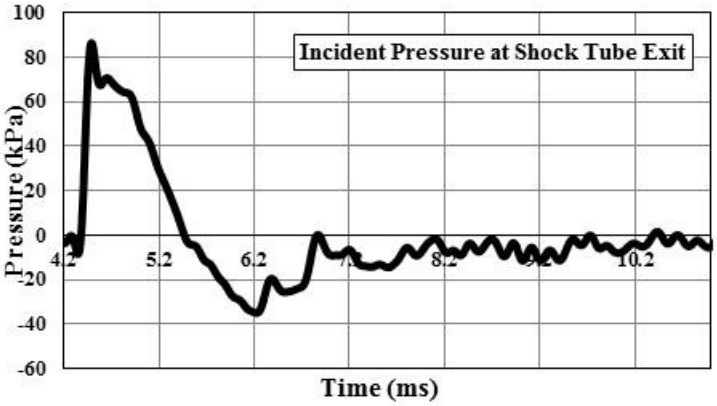

Figure 4.4: Incident shock wave profile measured at the shock tube exit.

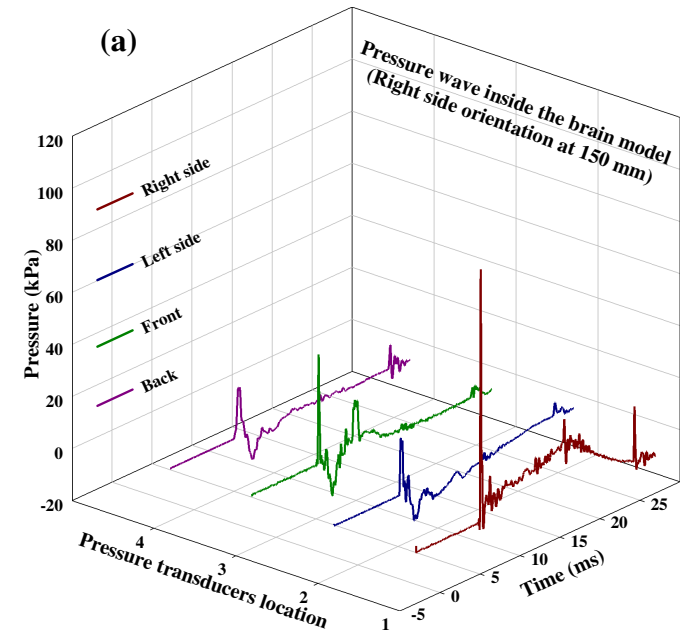
(a)
Pressure wave inside the brain model
(Right side orientation at 150 mm)
Right side
Left side
Front
Back
Pressure (kPa)
120
100
80
60
40
20
0
-20
Pressure transducers location
4
3
2
1
Time (ms)
-5
0
5
10
15
20
25

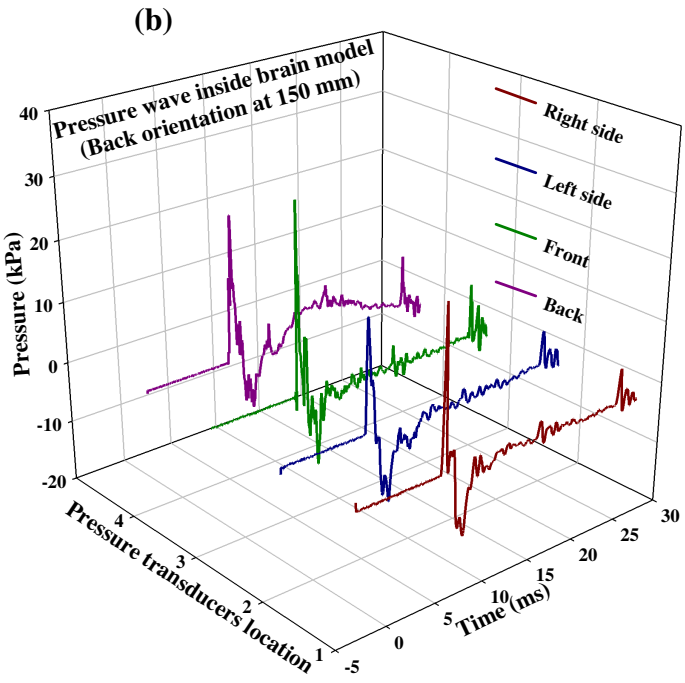
(b)
Pressure wave inside brain model
(Back orientation at 150 mm)
Right side
Left side
Front
Back
Pressure (kPa)
40
30
20
10
0
-10
-20
Pressure transducers location
4
3
2
1
Time (ms)
-5
0
5
10
15
20
25
30

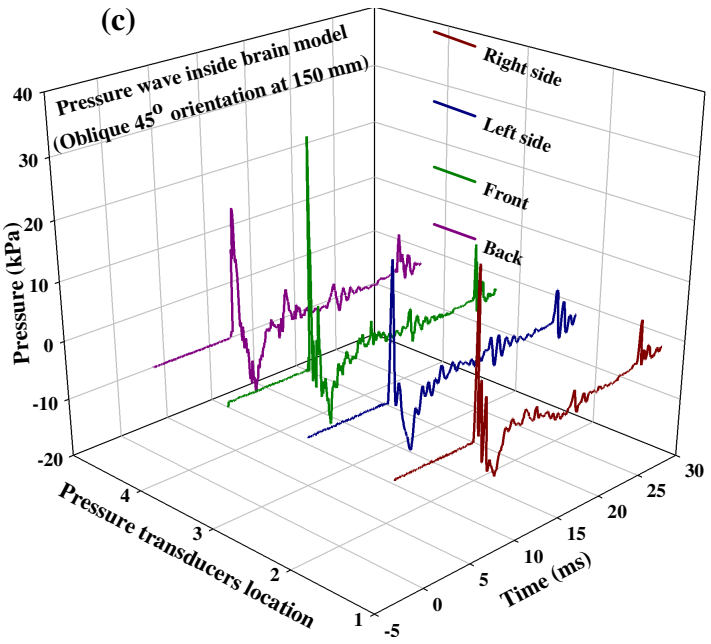

Figure 4.5: Pressure wave profile within the brain model after exposure to simulated blast shock wave at 150 mm from the shock tube exit with three brain model orientations right side (a), back (b) and oblique 45° (c)

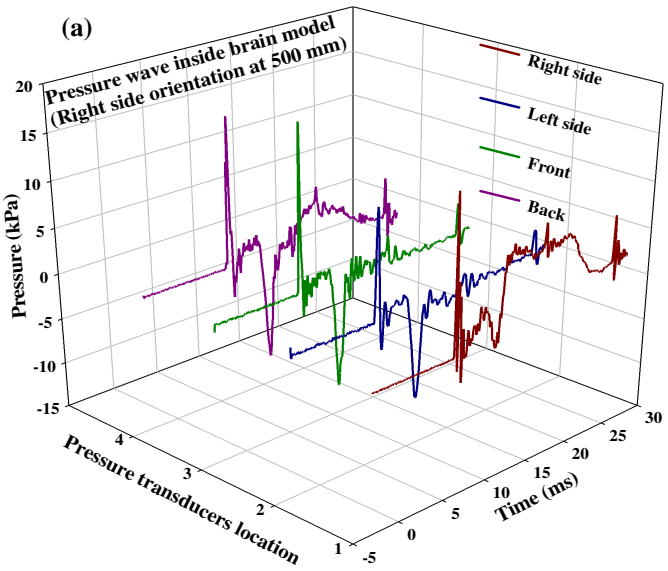
(a)
Pressure wave inside brain model
(Right side orientation at 500 mm)
Right side
Left side
Front
Back
Pressure (kPa)
20
15
10
5
0
-5
-10
-15
Pressure transducers location
4
3
2
1
Time (ms)
-5
0
5
10
15
20
25
30

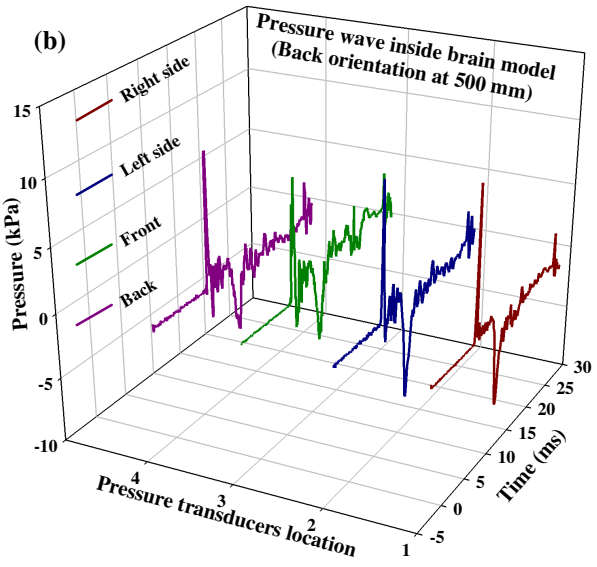
(b)
Pressure wave inside brain model
(Back orientation at 500 mm)
Right side
Left side
Front
Back
Pressure (kPa)
15
10
5
0
-5
-10
Pressure transducers location
4
3
2
1
Time (ms)
-5
0
5
10
15
20
25
30

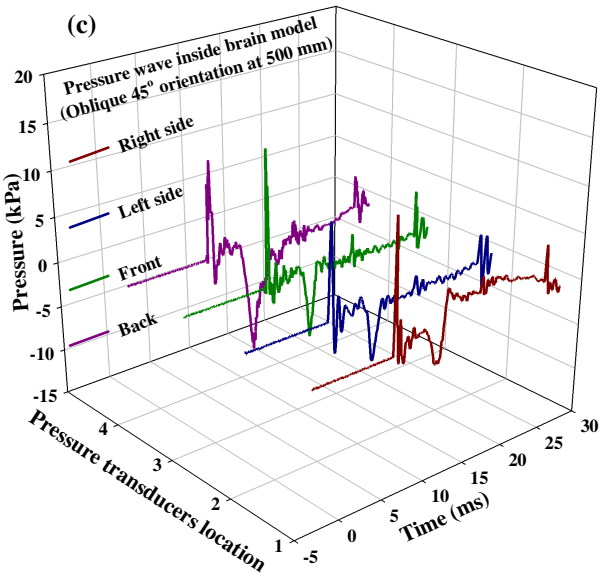

Figure 4.6: Pressure wave profile within the brain model after exposure to simulated blast shock wave at 500 mm from the shock tube exit with three brain model orientations right side (a), back (b) and oblique 45^{o} (c)

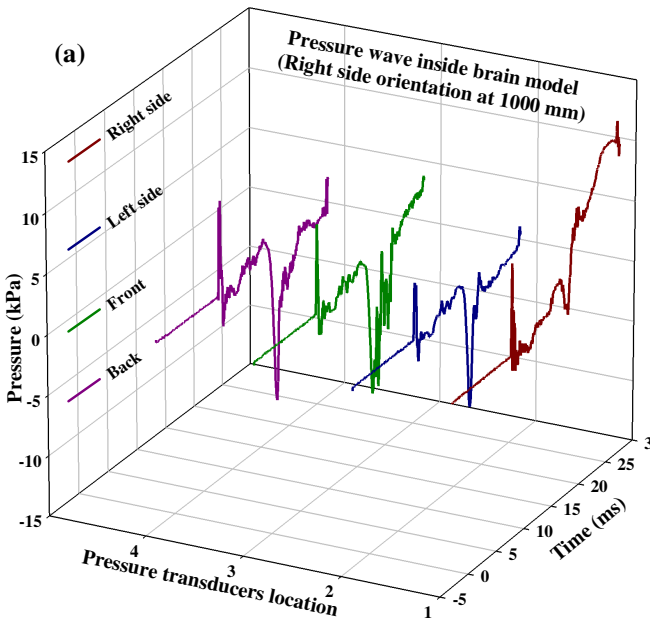
(a)
Pressure wave inside brain model
(Right side orientation at 1000 mm)
Right side
Left side
Front
Back
Pressure (kPa)
15
10
5
0
-5
-10
-15
Pressure transducers location
4
3
2
1
Time (ms)
25
20
15
10
5
0
-5

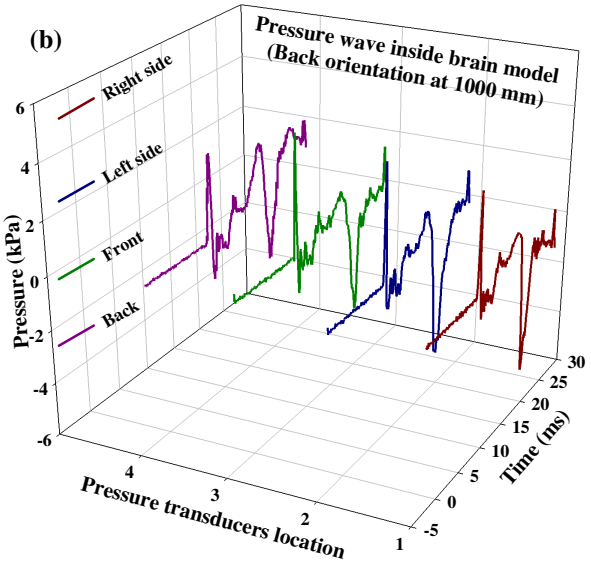
(b)
Pressure wave inside brain model
(Back orientation at 1000 mm)
Right side
Left side
Front
Back
Pressure (kPa)
6
4
2
0
-2
-4
-6
Pressure transducers location
4
3
2
1
Time (ms)
30
25
20
15
10
5
0
-5

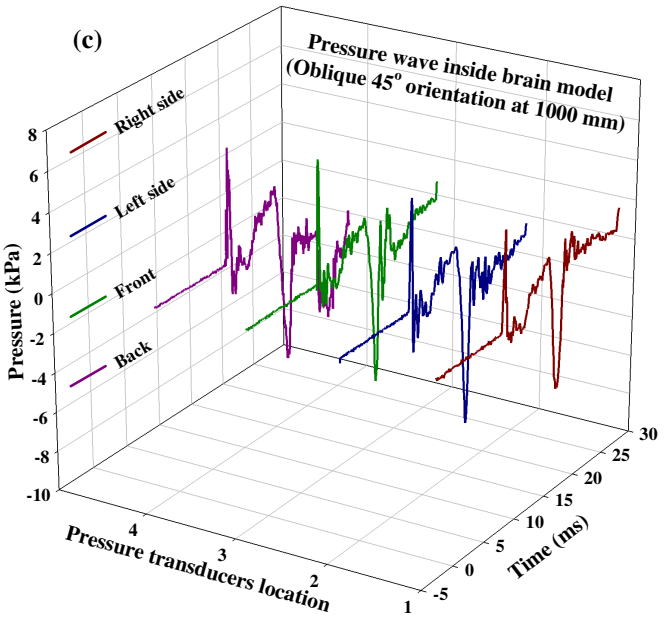

Figure 4.7: Pressure wave profile within the brain model after exposure to simulated blast shock wave at 1000 mm from the shock tube exit with three brain model orientations right side (a), back (b) and oblique 45° (c)

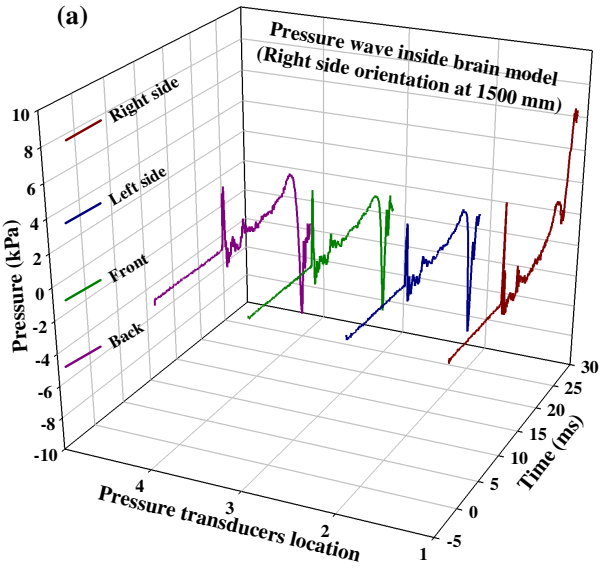
(a)
Pressure wave inside brain model
(Right side orientation at 1500 mm)
Right side
Left side
Front
Back
Pressure (kPa)
10
8
6
4
2
0
-2
-4
-6
-8
-10
Pressure transducers location
4
3
2
1
Time (ms)
30
25
20
15
10
5
0
-5

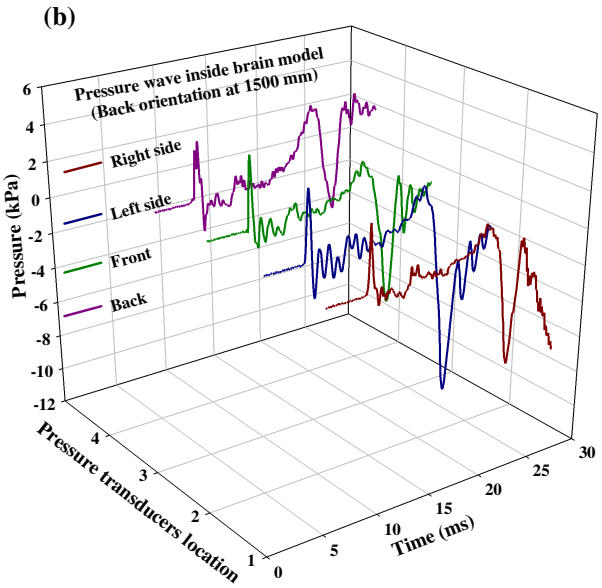
(b)
Pressure wave inside brain model
(Back orientation at 1500 mm)
Right side
Left side
Front
Back
Pressure (kPa)
6
4
2
0
-2
-4
-6
-8
-10
-12
Pressure transducers location
4
3
2
1
Time (ms)
0
5
10
15
20
25
30

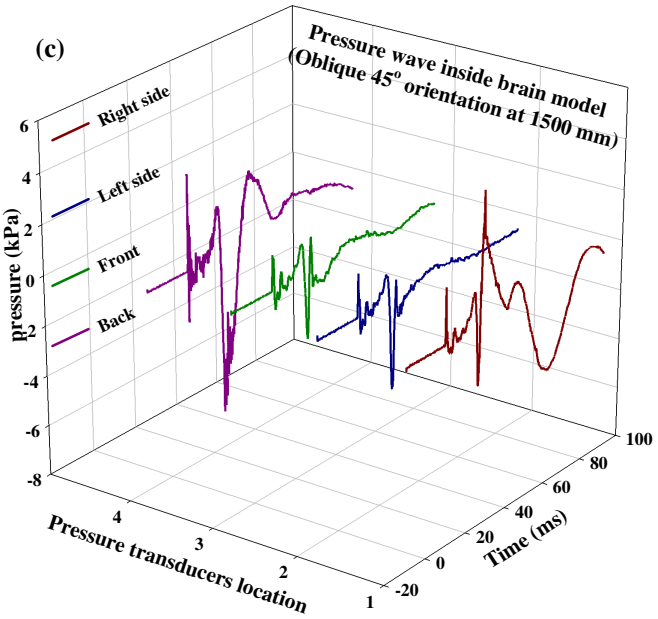

Figure 4.8: Pressure wave profile within the brain model after exposure to simulated blast shock wave at 1500 mm from the shock tube exit with three brain model orientations right side (a), back (b) and oblique 45° (c)

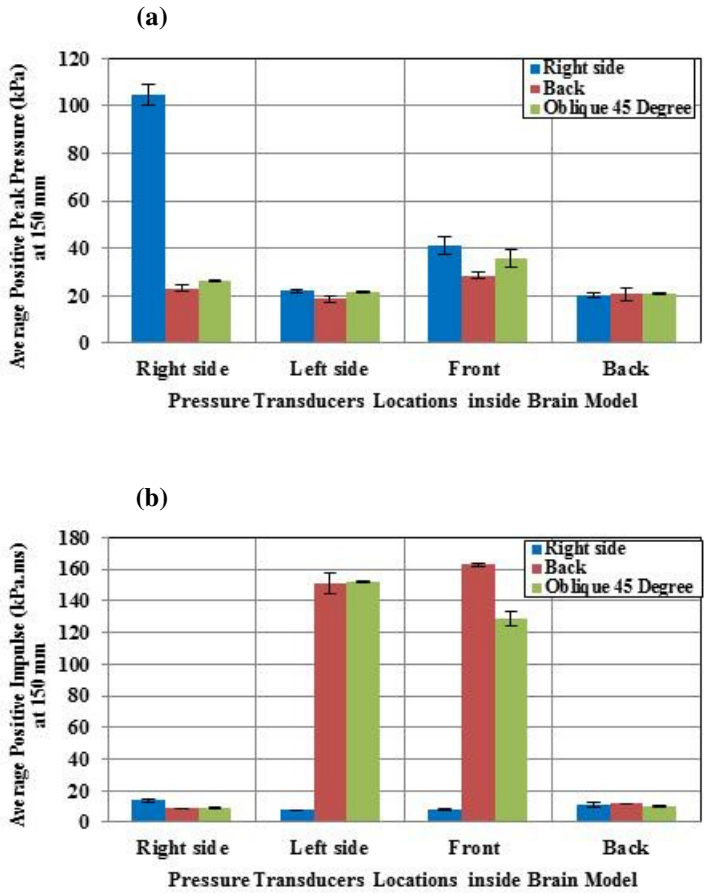

Figure 4.9: (a) Average Positive Peak Pressure (kPa). (b) Average Positive Impulse (kPa.ms) of three Brain Model orientations (Right side, Back, and Oblique 45^{o}) at 150 mm

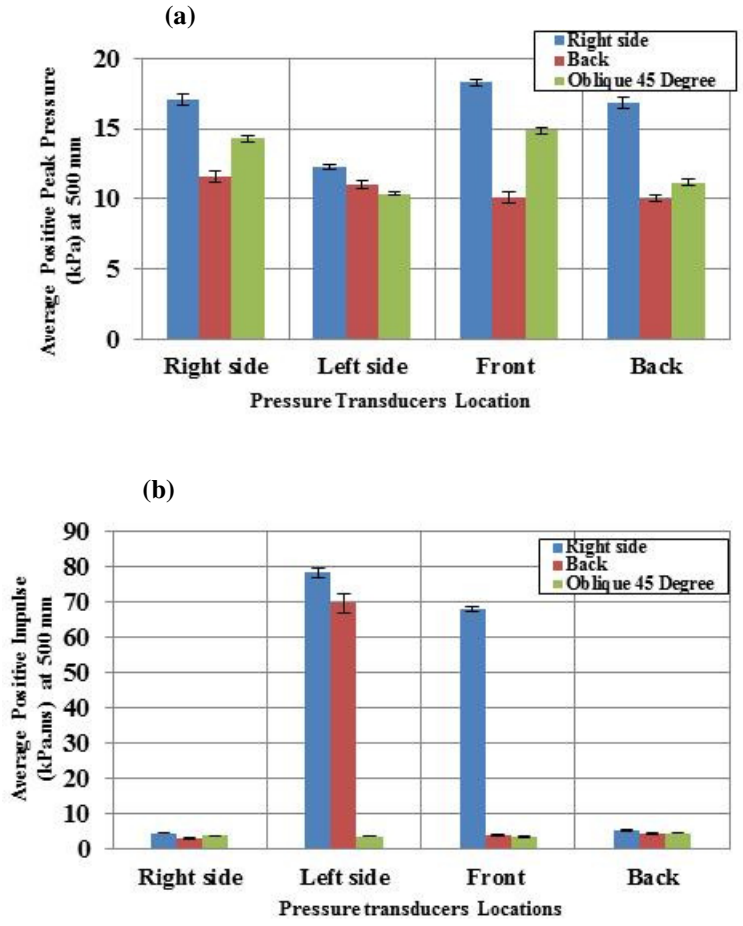

Figure 4.10: (a) Average Positive Peak Pressure (kPa). (b) Average Positive Impulse (kPa.ms) of three Brain Model orientations (Right side, Back, and Oblique 45^{o}) at 500 mm.

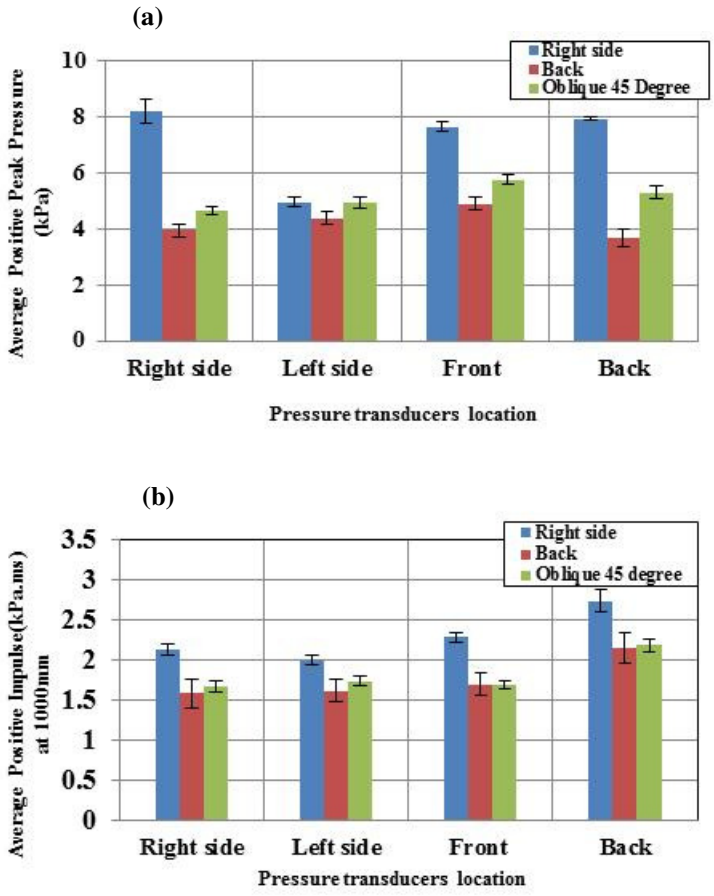

Figure 4.11: (a) Average Positive Peak Pressure (kPa). (b) Average Positive Impulse (kPa.ms) of three Brain Model orientations (Right side, Back and Oblique 45^{o}) at 1000 mm

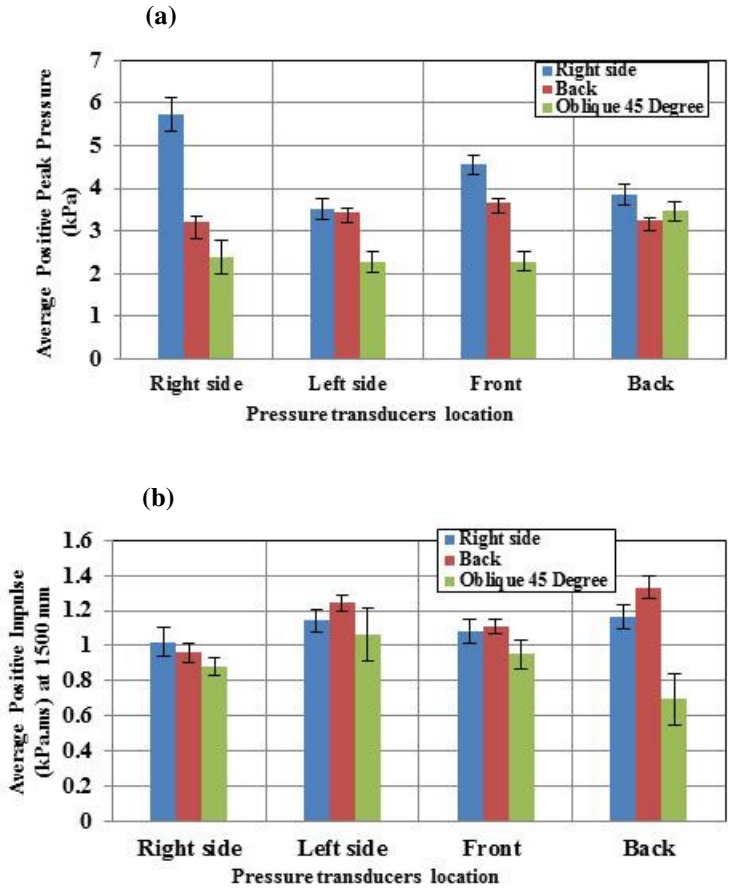

Figure 4.12: (a) Average Positive Peak Pressure (kPa). (b) Average Positive Impulse (kPa.ms) of three Brain Model orientations (Right side, Back, and Oblique 45^{o}) at 1500 mm.

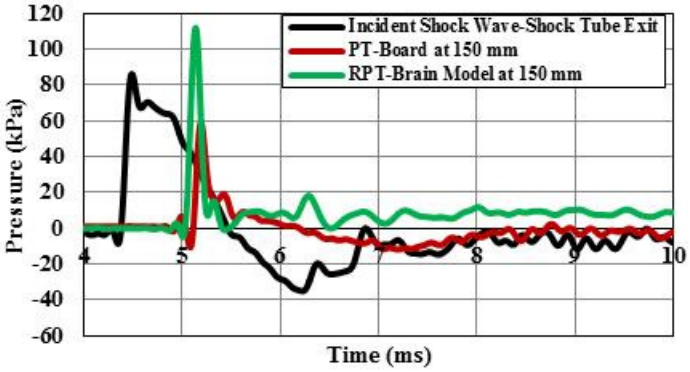

Figure 4.13: Pressure waveform at three different locations: Shock tube exit, PT mounted on air-foil board and RPT inside the brain model

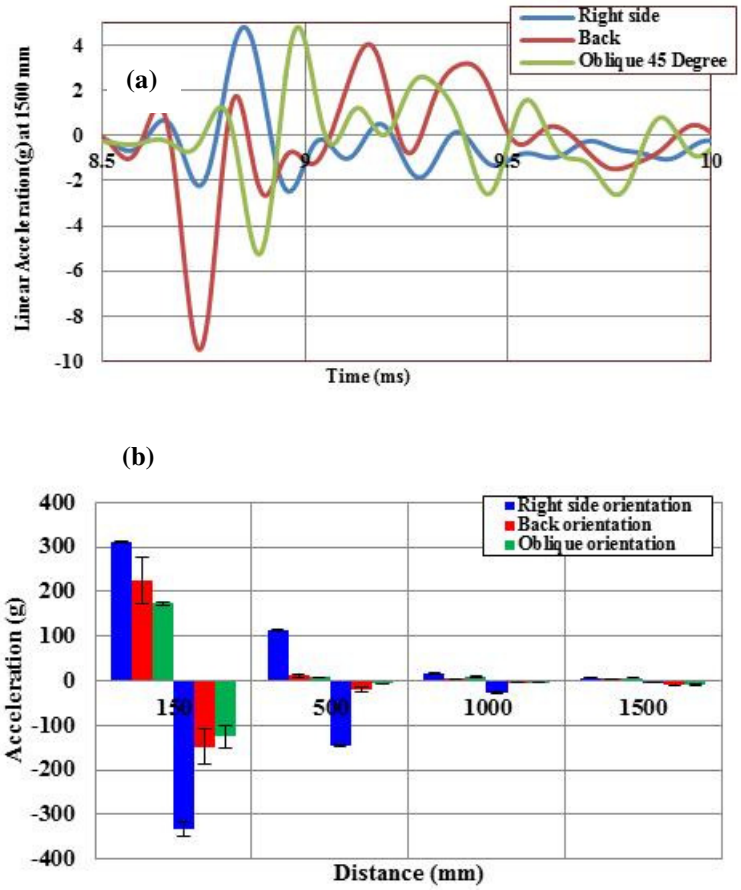

Figure 3.14: a) Acceleration profiles for the three Brain Model orientations. The accelerometer was facing the shock tube opening at 1500 mm. b) Average of the acceleration positive and negative values for three brain model orientations at four distances from shock tube exit.

Chapter 5: A physical head and neck surrogate model to investigate blast-induced mild traumatic brain injury

Neveen Awad, Wael W. El-Dakhakhni, Ammar Gilani

5.1 Abstract:

Introduction: Mild traumatic brain injury (m-TBI) resulting from the exposure to a blast shock wave is a challenging problem due to the broad long-term neurological deficits on the victims. The blast related injury is not only due to the prevalence of military conflicts, but also due to increase terrorist attacks and domestic/industrial accidents. The mechanisms of blast-induced mild traumatic brain injury (BImTBI) have been controversial for a long time and nowadays are one of the most attentive topics among the neurotrauma researches.

Materials and Methods: A physical head and neck model (PHNM) equipped with a surrogate gel brain was developed and its dynamic responses to a blast wave were evaluated using a predesigned compressed air-driven shock tube. The neck model was constructed and tuned to simulate the actual human neck stiffness. The history of intracranial pressure (ICP) at different locations within the brain was monitored with four miniature pressure transducers (PTs). The acceleration of the head as well as the brain model was recorded using two accelerometers mounted internally and outside the PHNM. The shock wave effects on the PHNM were examined at three distances from shock tube exit (150, 500 and 1000 mm) for four orientations of PHNM (front, back, left side and oblique 45^{o}).

Results: The PHNM was exposed to free-field blast tests with controlled reliable Positive Peak Pressure (PPP). The ICP amplitudes and profiles as well as the acceleration results vary according to the PHNM locations and orientations with respect to shock tube exit.

Conclusions: The most vital parameters of ICP wave profiles including PPP, positive phase duration (PPD), and positive impulse (PI) values were greatly affected by the PHNM locations/orientations with respect to the shock tube exit. The skull flexure response as a result of the blast wave/head interaction plays an important role in TBI by magnifying ICP. The significant increase of the intracranial negative pressure component values is hypothesized as the possible mechanism of the brain tissue cavitation and subsequent neurotrauma.

Keywords:

Blast-induced mild traumatic brain injury, Brain biomechanics, Explosions, intracranial pressure wave, physical head and neck model, Shock tube

5.2 Introduction

Exposure to a blast shock wave can result in brain damage with serious neurological manifestations. Clinical studies reported that emotional and cognitive abnormalities are the most frequent long-term impairments after mild blast injury. In general, human body injuries can occur when the degree of the biological system deformation exceeds its maximum injury tolerance, thus resulting in anatomical and physiological abnormalities [1]. Therefore, it is crucial to better understanding the injury mechanisms and define the brain responses in order to improve the protection techniques

and therapeutic approaches [2-4]. Nevertheless, there are limited information about the main causes of BImTBI, but wide range of related researches have suggested various mechanisms by which the primary blast wave may directly and indirectly damage the brain [5-7]. This includes the generation of shearing stresses in brain tissues and subsequent diffuse axonal injury (DAI) as a result of a shock wave infiltration at the gray-white matter interface [8, 9]. Another theory that has been postulated is the thoracic mechanism [10], whereas such mechanism may result in multi pathophysiological responses secondary to the lungs hyperinflation from blast overpressure infiltration. A vasovagal response is one of the most common subsequences, which triggers different body reactions including apnea, bradycardia, hypotension and subsequently cerebral hypoxemia [11]. On the other hand, mechanisms of the BImTBI were to cause brain damage by the direct head exposure to blast shock wave, the skull flexure and bulk acceleration of the head [12]. Previous studies using three-dimensional hydrodynamical simulations showed that the effect of non-lethal blast wave on the head may produce skull deformation by 50 μm [13]. This developed mechanical load is enough to produce damage to the brain tissues. In addition, the mechanisms of BImTBI may induce focal and/or diffuse brain injuries [14]. Brain edema is also an important example of the diffuse TBI lesions that occurs secondary to blast injuries [15]. The most common cause of developing the brain edema is the disruption of blood brain barrier (BBB) and the subsequent development of vasogenic edema [16]. The latter occurs when the water movement increase from the blood vessels to extracellular space in the brain parenchyma [17]. The brain edema is one of the most vital neurological abnormalities as it contributes

in many of central nervous system manifestations, such as elevation of ICP, impairment of cerebral perfusion and oxygenation as well as other ischemic brain lesions [18].

Experimental studies of traumatic brain injury mechanisms present challenge to be performed using in vivo or in vitro techniques. This is not only due to essential ethical and technical issues involving use of animals but also due to the major differences between the tested brain models and the human brain dynamic properties and responses [19]. Therefore, experimental study of human brain response to blast waves can only be achieved by creating physical head models with properties simulating those of humans [20]. In fact choosing an appropriate material to develop even a surrogate brain that possesses similar elastic properties to the human brain tissue to be able to study the mechanical mechanisms of blast shock wave on human neurotrauma is a challenge unto itself [21]. In the current research, the PHNM was developed using a surrogate skull and neck where the intracranial cavity is occupied with a silicone gel brain model. As the blast pressure wave can be transmitted through the skin, nasal opening and orbital cavity, a surrogate skin was accurately developed and equipped with nasal and orbital orifices [22]. To be able to monitor the development of pressure wave within the PHNM during blast tests, four PTs were embedded in different locations inside the brain model. In order to capture the inertial response of the PHNM, two accelerometers mounted on the skull and brain gel model were used. Analysis was performed to understand the effects of orientations/distances with respect to the shock tube exit and the resultant ICP as well as the relative acceleration between the brain gel and the PHNM. Tests were performed at

four different PHNM orientations corresponding to the anatomical locations of frontal (front), occipital (back), temporal (left side) and oblique 45° for the left-frontal bones at 150, 500, and 1000 mm with respect to the shock tube exit. The ICP was measured at the frontal (front), occipital (back), right temporal (right side) and left temporal lobes (left side) of the brain model. The accelerometers were attached to the brain and PHNM and aligned to the direction of shock wave propagation. For the current study, the right PT (RPT) was embedded in the brain's temporal lobe, the anatomical site of the limbic system, and slightly tilted toward the frontal lobe. The left PT (LPT) was embedded straight in the middle of the left hemisphere of the brain, while the front PT (FPT) and back PT (BPT) were implanted in the brain front and back in between the two cerebral hemispheres at the same level.

5.3 Materials and Methods

5.3.1 Skull of Physical Head Model

A human male Asian skull, Calvarium cut (BC-092, Bone Clones® Osteological reproduction, Canoga Park, CA 91304 USA) was used to perform the PHNM. The skull weighs about 870 g and has dimensions of 212.5 x 137.5 x 212.5 mm. It is made of polyurethane resin, which is widely used in orthopaedic applications due to its ability to mimic the human bone properties and geometry [23]. The polyurethane resins Young's modulus is about 6-7.5 GPa [24, 25], while the actual cortical bone is in the range of 7.46-12 GPa [26, 27].

5.3.2 Surrogate Brain Preparation

The method of preparing the brain model was described in previous study [28]. A plastic brain mold (SKS Sibley CO., El-Segundo, CA) of 190 x 160 x 100 mm was used to create a surrogate brain with simulated sulci and gyri giving the irregular characteristics of the outer surface of human brain. The brain mold was filled with 1400 g of Sylgard 527 A&B silicone gel which represents the average weight of an adult brain [28]. The two components of the gel were mixed in a one-to-one mass ratio and cured in the plastic mold, for at least one week at room temperature, before experiments commenced.

5.3.3 Structure of Surrogate Neck

Surrogate neck was developed using six steel disks (76 mm diameter) to simulate the cervical vertebrae and to use their centers to pass the sensors wires. Twelve silicone foam rubber rings (61 mm diameter and 9 mm thickness) were used to simulate the intervertebral discs which allow the flexible neck movements and also act as shock absorbers [29]. The physiological and anatomical functions of the intervertebral discs play an important role by which they can influence the head movement after exposure to blast shock wave. Two silicone foam rubber rings were attached on the top of the each steel disk. Between the first and second steel disk, a connection joint was made to allow for the skull flexion and extension movements. While, the second steel disk was connected to the remaining steel disks by four steel cables (0.38 mm diameter). These cables act as tendons that allow the head to move without restriction in all directions (Fig.

5.1). The cables that hold the surrogate neck components were extended to join four metal springs (4 mm aluminum sleeves), that are connected to four fixed hooks (111 x 158 mm). The skull was connected at the foramen magnum to the surrogate neck. Openings were created in the center of the silicone rubber rings, so the PTs' connection wires can go through the center openings of the steel disks as well as the rubber rings. The total neck length starting from the neck model connection with the skull up to the connection with the supported plate at the base was 160 mm. This corresponds to the average neck length of adult human and ought to be an important factor in the subsequent neck stiffness evaluation.[30].

5.3.4 Neck Stiffness Analysis

It is crucial to calibrate the surrogate neck such that it simulates the human neck as accurately as possible. As the dynamic neck stiffness and its corresponding flexion angle are fundamental in governing the movement of the PHNM, the performance of the surrogate neck was analyzed by testing the neck maximum flexion angle as a function of the applied load. The test was conducted using a load cell (22 Kg), an amplifier (1.7g Accel tool # 2273), and a string potentiometer (WPS-250-MK30-P10). In order to flex the neck, a steel cable was connected between the load cell and the skull anterior at the nose level. At the same level but from the back, the string pot was connected to the nose opening posterior (Fig.5.1). Therefore, by pulling the fisher string anterior, the applied force will be recorded by the load cell and the corresponding skull displacement will be measured by the string potentiometer. The corresponding moment (recorded load times the neck-length) and rotation of the skull (arc tan of the neck displacement to the neck

flexing length ratio) are then plotted and the slop of this curve represents the neck stiffness. The neck stiffness can be controlled by changing the number of springs connected to the steel cable (0.38 mm diameter). In the current study, up to four springs in each steel cable were examined to optimize the surrogate neck and to ensure that it performance mimics that of the actual human neck.

5.3.5 Surrogate Skin Preparation

A Linatex® premium rubber sheet (Dunrite® Rubber, Hamilton, ON Canada) with 1.5 mm thickness was used to cover the PHNM and simulate the skin. This material possesses similar elastic properties to human skin. The human skin and linatex rubber density values are 1.2 g/cc and 0.98 g/cc, while the tensile strength values are 27 x 10^3 kPa and 21 x 10^3 kPa, respectively. [31, 32]. The simulated skin was equipped with openings at the anatomical location of nasal and orbital orifices, which can act as paths for the shock wave. On the other hand, the exposed orbital cavities were occupied with cured silicone gel (sylgard 527) to resemble the eye globes.

5.3.6 Pressure-Time Profile and Acceleration Measurements of the PHNM

Four pressure transducers (PTs) capable of measuring transient/repetitive dynamic events with acceleration-compensation (Model type-2115B, Kistler Instrument Corp., Armherst NY 14228) were utilized to monitor ICP. The PTs were embedded intraparenchymally within the brain model at four locations (frontal (front), occipital (back), right temporal (right side) and left temporal lobes (left side)). Thereby, the diaphragm parts were inserted internally and the connector parts were projected

externally to be connected to the data acquisition systems. The LPT was placed near the upper layer of the brain model, while the RPT was inserted near its base. The FPT and BPT were inserted in between the two hemispheres at the same level within the brain model. Additionally, two accelerometers (4 x 2x 1 mm, weight 1.3 g, range ± 500 g, model 8732A500 micro K-Shear, Kistler Instrument Corp., Armherst NY 14228), were used to measure the brain model and the head acceleration. The two accelerometers were connected to the data acquisition system and were oriented in each test to always face the shock tube opening at any given orientation.

5.3.6.1 Data Acquisition System

Two identical 500 MHz high-speed data acquisition systems (Tektronix TDS744A) with four channels each were linked together and used to record the pressure/acceleration waveforms. To ensure signal capturing during the shock wave development, one of the data acquisition systems was set to act as the main trigger and the other as the auxiliary trigger.

5.3.6.2 Compressed Air-Driven Shock Tube

The PHNM experiments were performed using a compressed air driven shock tube that was developed and described in previous studies [28, 33]. The horizontally mounted shock tube consists of compression and expansion chambers of equal and constant cross section but have different length. The first chamber (shorter) contains compressed air, while the second volume (longer) is the expansion chamber, which is open to the

atmosphere. The chambers are 250 mm and 2000 mm long, respectively, while their outer diameter is 203 mm. The two chambers are separated by a metallic diaphragm and are tightly joined together using 16 steel bolts of 19 mm diameter. When the steel diaphragm ruptures suddenly due to extensive plastic deformation, the pressurized air is abruptly exposed to the area of low pressure. This creates a shock wave that propagates into two directions, the low pressure volume (expansion chamber) opened to the surrounding atmosphere and a rarefaction or expansion wave that propagates into the high pressure volume (compression chamber).

5.3.7 Steel Diaphragm Preparation

The technique by which the steel diaphragms are utilized to perform the blast test was discussed before in previous studies [28, 33]. Steel diaphragms of 0.127mm thick (Branded® Shim, Downers Grove, IL60515 USA) were prepared by cutting 16 holes using a punch set tool (SP-9 fractional, Trinity Brand Industries, INC, USA). The holes were created to match the bolts' location at the compression and expansion chambers of the compressed air-driven shock tube.

5.3.8 Statistical Analysis

All blast experiments were performed at least in triplicate for each PHNM orientation and distance, to be able to prove the reliability of the shock wave effects on the brain. Comparative analyses were performed with SPSS 13.0 for Windows operating system using One-Way ANOVA test to evaluate the variance of positive pressure values among the experiments. $P < 0.05$ was considered statistically significant.

5.4 Results and Discussion

Due to the increase number of incidents related BImTBI, many studies have been conducted to elucidate the various etiological mechanisms for better short and long-term injury managements. Some of the suggested injury mechanisms were attributed to direct cranial transmission, skull flexure; acceleration/deceleration and brain cavitation [34, 35]. The current research focuses on understanding the ICP responses to simulated blast shock wave in the range that can induce mTBI.

5.4.1 Characterization of Resultant Blast Shock Waves

The aim of the current study is to investigate the mechanical responses of PHNM to simulated blast shock waves. The experiments were performed by utilizing the predesigned and calibrated compressed air-driven shock tube at the Applied Dynamics Lab, McMaster University. The consistent shock waves were obtained by controlling the compressed air triggering pressure using a pre-tested steel diaphragm with a thickness of 0.127 mm [33]. This pressure causes the steel diaphragm to rupture resulting in the instantaneous release of the pressured air from compression chamber to the expansion chamber. The results of previous calibration study as well as the current study show that the triggering pressure in each blast test was about 204 kPa. Moreover, the pressure profiles at the tested locations inside and outside shock tube follow the Friedlander waveform fairly well. This blast experimental setup minimizes the variation of blast loading parameters for the subjects tested inside or outside shock tube [36].

5.4.2 Measurements of Surrogate Neck Stiffness

The neck plays a vital role in TBI, as it can transmit enough energy to the head, even without a direct impact to the head itself, inducing brain injury [37]. In current study, the stiffness of the neck was measured using a test setup performed by attaching 22 kg load cell to the head anterior and a string pot posterior at the same level of the load cell. Figure 5.2 shows the relationship between the moment applied on the skull and the corresponding neck flexion angles. It was reported that the normal range of the neck flexion angle is 15° – 30° depending on the cervical vertebrae level [29, 38] and Figure 5.2 suggested that using one spring per each tendon (the four steel cables) allows for this range of movement. In addition, Figure 5.3 shows the resultant average of the neck stiffness by using up to four springs. The results show that by utilizing one spring, the measured neck stiffness of the PHNM resembles the actual neck stiffness [20]. The developed surrogate neck allows simulating an important part of the blast mechanical mechanism as the skull flexure resulting from direct blast wave impact contributes to the brain damage [13]. This effect occur secondary to the blast pressure propagation into the brain after head movements [7, 39]. For instance, as the shock wave propagates towards the PHNM, the neck moves in the wave direction causing coup and counter coup injury of the brain. Once the shock wave front reaches the PHNM sudden head movement occurs. With further wave propagation, the shock front engulfs the PHNM, allowing a gradual pressure wave transmission through the skull and ultimately the brain. This will

eventually contributes to the intensity of the pressure wave which builds up inside the brain model and this will be discussed further in the following sections.

5.4.3 Intracranial Pressure Response

The ICP measured during blast tests is highly dependent on the exact location of the PTs within the brain gel model relative to the shock wave direction and the skull geometry as well as the variations in the bones thicknesses. For instance, the frontal and occipital bones are thicker (6.3, 7.7 mm, respectively) than the temporal and parietal bones (3.9, 5.8 mm, respectively) [40]. Figure 5.4 shows the PHNM with the PTs embedded inside the brain model. The ICP waves measured by the embedded PTs that are aligned with the incoming blast wave for the four tested orientations are shown in Figure 5.5. For each orientation, the test was conducted at three different locations relative to shock tube exit. For a given orientation, the amplitudes of the PPP gradually decrease as the PHNM gets far from shock tube exit. Furthermore, the ICP waveforms are dependent on the PHNM orientation with respect to the incoming blast wave front. For instance, with the front orientation (Fig. 5.5a) the measured pressure wave by FPT shows a distinct peak followed by a gradual decay that tracks Friedlander wave. On the other hand, the pressure waveforms measured by the BPT, LPT, and RPT (Fig. 5.5b, c, and d, respectively) at 150 and 500 mm exhibited different behavior. As can be observed from these plots, once the peak overpressure is reached, the pressure decays very rapidly and is directly followed by negative pressure phase. At 1000 mm, a time interval appears between the PPD and negative phase duration (NPD). Therefore, after PPD ends, the

pressure wave slightly oscillates about atmospheric pressure then the NPD starts. The duration of this period varies with respect to the PHNM orientation for a given PT location inside the brain model. Additionally, Figure 5.6 demonstrates a comparison between the average values of PPP and NPP (Fig. 5.6a, b, and c) as well as the PPD and PI (Fig. 5.6d, f, and e) measured by the PTs inside PHNM. The figure clearly shows that the pressure waves recorded by BPT, LPT, and RPT have high NPP values compared to FPT at the three tested locations for all PHNM orientations. Furthermore, the figure displays the correlation among the pressure wave parameters, PPP, PPD, and PI. By comparing the PPD average values of the pressure waves measured inside the brain model, it is clear that the front orientation had the longest PPD and highest PI for the pressure waves measured by FPT for all locations. This indicates that even if the pressure wave possesses low PPP, damage still can occur depending on the impulse value. Figure 5.7 presents all the measured ICP waves and it clearly shows that the waveforms measured at a given distance and orientation has similar profiles irrespective of the PT location inside the brain model. However, the pressure amplitudes vary depending on the PT location inside brain model as well as the distance from shock tube exit due to the pressure amplitude decay with increasing the shock wave travel path. Moreover, Figure 5.7 shows a distinct signature represented by a small positive, or negative, peak at the very early stage of the measurements and immediately after the blast wave front hits the head. This peak appears near the arrival time of the blast wave front which is about 5 ms, 6 ms and 7.5 ms for tested locations (150 mm, 500 mm, and 1000 mm, respectively). These early peaks show a positive amplitude for the impact site and negative amplitude in

the opposite site which correlates to the coup and countercoup injury sites. Additionally, they are followed by the other significant positive and negative peaks that may be generated as a subsequent effect from the brain translational and rotational movements following the blast and PHNM interactions. This can be associated with the main difference of shock wave direct and indirect impacts. At 150 mm from the shock tube exit (Fig. 5.7-group a), the first positive or negative peaks are more prominent comparing to the other distances. This indicates that for a given blast event, the closer to the blast site, the higher the potential of direct and indirect blast injuries to occur. On the other hand, the more the distance from the explosion location, the lower effect of direct injury and, instead the indirect blast impact will be the leading cause of injury. Moreover, the external shock wave load can also lead to skull deformation, which in turn applies an additional pressure on the brain and subsequently contributes in the sudden change of intracranial pressure. Further, at 500 mm the developed ICP waves for all orientations display a bifid PPP with small negative pressure in between. This is followed by NPD, which is characterized by the large amplitude of NPPs comparing to the PPP at the same distance (Fig. 5.7-group b). Figure 5.7-group c presents the developed pressure waves at 1000 mm. For this group, the PPD is followed by a period of oscillation around atmospheric pressure and the NPD are associated with a relatively large NPP equating to the PPP at the same distance. In general, the development of positive and negative pressures creates a compression and tension regions in the brain at the coup and counter coup sites. These abrupt changes of intracranial pressures at different brain regions are considered one of the main causes of the brain injuries. For instance, DAI, which may

develop as a result of the changes in the cell volume and density or due to the relative movement of the brain tissues at different speeds when exposed to blast [9, 41]. In addition, the significant increase in the negative pressure inside the brain model is considered as the possible mechanism of the intracranial cavitation that may induce blood vessels rupture and subsequently the brain tissue and cellular damage [42].

5.4.4 Comparison of Positive Peak Pressure and Positive Impulse

The analysis of the pressure waves for the four tested orientations demonstrates that the average values (Fig. 5.8a, b, and c) varied depending on the PTs locations inside the brain model at given distances and orientations with respect to the shock tube. The right side and back locations experienced higher amplitude compared to the left side and front for each tested distance from shock tube. For instance, the average pressure values recorded at RPT, BPT, LPT, and FPT for the front orientation at 150 mm were 12.25, 11.9, 5.7, and 7.7 kPa, respectively. As the RPT is located in the anatomical site of the temporal lobe and showed higher average PPP, this suggests a potential brain injury at this location. The hippocampus, one of the limbic system structure within the temporal lobe, plays a significant role in the long-term memories and its impairment results in memory deficit and cognitive dysfunction [43]. This finding is consistent with a previous study [39], in which the head and neck flexion loads (blast wave impacts to the back PHNM) induced visible brain damage comparing to the extension load (blast wave impacts to the front PHNM). The blast/PHNM interaction is a function of the total impulse (area under the pressure-time profile) [44]. This suggests that the PPD, which is

part of the impulse calculation, has a vital role in determining the intensity of the shock wave effects and subsequent brain injury. The measurements at FPT depict longer PPD at each tested distance for front orientation compared to other PTs readings. Subsequently, the average values for the same orientation at FPT revealed higher value (10.2 kPa.ms) in correlation to the back, right side and left side measurements (7.2, 8.3. and 4.2 kPa.ms, respectively). In contrast to the average PPP values, the PI results were apparently dependent on the location and orientation with respect to shock tube exit. For instance, for front orientation at 150 mm a high PI value was measured at FPT, while both back and oblique orientations showed highest PI at BPT (Fig. 5.8d). Finally, for a given distance, the left orientation depict higher PI value at LPT (Fig. 5.8d). At 500 mm, the highest PI values were associated with different orientations and location of PT inside the brain model. High PI values were calculated at FPT and RPT for front orientation, BPT with back orientation, and LPT for oblique as well as left orientations (Fig. 5.8e). At 1000 mm (Fig. 5.8f) the highest PI values where at FPT, BPT, and RPT, while LPT measured pressure was relatively low for each tested orientation. In general, the parameters PPP, PPD and PI of blast wave and subsequently the intracranial pressure are considered the key parameters needed to describe root cause of BImTBI [1].

5.4.5 PHNM Acceleration Analysis

Blast shock wave generated from an explosion have the ability to induce significant brain damage without visible signs of external head injuries [45]. When the shock wave propagates in the air away from the source, it generates positive pressure phase as well as

a blast wind followed by a negative pressure phase [46]. Each blast shock wave component plays an important role in primary TBI due to the development of blast mechanical forces applied on the head and then transmitted to the brain tissues [14, 47]. The skull acceleration and the accompanied brain mass inertia resulting from the blast wave is an important mechanism that can induce graded levels of diffuse brain injuries [48]. Both linear and angular accelerations have a crucial role in the TBI due either to the development of pressure gradient or the shear stress respectively [37]. In the current research, the brain and head linear accelerations were monitored using two accelerometers that always align with the shock wave propagation direction at each blast test. The accelerations profiles and subsequent head and neck movement directions changed according to the orientations of the PHNM, which include flexion, extension and lateral flexion for back, front and side or oblique orientations, respectively. Figure 5.9 shows the acceleration profiles of the brain model and the whole PHNM during blast tests at different tested locations and orientations. The amplitude values and patterns of the brain model acceleration showed variations depending on the locations and orientations of PHNM with respect to the propagation of the blast wave. At 150 mm, the front, back and left side orientations showed one acceleration pulse at the arrival time of the blast wave to PHNM, while the oblique orientation displayed three positive acceleration pulses, one at the arrival time (5 ms) and the other two pulses are between the 8^{th} and 9^{th} ms. It was observed that during the oblique orientation test, the head moved in a diagonal direction at the time of the shock wave/head interaction followed by flexion and extension movements. The first peak might be attributed to the PHNM movement in the

same direction as the blast wave propagates, while the latter two peaks on the acceleration plot might be attributed to the subsequent flexion and extension movements. The peak acceleration for the front orientation has the highest value, which followed by the left side, oblique then the back orientation. Nevertheless, the amplitudes of the brain model acceleration decrease for all orientations as the PHNM moves away from the source of the shock wave, they remain higher for the front orientation at 500 mm and for the front as well as the left orientations at 1000mm. The acceleration patterns of the brain model at 500 mm and 1000 mm for all orientation show high frequency content long after the end of the blast wave. This can be attributed to an excessive vibration in the brain gel model. On the other hand, the bulk acceleration of the head displayed different patterns and amplitudes comparing to the brain model at a given distance and orientation. It is observed that the acceleration positive and negative amplitudes are the highest for the back orientation at 150 mm, however, the highest acceleration peaks at 500 mm and 1000 mm are for the left orientation comparing to other peaks at the same distances. By comparing the average positive peak values of the brain model acceleration to the bulk acceleration (Fig. 5.10a & b), it can be clearly shown that the brain model peak accelerations are inversely proportional to the severity of head movements. For instances, the brain model acceleration is higher than that of the PHNM for the front orientation (282 g and 97 g, respectively), while for the back orientation, the PHNM acceleration is higher than the brain model acceleration (425 g and 16 g, respectively). Further, there is an observed correlation between the peak acceleration values and the tested orientations. This is demonstrated mainly at the 150 mm where the brain model peak acceleration

decreases from the maximum value at the front orientation followed by oblique, left side and then back orientations. On the other hand at the same given distance, the PHNM peak acceleration follow the opposite sequence of the brain, as it attains its maximum at the back orientation then decreases as while moving toward the left side, oblique and front orientations. These results emphasize that the linear acceleration plays a significant role in brain injury by its direct effect and by augmenting the transmitted blast wave intracranially. The PHNM can be used for further investigations to validate computational models of BImTBI and address the acceleration and other mechanisms in the brain tissue damage.

5.5 Conclusions

Blast tests were performed using a compressed air-driven shock tube and a physical head and neck model to address the effects of blast shock wave on the human head. The blast test setup proves the ability to provide reliable results inside and outside the shock tube making it suitable to be used in other related BImTBI using wide range of physical head models or animal models. In addition, the experimental data demonstrated the correlation of external blast loading, which is in the range of inducing mild traumatic brain injury, and the internal biomechanical responses. This study provides crucial information that can be used for further studies related to the blast mechanical mechanisms on the brain injury. Results show different patterns and durations of the intracranial pressure histories depending on the PHNM orientations and locations with respect to the shock tube exit. In addition, the ICP results illustrate that the skull flexure,

as a result of blast wave dynamic interaction with the PHNM, can lead to pressure oscillation inside the brain model. On the other hand, the resultant positive and negative pressures in the PHNM were at the levels that can induce a mild traumatic brain injury in animal models, where the brain damage is only detected microscopically with no gross changes [49]. It can be concluded that sudden fluctuations of intracranial pressure may be a dominant injury mechanism in the BImTBI investigated in the current study. This study suggests that the nearer we get to the blast site, both direct and indirect blast injuries will contribute to the total damage within the brain, and as we move away from the explosion location, the effect of direct injury is reduced and the indirect blast impact might be considered the main cause of injury. Additionally, the head movements after shock wave impact may have minimal contribution on the brain linear acceleration. Therefore, more investigations are required to address the relation between the skull movements and the brain angular acceleration. Furthermore, to improve the brain injury prediction, the current study provides valuable quantitative data that can be utilized in a computer simulation of BImTBI. As the traumatic brain injury is a complex problem, better understanding of the blast injury mechanisms is essential for early diagnosis and improves the health management procedures.

5.6 Acknowledgments

The authors gratefully acknowledge Kent Wheeler and Paul Heerema at the Applied Dynamics Lab for their help and useful discussions.

5.7 References

1. Effgen, G.B., et al., *A Multiscale Approach to Blast Neurotrauma Modeling: Part II: Methodology for Inducing Blast Injury to in vitro Models.* Frontiers in neurology, 2012. **3**: p. 23-23.
2. Malojcic, B., et al., *Consequences of mild traumatic brain injury on information processing assessed with attention and short-term memory tasks.* Journal of Neurotrauma, 2008. **25**(1): p. 30-37.
3. Trudeau, D.L., et al., *Findings of mild traumatic brain injury in combat veterans with PTSD and a history of blast concussion.* Journal of Neuropsychiatry and Clinical Neurosciences, 1998. **10**(3): p. 308-313.
4. Thompson, J.M., K.C. Scott, and L. Dubinsky, *Battlefield brain Unexplained symptoms and blast-related mild traumatic brain injury.* Canadian Family Physician, 2008. **54**(11): p. 1549-1551.
5. Sundaramurthy, A., et al., *Blast-induced biomechanical loading of the rat: an experimental and anatomically accurate computational blast injury model.* Journal of Neurotrauma, 2012. **29**(13): p. 2352-+.
6. Cernak, I., et al., *Neuroendocrine responses following graded traumatic brain injury in male adults.* Brain Injury, 1999. **13**(12): p. 1005-1015.
7. Chafi, M.S., G. Karami, and M. Ziejewski, *Biomechanical assessment of brain dynamic responses due to blast pressure waves.* Annals of Biomedical Engineering, 2010. **38**(2): p. 490-504.
8. Garman, R.H., et al., *Blast exposure in rats with body shielding is characterized primarily by diffuse axonal injury.* Journal of Neurotrauma, 2011. **28**(6): p. 947-959.

9. Gieron, M.A., J.K. Korthals, and C.D. Riggs, *Diffuse axonal injury without direct head trauma and with delayed onset of coma.* Pediatric Neurology, 1998. **19**(5): p. 382-384.

10. Courtney, A.C. and M.W. Courtney, *A thoracic mechanism of mild traumatic brain injury due to blast pressure waves.* Medical Hypotheses, 2009. **72**(1): p. 76-83.

11. Cernak, I., et al., *Involvement of the central nervous system in the general response to pulmonary blast injury.* Journal of Trauma-Injury Infection and Critical Care, 1996. **40**(3): p. S100-S104.

12. Chavko, M., et al., *Relationship between orientation to a blast and pressure wave propagation inside the rat brain.* Journal of Neuroscience Methods, 2011. **195**(1): p. 61-66.

13. Moss, W.C., M.J. King, and E.G. Blackman, *Skull Flexure from Blast Waves: A Mechanism for Brain Injury with Implications for Helmet Design.* Physical Review Letters, 2009. **103**(10): p. 4.

14. Kocsis, J.D. and A. Tessler, *Pathology of blast-related brain injury.* Journal of Rehabilitation Research and Development, 2009. **46**(6): p. 667-671.

15. Chen, Y., W. Huang, and S. Constantini, *Concepts and strategies for clinical management of blast-induced traumatic brain injury and posttraumatic stress disorder.* Journal of Neuropsychiatry and Clinical Neurosciences, 2013. **25**(2): p. 103-110.

16. Unterberg, A.W., et al., *Edema and brain trauma.* Neuroscience, 2004. **129**(4): p. 1021-1029.

17. Nimmo, A.J., et al., *Neurogenic inflammation is associated with development of edema and functional deficits following traumatic brain injury in rats.* Neuropeptides, 2004. **38**(1): p. 40-47.

18. Strbian, D., et al., *The blood-brain barrier is continuously open for several weeks following transient focal cerebral ischemia.* Neuroscience, 2008. **153**(1): p. 175-181.

19. Ganpule, S., et al., *Mechanics of blast loading on the head models in the study of traumatic brain injury using experimental and computational approaches.* Biomechanics and Modeling in Mechanobiology, 2013. **12**(3): p. 511-531.

20. McGill, S.M., et al., *Passive stiffness of the human neck in flexion, extension, and lateral bending.* Clinical Biomechanics, 1994. **9**(3): p. 193-198.

21. Sogbesan, E., *Design and analysis of blast induced traumatic brain injury mechanism using a surrogate headform: instrumentation and outcomes*, in *Mechanical & Materials Engineering*2011, University of Nebraska-Lincoln.

22. Saljo, A., et al., *Neuropathology and pressure in the pig brain resulting from low-impulse noise exposure.* Journal of Neurotrauma, 2008. **25**(12): p. 1397-1406.

23. V. Shim, J.B., C. Josten and I. Anderson *Use of polyurethane foam in orthopaedic biomechanical experimentation and simulation*, 2012, Creative Commons Attribution License: licensee InTech. p. 171-200.

24. Orozco, R., *Effects of toughened matrix resins on composite materials for wind turbine blades*, in *Chemical Engineering*1999, Montana State University-Bozeman.

25. Stadelmann, V.A., et al., *Calcium phosphate cement augmentation of cancellous bone screws can compensate for the absence of cortical fixation.* Journal of Biomechanics, 2010. **43**(15): p. 2869-2874.

26. Motherway, J.A., et al., *The mechanical properties of cranial bone: The effect of loading rate and cranial sampling position.* Journal of Biomechanics, 2009. **42**(13): p. 2129-2135.

27. Hubbard, R.P., *Flexure of layered cranial bone.* Journal of Biomechanics, 1971. **4**(4): p. 251-263.

28. Neveen Awad, A.G., and Wael El-Dakhakhni, *Analysis of blast shock wave effects on surrogate brain gel model for traumatic brain injury assessment*: Submitted July 2014 to International Journal of Impact Engineering.

29. Bogduk, N. and S. Mercer, *Biomechanics of the cervical spine. I: Normal kinematics.* Clinical Biomechanics, 2000. **15**(9): p. 633-648.

30. Schaap, P., *Mathematical modelling of dummy headneck assemblies with MADYMQ*, in *Computational and Experimental Mechanics Group, Department of Mechanical Engineering*1992, Eindhoven University of Technology

31. A.J. Gallagher, A.N.A., K. Bruyere, M. Otténio, H. Xie, M.D. Gilchrist, *Dynamic tensile properties of human skin*, in *IRCOBI Conference* 2012. p. 494-502.

32. Richard H. Unverzagt, R., Ga. , *Cover for ballistic target assembly*, 1988, Linatex Coporation of America, Stafford Springs, Conn. : USA.

33. Neveen Awad, W.W.E.-D., and Ammar Gilani, *Compressed air-driven shock tube system to simulate blast-induced mild traumatic injuries*: Submitted July 2014 to Shock Waves Journal

34. Nakagawa, A., et al., *Biological and mechanical profile of bench top blast wave traumatic brain injury model in rat.* Journal of Neurosurgery, 2010. **113**(2): p. A415-A415.

35. Bass, C.R., et al., *Brain injuries from blast.* Annals of Biomedical Engineering, 2012. **40**(1): p. 185-202.

36. Chandra, N., et al., *Evolution of blast wave profiles in simulated air blasts: experiment and computational modeling.* Shock Waves, 2012. **22**(5): p. 403-415.

37. Albert I. King, K.H.Y., Liying Zhang and Warren Hardy, *Is head injury caused by linear or angular acceleration?* , in *Mild Traumatic Brain Injury Subcommittee, National Football League* 2003, Wayne State University IRCOBI Conference - Lisbon (Portugal). p. 1-12.

38. Grip, H., *Biomechanical assessment of head and neck movements in neck pain using 3D movement analysis*, in *Department of Radiation Sciences*2008, Umeå University, Sweden.

39. Krave, U., M. Al-Olama, and H.A. Hansson, *Rotational acceleration closed head flexion trauma generates more extensive diffuse brain injury than extension trauma.* Journal of Neurotrauma, 2011. **28**(1): p. 57-70.

40. H.A.M. Mahinda , O.P.M., *Variability in thickness of human skull bones and sternum – an autopsy experience.* Journal of Forensic Medicine and Toxicology, 2009. **26**(2): p. 6.

41. Smith, D.H., D.F. Meaney, and W.H. Shull, *Diffuse axonal injury in head trauma.* Journal of Head Trauma Rehabilitation, 2003. **18**(4): p. 307-316.

42. Nakagawa, A., et al., *Mechanisms of primary blast-induced traumatic brain injury: insights from shock-wave research.* Journal of Neurotrauma, 2011. **28**(6): p. 1101-1119.

43. Cernak, I., et al., *Cognitive deficits following blast injury-induced neurotrauma: possible involvement of nitric oxide.* Brain Injury, 2001. **15**(7): p. 593-612.

44. Zhang, J.Y., et al., *Experimental study of blast-induced traumatic brain injury using a physical head model*, in *Stapp Car Crash Journal, Vol 53*, A.I. King, J.W. Melvin, and L.W. Schneider, Editors. 2009, Soc Automotive Engineers: Warrendale. p. 215-227.

45. Wang, Y., et al., *Tightly Coupled Repetitive Blast-Induced Traumatic Brain Injury: Development and Characterization in Mice.* Journal of Neurotrauma, 2011. **28**(10): p. 2171-2183.

46. Leonardi, A.D., et al., *Intracranial pressure increases during exposure to a shock wave.* Journal of Neurotrauma, 2011. **28**(1): p. 85-94.

47. N. Awad, L.D., *Neurological manifestations related to blast injury.* Accepted (August 2011) for publication in the European Neurological Journal.

48. Li, X.Y., et al., *Diffuse axonal injury induced by simultanous moderate linear and angular head accelerations in rats.* Neuroscience, 2010. **169**(1): p. 357-369.

49. Donovan, V., et al., *Repeated mild traumatic brain injury results in long-term white-matter disruption.* Journal of Cerebral Blood Flow and Metabolism, 2014. **34**(4): p. 715-723.

5.8 List of Figures

Figure 5.10: (a) Brain acceleration and (b) Skull acceleration at 150 mm, 500 mm and 1000 mm for all orientations relative to shock tube exit.

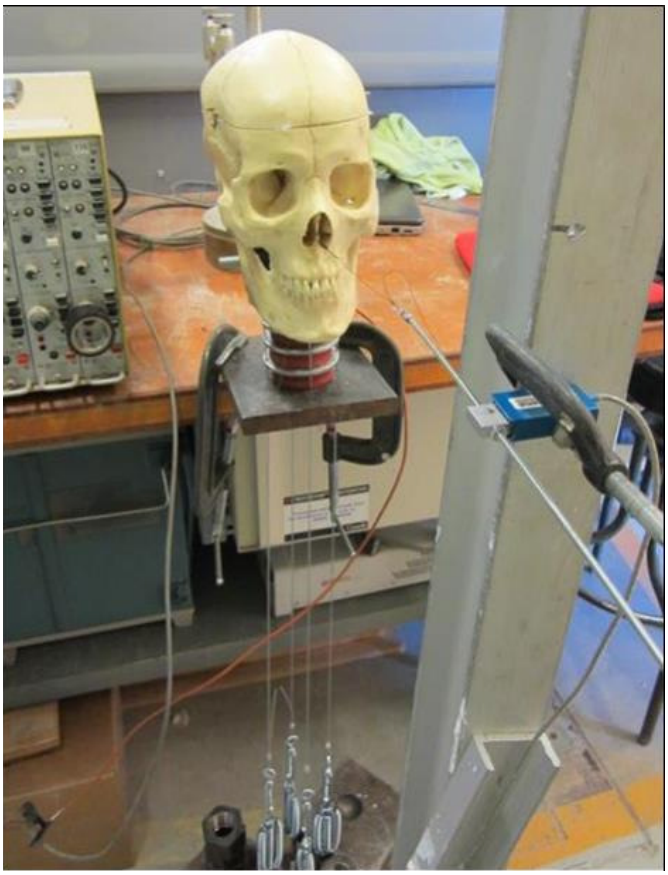

Figure 5.1: Experimental setup of the neck stiffness evaluation test

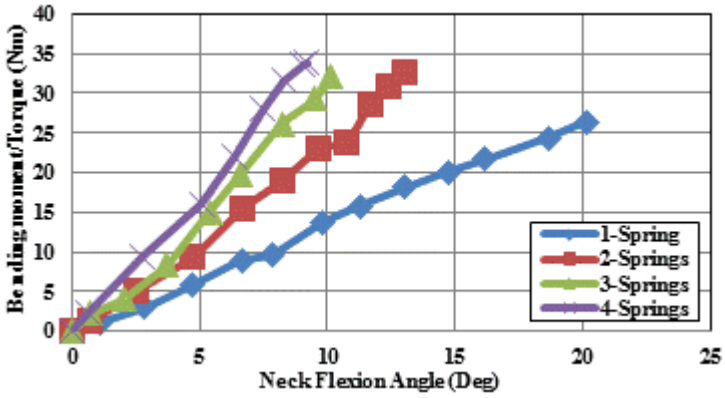

Figure 5.2: Relationship between the forces applied on the skull and the corresponding neck flexion angles

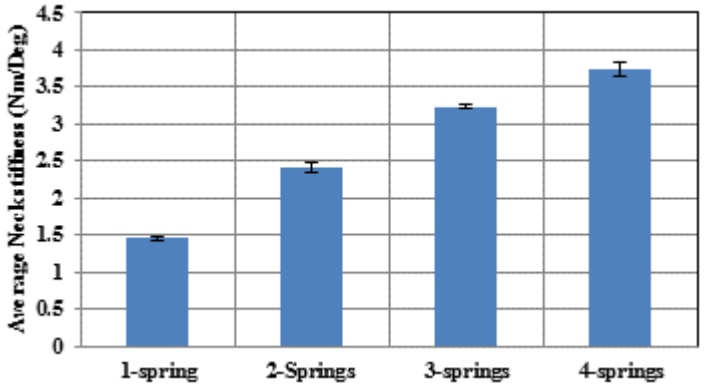

Figure 5.3: Average neck stiffness values using different spring numbers at each cable

Figure 5.4: Brain model inside the skull with inserted pressure transducers and accelerometer.

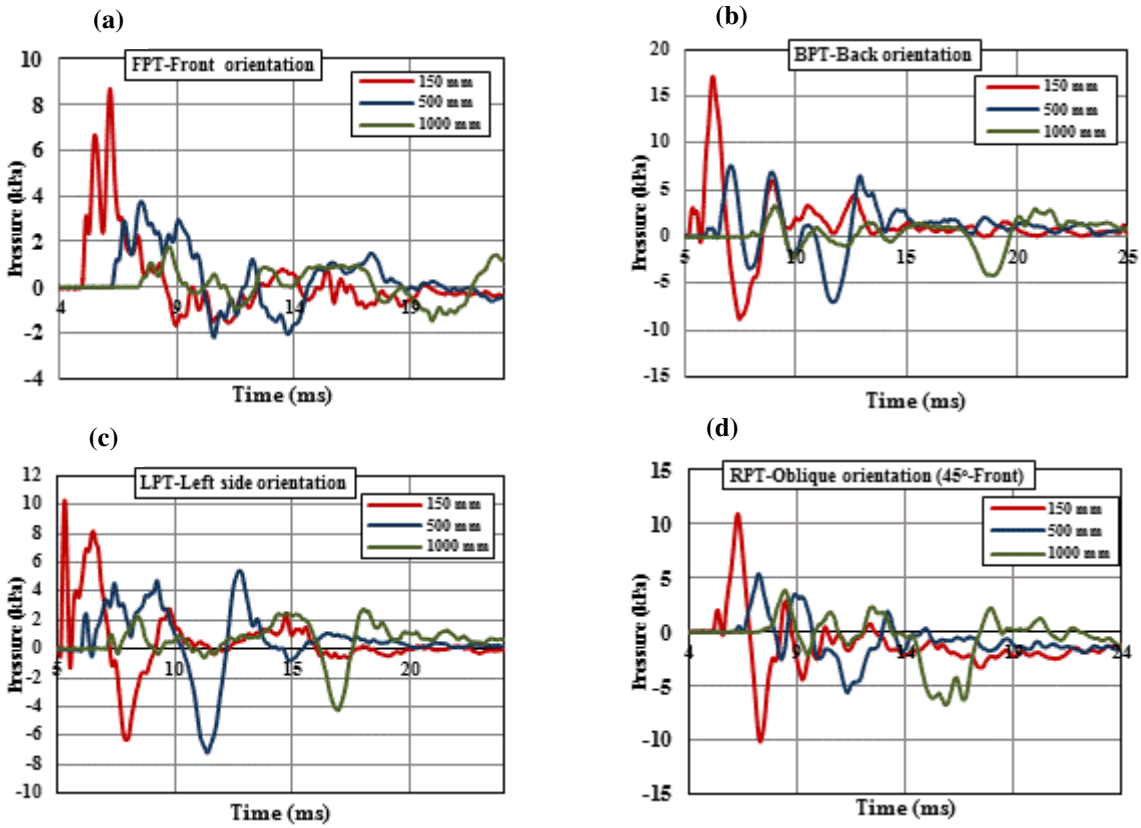

Figure 5.5: Pressure wave forms at all pressure transducers (PT) locations inside PHNM at 150, 500 and 1000 mm for all orientations (front, back, left side and oblique 45^{o}) (a). Front PT (FPT), (b) Back PT (BPT), (c) Left side PT (LPT), and (d) Right side PT (RPT).

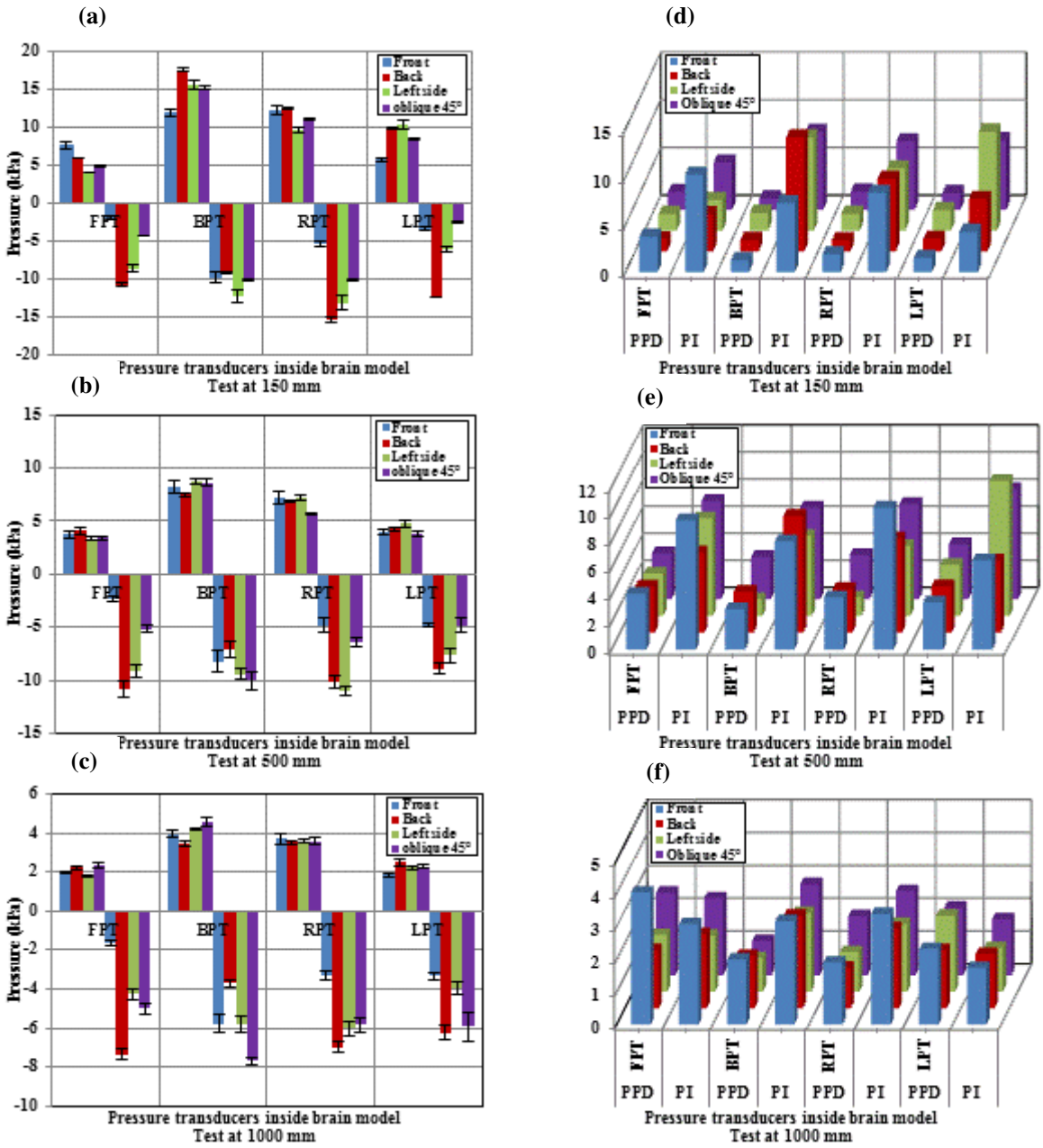

Figure 5.6: Right side shows the average values of positive and negative peak pressure recorded by all pressure transducers (PTs) inside PHNM at 150 mm (a), 500 mm (b) and 1000 mm (c) and the left side shows the average PPD (ms) and PI (kPa.ms)of the pressure measured inside PHNM at 150 mm (d), 500 mm (e) and 1000 mm (f) for all orientations (front, back, left side and oblique 45^{o})

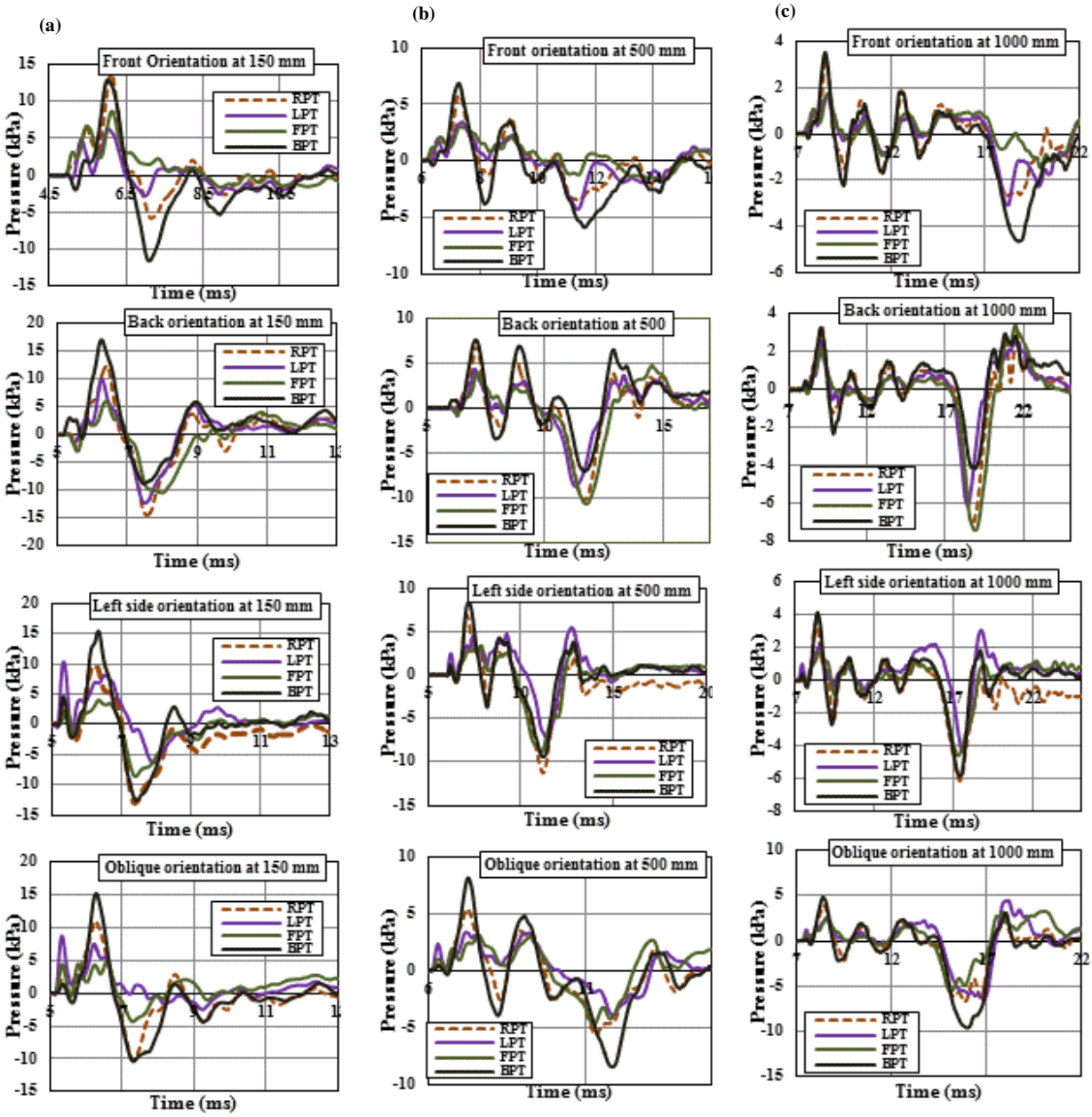

Figure 5.7: Pressure wave forms at all pressure transducers inside PHNM at 150 mm (group-a) 500 mm (group-b) and 1000 mm (group-c) for the orientations front, back, oblique 45^{o} and left side.

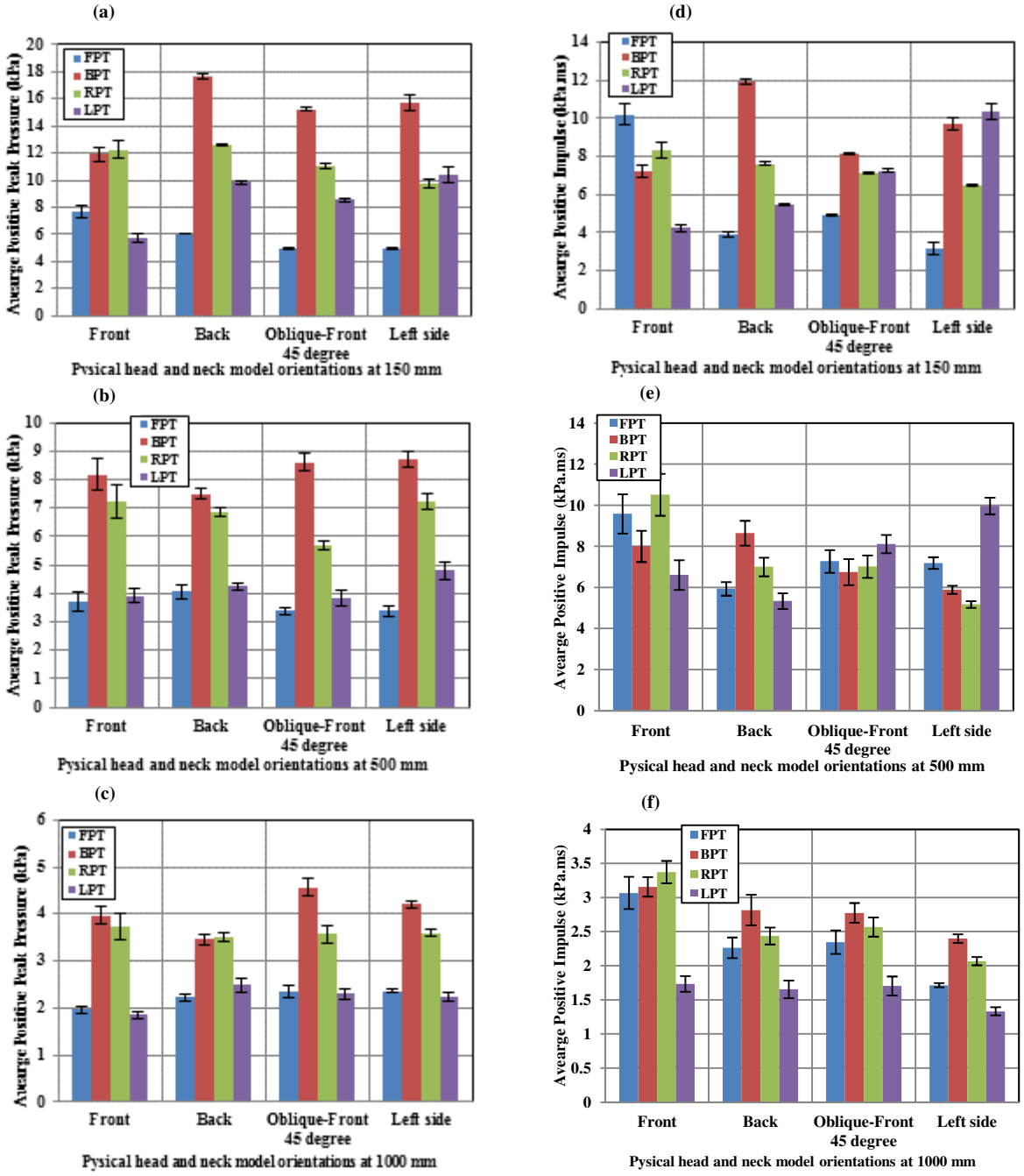

Figure 5.8: Demonstrates the average positive peak pressure (right column) and the average positive impulse (left column) of the PHNM at 150, 500, and 1000 mm for all orientations (front, back, oblique 45^{o} and left side).

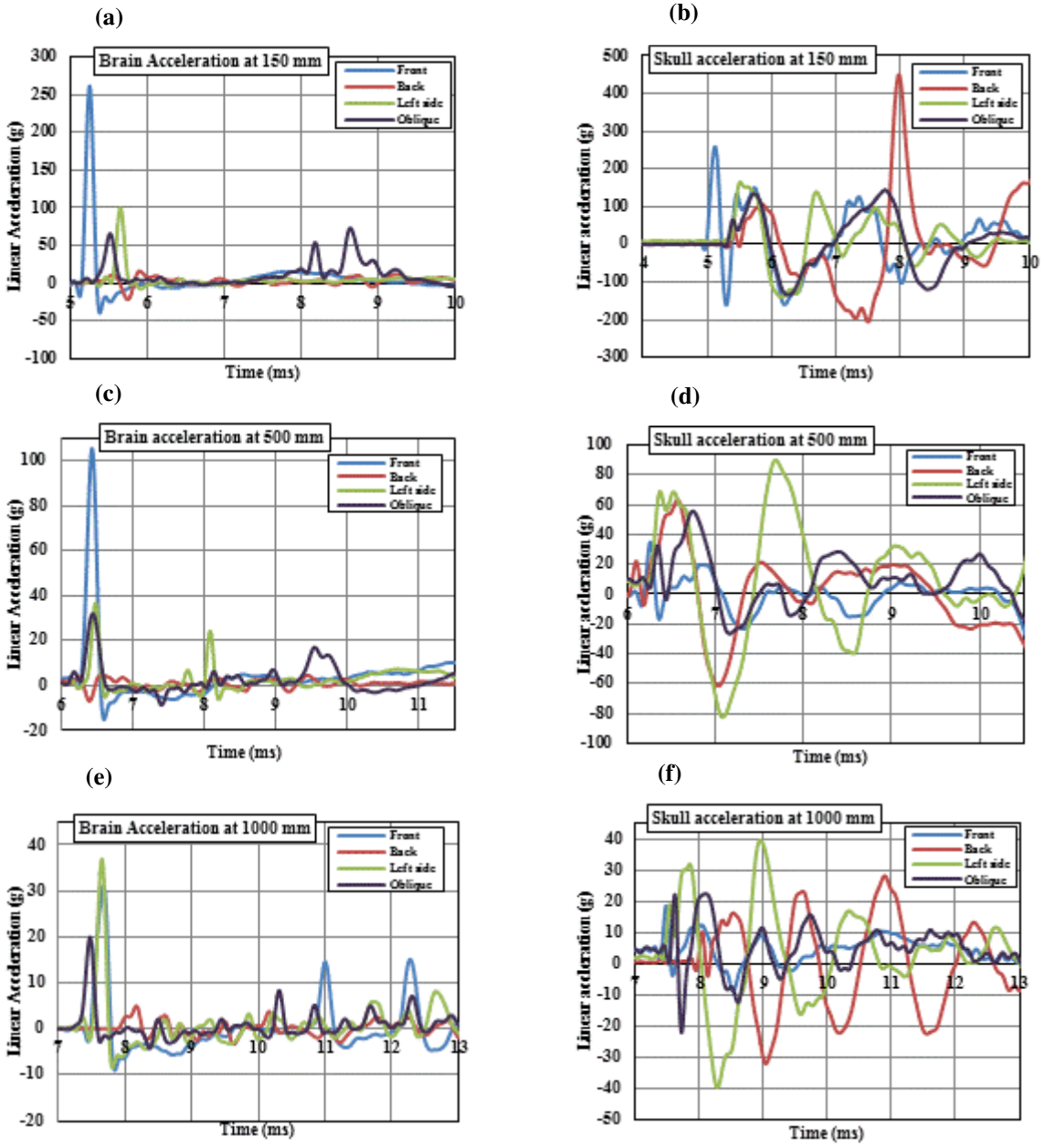

Figure 5.9: Brain and skull acceleration at a, b)150 mm c, d) 500 mm e, f) 1000 mm for all orientations relative to shock tube exit

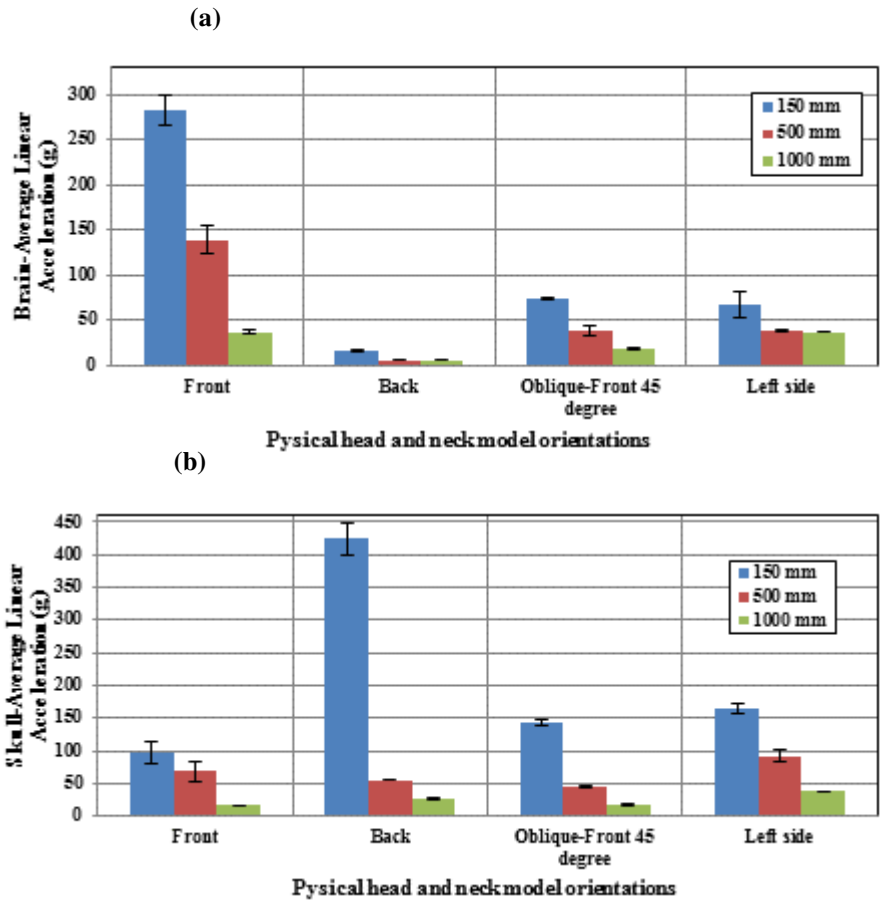

Figure 5.10: (a) Brain acceleration and (b) Skull acceleration at 150 mm, 500 mm and 1000 mm for all orientations relative to shock tube exit.

Chapter 6: Summary, Conclusions and Recommended Future Studies

6.1 Summary and Conclusions

Blast-induced traumatic brain injuries (b-TBIs) have been considered as the signature wound of various explosions events in military conflicts or domestic and industrial accidents. b-TBIs may result from primary (blast wave), secondary (shrapnel), tertiary (victim hit surrounding objects or ground) or quaternary (heat, toxic gases, or dust) blast injuries. The primary blast brain injury is a serious health problem that may contribute to a substantial number of brain dysfunctions. Due to the lack of essential related information required to protect against or assess for early diagnosis and managements, a better understanding of blast wave interactions with models is demanded. This work has been carried out to generate blast waves and study their interactions with gel brain model and physical head and neck model (PHNM). This work investigates different wave components that may be influenced by the orientation and location of the tested models from the blast source.

Compressed air-driven shock tube was designed and numerically analyzed using finite element analysis (FEA). The numerical analysis was performed by utilizing LS-DYNA. Experimental validation of the shock tube numerical model was conducted to calibrate and replicate free field blast waves for further studies related to the blast-induced mild traumatic brain injury (BImTBI). Two metallic diaphragms (steel and brass) were utilized in the calibration tests using three different thicknesses for each type (0.127, 0.076, and 0.025 mm). The pressure wave inside and outside the shock tube were

monitored using four pressure transducers (PTs) inserted at different locations internally and additional four PTs mounted on air-foil board at 50, 100, 150 and 450 mm externally. The experimental results revealed reduction in peak pressure and impulse by moving away from shock tube exit. By comparing the results of the FEA model and shock tube experiments shows good correlation with no significant difference at the four locations outside the shock tube exit. Analysis of experimental results revealed variations in the resultant shock wave parameters depending on the tested diaphragm type and thickness. Therefore, it was concluded that the generated shock wave can be controlled by altering the diaphragm type for various blast related applications. The 0.127 mm steel diaphragm showed reliable results through all performed tests. This was manifested in the key parameters of blast shock wave including positive peak pressure (PPP), positive phase duration (PPD), and positive impulse (PI) were consistent at any examined distances from shock tube exit. The previous finding was further affirmed using statistical analysis.

Experiments of gel brain model were carried out using the compressed air-driven shock tube as a source of reliable shock waves in the range that can induce mTBI. Experimental studies were performed to assess the wave propagation modes within the brain model in relation to different brain model orientations and distances with respect to the shock tube exit. The brain model was developed by using silicone gel (Sylgard 527 A & B). A compression test using Instron was performed to examine the silicone gel elastic properties. Analysis of compression test results revealed that the silicone gel can be used to develop a brain model as it possesses elastic properties similar to the actual brain tissue. Internal brain model pressure and acceleration were measured using four PTs

embedded internally and an accelerometer, respectively. The experiments were performed at four distances (150, 500, 1000 and 1500 mm) and for three orientations (right side, back and oblique 45°). At the 150 mm distance from shock tube exit, the pressure waves showed a positive phase followed directly by a negative phase pressures that are similar to the incident shock wave profile. For other tested locations, a gap between positive and negative phases appeared and it increases with increasing distance from the shock tube exit .At the same time, the PPP decreases while the negative peak pressure (NPP) increases. This suggests that by increasing the distance from shock wave source the effect of the incident pressure reduces, while the effect of reflected pressure increases. It has been suggested that NPP is the main cause of developing the brain cavitation. Further investigation is required to address the risk of cavitation as a possible brain injury mechanism. Results showed that the PI values for any tested orientations were similar at the far distances. This suggests that by moving away from the shock wave source the effects of orientation factor on the brain injury are reduced.

Further investigations of mTBI mechanisms were conducted utilizing a physical head and neck model (PHNM) and was covered with a surrogate skin. The PHNM consisted of a skull occupied with silicone gel brain model and connected to a neck model that was designed and constructed at Applied Dynamics Lab. The neck model stiffness was tested aiming to mimic the actual neck. The PHNM was exposed to a blast wave generated from the previously designed shock tube. Four different PHNM orientations corresponding to the anatomical locations of frontal (front), occipital (back), temporal (left side) and oblique 45° for the left-frontal bones at 150, 500, and 1000 mm

with respect to the shock tube exit were examined. The intracranial pressure (ICP) was recorded using four PTs embedded intraparenchymally at right and left temporal lobes, frontal, and occipital lobes. The brain acceleration as well as the bulk acceleration was recorded using two accelerometers inserted on the brain model internally and on the head externally. The resultant positive and negative pressures recorded intracranially were at the nonlethal levels which could lead to mTBI as previously reported in other studies using animal models. The results suggest that both direct and indirect blast injuries will contribute to the total damage within the brain as we get closer to the blast site. While as we move away from the detonation, the effect of direct injury is reduced and the indirect blast impact might be considered the main cause of injury. Further, in accordance with the PHMN orientations there were alteration in the recorded waveforms that may result from the effects of the skull irregular shape and thickness of the cranial bone, which can influence the wave propagation intracranially. Analysis of acceleration results showed that head movements after PHNM and shock wave interaction may have minimal contribution on the brain linear acceleration. The blast-induced traumatic brain injury is a challenge health care problem and better understanding of its mechanisms is crucial to prevent the development of chronic neurological dysfunctions through the early diagnosis and improvement of the health management procedures.

6.2 Recommended Future Studies

The results of this research revealed that the blast test setup is to provide reliable results inside and outside the shock tube. Therefore, this system is considered suitable to

be used in other related BImTBI researches in accompanied with a wide range of tested subjects. This includes not only physical head and small/large animal models, but also using in vitro models to examine the biochemical responses after exposure to mild range of blast shock wave. Investigations of moderate and severe TBI require obtaining a shock wave with high amplitude. Using a thicker metallic diaphragm that can be punctured with mechanically-operated sharp metal striker when the air inside the compression chamber reaches the required pressure will promote a wide range of reliable shock waves. Moreover, the PHNM can be modified by mimicking other intracranial structures that may influence the wave propagation within the brain, for instance, the cerebrospinal fluid (CSF) and Dura mater. Further investigations are suggested to study the effect of both linear an angular acceleration after exposure to simulated blast for better understanding of their role combined in TBI.

The results of this study provide fundamental information that might help further studies related to the mechanical mechanisms of blast-induced brain injuries. The prominent negative peak pressure at certain tested locations and for specific model orientations with respect to shock tube exit suggests that further investigations may be required to evaluate the cavitation mechanism in developing brain dysfunctions. Valuable quantitative data obtained from the current study could be the foundation for a computer simulation of BImTBI aiming to improve the brain injury prediction.